

AD-A009 327

ANNUAL RESEARCH REPORT 1 JULY 1973 -  
30 JUNE 1974

Armed Forces Radiobiology Research  
Institute

Prepared for:  
Defense Nuclear Agency

30 June 1974

DISTRIBUTED BY:

**NTIS**

National Technical Information Service  
U. S. DEPARTMENT OF COMMERCE

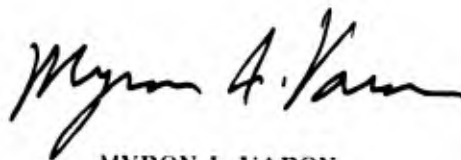
## FOREWORD

This report describes, in brief summary, the scientific accomplishments of the Armed Forces Radiobiology Research Institute (AFRRI) for the period 1 July 1973 to 30 June 1974.

During this period, the broadened research program of the AFRRI led to significant contributions in biomedical research. The Behavioral Sciences Department continued to provide biological data relevant to nuclear combat operations, particularly the employment of nuclear weapons in tactical or theater nuclear warfare. A significant result of the scientific effort within the Experimental Pathology Department was the award of a contract by the National Heart and Lung Institute to AFRRI to conduct research on "Improved Preservation of Granulocytes for Transfusion."

In this report, the majority of the technical summaries of the Neurobiology Department have appeared in the open literature and have led to numerous collaborative efforts with distinguished scientists including two Nobel laureates. The nuclear medicine and biochemistry efforts of the Radiation Biology Department led to numerous clinical applications of this Department's research. The 1st Invitational Symposium on the Serodiagnosis of Cancer, jointly sponsored by the AFRRI, the Laboratory Service of the National Naval Medical Center, and the American Society of Clinical Pathologists was a highlight of fiscal year 1974.

The Institute's accomplishments would not have been possible without the continued support of numerous agencies. Appreciation is extended to the Surgeons General who have continued to provide the highly trained and qualified scientific personnel required by such a diversified research program. Financial support was provided by the Navy Toxicology Unit, the Office of Naval Research, the U. S. Army Medical Research and Development Command, the Food and Drug Administration and the National Institutes of Health.



MYRON I. VARON  
Captain MC USN  
Director

## TABLE OF CONTENTS

	Page
PATHOPHYSIOLOGICAL STUDIES OF POTENTIALLY TOXIC SUBSTANCES.	
Schneider, N. R. and Baum, S. J. ....	1
BIOLOGICAL EFFECTS OF ELECTROMAGNETIC PULSES. Skidmore, W. D.,	
Baum, S. J. and Wyant, D. E. ....	3
EXPERIMENTAL COMMUNICATING HYDROCEPHALUS IN THE PRIMATE:	
ULTRASTRUCTURAL AND PATHOPHYSIOLOGICAL STUDIES. Flor, W. J. ..	5
A TECHNIQUE FOR THYMECTOMY IN THE ADULT RAT. Cloud, C. L. and	
Ledney, G. D. ....	7
SUPPRESSION OF SECONDARY DISEASE BY <u>IN VITRO</u> EXPOSURE OF MIXTURES	
OF LYMPHOID AND STEM CELLS TO PURIFIED ANTILYMPHOCYTE	
ANTIBODY. Ledney, G. D., Exum, E. D., Crawford, R. M., Galley, C. B.	
and Walker, R. I. ....	10
INDUCTION OF SPECIFIC IMMUNOLOGIC UNRESPONSIVENESS IN RATS USING	
ANTIGENIC STIMULATION AND CYTOXAN. Fink, M. P., Cloud, C. L.	
and Ledney, G. D. ....	11
ENDOTOXIN EFFECTS OF MOUSE LIVER ADENYL CYCLASE. Donlon, M. A.	
and Walker, R. I. ....	14
HEMATOPOIETIC STEM CELL RENEWAL IN THE POSTIRRADIATED ANIMAL.	
McCarthy, K. F. ....	16
FEEDBACK MECHANISMS BETWEEN INFLAMMATORY AREAS AND THE	
GRANULOPOIETIC MICROENVIRONMENT. Wyant, D. E. and Baum, S. J. ..	
DEVELOPMENT OF CLINICAL APPROACHES FOR THE TREATMENT OF	19
RADIATION SICKNESS AND GRAFT VERSUS HOST DISEASE THROUGH	
MANAGEMENT OF THE INTESTINAL FLORA. Walker, R. I. and	
Ledney, G. D. ....	22
THE PHARMACOKINETICS OF SODIUM NITRITE AND ITS RELATIONSHIP TO	
METHEMOGLOBINEMIA IN SELECTED MAMMALS. Schneider, N. R. ....	
CONTROL OF WHITE CELL POPULATION IN THE POSTIRRADIATED ANIMAL.	24
MacVittie, T. J., McCarthy, K. F. and Baum, S. J. ....	26
EVALUATION OF THE BIOLOGIC ACTIVITY OF ATTENUATED ENDOTOXIN.	
Galley, C. B., Walker, R. I., Ledney, G. D. and Gambrill, M. R. ....	29
PROTEIN-BOUND CARBOHYDRATES AS BIOCHEMICAL CRITERIA IN DIAGNOSIS	
AND PROGNOSIS OF MALIGNANT NEOPLASIA. Evans, A. S. ....	
ALTERATIONS OF SERUM SIALIC ACID LEVELS IN MINIATURE SWINE AFTER	31
SPLIT DOSE EXPOSURE TO <sup>60</sup> Co RADIATION. Sobocinski, P. Z. and	
Taylor, J. F. ....	33
AUTOMATED DETERMINATIONS FOR SERUM SIALIC ACIDS AND HEXOSAMINES.	
Mathewson, N. S. and Sobocinski, P. Z. ....	33
GLYCOPROTEINS IN DIABETES. Woods, R. J. O. and Sobocinski, P. Z. ....	
EXPERIMENTAL INDUCTION OF NEUROGENIC TUMORS IN MINIATURE SWINE	37
(NEUROGENIC TUMOR MODEL). Ekstrom, M. E. ....	
DEVELOPMENT OF A HYPOTHROMBOGENIC BLOOD OXYGENATOR MEMBRANE.	
Weathersby, P. K. ....	38
TECHNETIUM-99m PHOSPHATE BONE IMAGING: A METHOD FOR ASSESSING	
BONE GRAFT HEALING. Stevenson, J. S., Bright, R. W., Dunson, G. L.	
and Nelson, F. R. ....	39
TECHNETIUM-99m PYROPHOSPHATE: COMPARISON OF ED <sub>50</sub> FOR TETANY	
AND ACIDOSIS WITH ACUTE LD <sub>50</sub> . Stevenson, J. S., Eckelman, W. C.,	
Sobocinski, P. Z., Barron, E. L. and Levin, S. G. ....	44

	Page
TECHNETIUM-99m PYROPHOSPHATE FOR BONE IMAGING. Eckelman, W. C., Reba, R. C., Kubota, H. and Stevenson, J. S. ....	46
EVALUATION OF HEALING OF MANDIBULAR BONE GRAFTS IN DOGS BY QUANTITATIVE TECHNETIUM-99m POLYPHOSPHATE BONE IMAGING. Kelly, J. F., Cagle, J. D., Stevenson, J. S. and Adler, G. J. ....	48
CORRELATION OF GAMMA CAMERA AND FLOWMETER DETERMINED RENAL BLOOD FLOW MEASUREMENTS. Kirchner, P. T., Gray, F. C., Short, D. B. and Filo, R. S. ....	49
TECHNETIUM-99m METHOTREXATE STUDIES. Kirchner, P. T., ....	50
A QUALITATIVE AND QUANTITATIVE COMPARATIVE ANALYSIS OF SCINTILLATION CAMERA TOMOGRAPHY WITH THE LATEST CONVENTIONAL IMAGING TECHNIQUES. McManaman, V. L., Sinclair, M. D. and Stevenson, J. S. ....	51
TECHNETIUM-99m POLYPHOSPHATE RENAL IMAGING. Sinclair, M. D. and Stevenson, J. S. ....	52
INSTRUCTION IN NUCLEAR MEDICINE. Stevenson, J. S. ....	53
LEAD SHIELD TO IMPROVE DETECTION OF HIGH-ENERGY PHOTONS BY SCINTILLATION CAMERAS. Stevenson, J. S. ....	55
MEASUREMENT OF CATHEPSIN D ACTIVITY ON BIOLOGICAL SAMPLES OBTAINED FROM IRRADIATED RATS. Snyder, S. L. and Sobocinski, P. Z. ..	57
A CRITICAL EVALUATION OF 1,10-PHENANTHROLINE AS A REAGENT FOR SIALIC ACID DETERMINATIONS. Snyder, S. L., Mathewson, N. S. and Sobocinski, P. Z. ....	57
TECHNETIUM-99m METHOD OF HIP SCANNING TO DETECT EARLY ASEPTIC NECROSIS. Stevenson, J. S. and Nelson, F. R. ....	60
RADIONUCLIDE ANGIOCARDIOGRAPHY. McManaman, V. L. and Stevenson, J. S. .	62
CEREBRAL AND CAROTID RADIOANGIOGRAPHY. McManaman, V. L., Stevenson, J. S. and Thrall, J. H. ....	63
A COMPUTER SERVICE FOR ANALYZING CLINICAL SCINTIGRAPHIC DATA. McManaman, V. L. and Stevenson, J. S. ....	64
FACTORS AFFECTING THE DIAGNOSTIC RELIABILITY OF SCINTILLATION CAMERA FILM IMAGES. McManaman, V. L., Stevenson, J. S. and Sinclair, M. D. ....	65
EFFECTS OF IONIZING RADIATION ON PHYSICAL ACTIVITY. Curran, C. R. and Franz, C. G. ....	69
THE INCIDENCE OF BEHAVIORAL INCAPACITATION AS A FUNCTION OF PULSED WHOLE-BODY HIGH NEUTRON RADIATION DOSE. Young, R. W. and Middleton, G. R. ....	69
EMESIS FOLLOWING EXPOSURE TO IONIZING RADIATION. Middleton, G. R. and Young, R. W. ....	71
BEHAVIORAL TOXICOLOGY. Young, R. W., Middleton, G. R., Franz, C. G. and Curran, C. R. ....	73
THE EFFECTS OF PROPYLENE GLYCOL DINITRATE VAPORS ON VISUAL EVOKED RESPONSE AND FREE OPERANT AVOIDANCE TASK. Mattsson, J. L. and Crock, J. W. ....	75
THE EFFECTS OF SULFOLANE ON SHOCK ELICITED AGGRESSION. Middleton, G. R. and Young, R. W. ....	77
EARLY DETECTION OF CENTRAL NERVOUS SYSTEM DAMAGE. Mattsson, J. L. and Levin, S. G. ....	79
HIPPOCAMPAL BIOELECTRIC PATTERNS AND BEHAVIOR. Teitelbaum, H. ....	80
CHANGES IN BRAIN BIOELECTRICAL ACTIVITY AS A RESULT OF REPEATED MORPHINE ADMINISTRATION. Teitelbaum, H., Catravas, G. N. and Blosser, J. C. ....	80



	Page
MOLECULAR STUDIES OF OPIATE TOLERANCE AND DEPENDENCE IN THE MAMMALIAN BRAIN. Catravas, G. N., Takenaga, J. and McHale, C. G. ....	81
NEURONAL AMINO ACID METABOLISM. Zeman, G. H. and Catravas, G. N. ....	83
CEREBRAL BLOOD FLOW IN EXPERIMENTAL SUBARACHNOID HEMORRHAGE. Martins, A. N., Koblaine, A. I., Doyle, T. F. and Newby, N. ....	83
EXPERIMENTAL POSTIRRADIATION MYELOPATHY. Fein, J. M. and Di Chiro, G. ....	85
EFFECTS OF IONIZING RADIATION ON SINGLE AND SIMPLE NERVE NETWORKS IN <u>APLYSIA CALIFORNICA</u> . Willis, J. A. and Carpenter, D. O. ....	86
CEREBRAL ISCHEMIA: LOCAL OXYGEN UTILIZATION AFTER MIDDLE CEREBRAL OCCLUSION. Fein, J. M. ....	87
CEREBRAL VASOSPASM. Fein, J. M. ....	89
NEUROTRANSMITTERS IN THE NERVOUS SYSTEM OF <u>APLYSIA</u> . Zeman, G. H., Yarowsky, P. J. and Carpenter, D. O. ....	90
CELL CULTURE OF NEURONAL TISSUES. Shain, W. G., Jr., Myers, P. R., Morantz, R. A. and Chock, E. S. ....	93
OPIATE EFFECTS ON BRAIN TYROSINE. Cohan, S. L. and Abbott, J. R. ....	99
THE EFFECTS OF OPIATES ON RNA POLYMERASE ACTIVITY <u>IN VIVO</u> . Darden, J. H. and Catravas, G. N. ....	100
MECHANISM OF MORPHINE ANTAGONISM OF RESERPINE-INDUCED DEPLETION OF BRAIN CATECHOLAMINES. Blosser, J. C. and Catravas, G. N. ....	101
FUNCTIONAL PROTEINS IN THE MEMBRANES OF NEURONS. Shain, W. G., Jr., Carpenter, D. O., Livengood, D. R. and Chock, E. S. ....	102
NEURORADIOLOGY CORRELATIONS. Shatsky, S. A., Evans, D. E., Alter, W. A., III and Armbrustmacher, V. ....	106
CARDIAC ARRHYTHMIAS RESULTING FROM EXPERIMENTAL HEAD INJURY. Evans, D. E., Alter, W. A., III and Shatsky, S. A. ....	109
EFFECT OF $\text{PaCO}_2$ CHANGES ON THE RATE OF FORMATION OF CEREBROSPINAL FLUID IN THE MONKEY. Martins, A. N., Koblaine, A. I. and Doyle, T. F. ..	111
THE EFFECTS OF TRAUMATIC INJURY ON SPINAL CORD BLOOD FLOW. Doyle, T. F., Koblaine, A. I. and Martins, A. N. ....	112
SENSORY RECEPTOR PHYSIOLOGY. Wiederhold, M. L. and Gallin, E. K. ....	113
STATE OF IONS AND WATER IN LIVING CELLS AND SOLUTIONS. Carpenter, D. O., McCreery, M. J. and Bidinger, J. ....	117
IONIC MECHANISMS UNDERLYING NEURONAL THERMOSENSITIVITY. Pierau, F. -K. and Carpenter, D. O. ....	119
ELECTROPHYSIOLOGICAL STUDIES ON THE LOBSTER CARDIAC GANGLIA. Livengood, D. R. ....	121
BIODYNAMICS AND PATHOPHYSIOLOGY OF TRAUMATIC UNCONSCIOUSNESS. Ommaya, A. K., Thibault, L. E. and Carpenter, D. O. ....	123
STUDIES INTO THE MECHANISM OF ALCOHOL-INDUCED PHYSICAL DEPENDENCE IN THE RAT. Hunt, W. A. ....	125
THE BRAIN AS AN IMMUNOLOGICALLY PRIVILEGED SITE. Morantz, R. A. and Shain, W. G., Jr. ....	127
IDENTIFICATION OF SPECIFIC OPIATE RECEPTORS IN CULTURED CELLS. Blosser, J. C. and Shain, W. G., Jr. ....	128
SPINAL CORD BLOOD FLOW MEASURED BY THE HYDROGEN CLEARANCE TECHNIQUE. Doyle, T. F., Koblaine, A. I. and Martins, A. N. ....	130
VENTRICULOCISTERNAL PERFUSION STUDIES IN THE MONKEY. Martins, A. N. and Doyle, T. F. ....	131
COMPUTERIZED AXIAL-TRANSVERSE TOMOGRAPHY: THE ACTA SCANNER. Kiker, W. E., Hinz, T. W. and Ledley, R. S. ....	132
INTRACRANIAL PRESSURE SENSOR DEVELOPMENT. Hermann, G. L. and Kiker, W. E. ....	136

	Page
DEVELOPMENT OF A PROTOTYPE BURN WOUND DRESSING. Meaburn, G. M., Cole, C. M., Hosszu, J. L., Wade, C. W. and Eaton, J. C. ....	137
PHOTONUCLEAR PRODUCTION OF POTASSIUM-38. Cole, C. M., Gray, F. C., Meaburn, G. M. and Stevenson, J. S. ....	139
ORGANOMETALLIC DOSIMETERS. Meaburn, G. M., Hosszu, J. L. and Kiker, W. E. ....	140
FREE RADICAL REACTIONS: RADIATION-INDUCED OPTICAL CHANGES IN AQUEOUS DNA SOLUTIONS. Meaburn, G. M. and Hosszu, J. L. ....	143
INDEX TO PRINCIPAL INVESTIGATORS .....	145

## **PATHOPHYSIOLOGICAL STUDIES OF POTENTIALLY TOXIC SUBSTANCES**

**Principal Investigators:** *N. R. Schneider and S. J. Baum*

**Collaborator:** *M. E. Andersen, Navy Toxicology Unit*

The objective of this research was to measure and determine the physiological and metabolic pathways of cyclotrimethylenetrinitramine (RDX) following oral, intraperitoneal and intravenous administration; its toxic and resultant pathological effects on the various organ systems; and the development of proper therapeutic and prophylactic procedures.

It was apparent during the course of experimentation that the two different consignments of RDX utilized did not quantitatively resemble each other in dose response relationships. Since physical assay by gas chromatography showed no variation in chemical activity between the two batches, this phenomenon was apparently related to particle size. Consequently, dosage per unit of body weight cannot be used as the sole indicator of expected RDX toxicity. Because of the enhanced absorption of the RDX in the small particle size, experiments utilizing this material were designed accordingly.

The oral acute distribution study was continued. Fasted rats were given 100 mg RDX (c.p.\*)/kg body weight. A group of 10 rats was utilized for serial sampling up to and including 8 hours after administration. These animals were previously prepared by anesthetizing them with chloral hydrate and implanting femoral artery and urinary bladder catheters, then permitting recovery for 24 hours before dosing. All animals in the 8-hour catheterized group had at least one seizure. The plasma concentrations in the catheterized group were higher than expected and often exceeded 5 µg/ml, the threshold of seizures reported in the intraperitoneal uptake study.

The differences in RDX concentrations between the catheterized and noncatheterized 8-hour groups were apparently related to the procedure involving chloral hydrate anesthesia and surgery the day before the animals received RDX. Histopathological examinations of tissues collected at euthanasia are in progress. Both light and electron microscopy are being employed to investigate both the cellular and subcellular effects of RDX toxicity.

A series of experiments involving repeated low level exposure to RDX were performed to investigate the effects of oral chronic distribution in the rat. RDX was administered at a dosage of 20 mg (f.p.†)/kg per day per os. An apparent stress related chronic respiratory disease produced approximately 25 percent lethality in the

---

\* Coarse particle size

† Fine particle size

RDX dosed animals. All control animals survived, exhibiting a normal growth curve. The data from the above experiment indicate that low levels of RDX were present in plasma, urine, feces and tissues of rats chronically administered daily low doses, but concentrations were so erratic on a day to day basis that no predictable trends were apparent. No accumulation of RDX was evident at the administered dosage level of 20 mg/kg per day. Plasma samples generally contained less than 2.5  $\mu\text{g}$  RDX/g. Tissue concentrations were generally less than 6  $\mu\text{g}$  RDX/g with an occasional sample exhibiting a concentration up to four times higher. No specific target organ was perceived during the course of the experiment.

Another oral chronic distribution study was conducted on rats given a water solution saturated with RDX instead of regular drinking water. The solution contained approximately 60  $\mu\text{g}$  RDX (f.p.)/ml. Animals maintained on the RDX saturated water solution exhibited a similar growth curve as the controls. Both groups consumed a similar amount of water, which was approximately 50 ml/day. Analysis of blood samples as well as tissue analysis has not yet been completed.

A definitive study was initiated to determine the percentage of an oral dose of RDX excreted in the feces. Sunderman reported, on the basis of two rats, that 40-90 percent of RDX is excreted chiefly in the feces over a period of 2 to 3 weeks after a single administered dose.<sup>1</sup> In our study, 10 rats were given a single dose (50 mg RDX (f.p.)/kg). The data indicate that an extremely small amount of the parent compound was excreted during this time. The total RDX output in the feces ranged from 47.75 to 103.84  $\mu\text{g}$  RDX. This amount is only 1-2 percent of the total original dosage of RDX administered. It is suspected that the RDX concentration reported by Sunderman includes metabolites in addition to the parent compound. <sup>14</sup>C-labeled RDX is being utilized in an attempt to identify the percentage of parent compound and possible metabolites excreted in the feces.

Because the miniature swine resembles man in many physiological, biochemical, and physical parameters, the experiments investigating the acute distribution of RDX in the biological system were expanded to include this species. A group of eight animals was administered RDX at a dosage of 100 mg RDX (f.p.)/kg. The data obtained indicate that plasma concentrations during the first 6 hours did not reach levels which had produced seizures in rats, and generally ranged from 0.9 to 3  $\mu\text{g}$ /ml. Urine concentrations were within a similar range, and not two to three times higher than plasma as exhibited in the rat. However, at 24 hours, plasma concentrations in five of the eight pigs approached or exceeded the seizure threshold of 5  $\mu\text{g}$  RDX/ml. Two of these pigs were suspected of having seizures during the night, a third was observed in a full seizure at  $T_0+23\frac{1}{2}$  hours, and one died at approximately  $T_0+22$  hours. The 24-hour plasma concentrations of these five pigs ranged from 3.6 to 18.2  $\mu\text{g}$ . The tissue concentrations of RDX in the miniature pig for brain, heart, liver, kidney and body fat generally ranged from 3 to 10  $\mu\text{g}$ /ml. RDX did not accumulate preferentially in any one tissue in these experiments. Tissue concentrations for the stomach and spiral colon often exceeded 45  $\mu\text{g}$ /g (107  $\mu\text{g}$ /g of stomach in the one lethality).

Investigations are being made to determine whether or not RDX is physically bound to the mucosa of the gut. Histopathological examinations of tissues collected at euthanasia are in progress.

#### REFERENCE

1. Sunderman, F. W. Hazards to the health of individuals working with RDX(B). National Defense Research Committee of the Office of Scientific Research and Development Report OSRD No. 4174, 1944. Arlington, Virginia, Armed Services Technical Information Agency ATI-31099, 1960.



#### BIOLOGICAL EFFECTS OF ELECTROMAGNETIC PULSES

**Principal Investigators:** W. D. Skidmore, S. J. Baum and D. E. Wyant

**Technical Assistance:** J. L. Atkinson and R. T. Brandenburg

The objective of this research was to determine biological effects of chronic exposure to pulsed electromagnetic radiation.

One year ago it was reported that rodents exposed to  $10^8$  pulses during 38 weeks from the AFRRI electromagnetic pulse (EMP) simulator showed no acute biological effects. This study was continued for another year and results are reported for rodents exposed to  $2.4 \times 10^8$  pulses during 90 weeks of exposure. At this time the rats are 2 years old and are approaching the end of their life-span.

Last year it was reported that reticulocytes appear to have been elevated after EMP irradiation while platelets decreased, although both counts remained within acceptable levels. These apparent differences disappeared during the 2nd year of exposure (Figures 1 and 2). It is clear now that EMP irradiation did not affect peripheral blood counts. As may be seen from Table I, there is no evidence that hematological parameters are affected by EMP exposure. Fertility tests showed no difference in the capability of irradiated rat males to impregnate female rats as compared with nonirradiated controls. The progeny of these matings showed no abnormalities. Histological studies indicated no late effects (tumors, shortening of life-span, etc.). It appears that continuous exposure to EMP radiation (five pulses per second and a peak field intensity of 447 kV/m) represented no biological hazards to rodents.

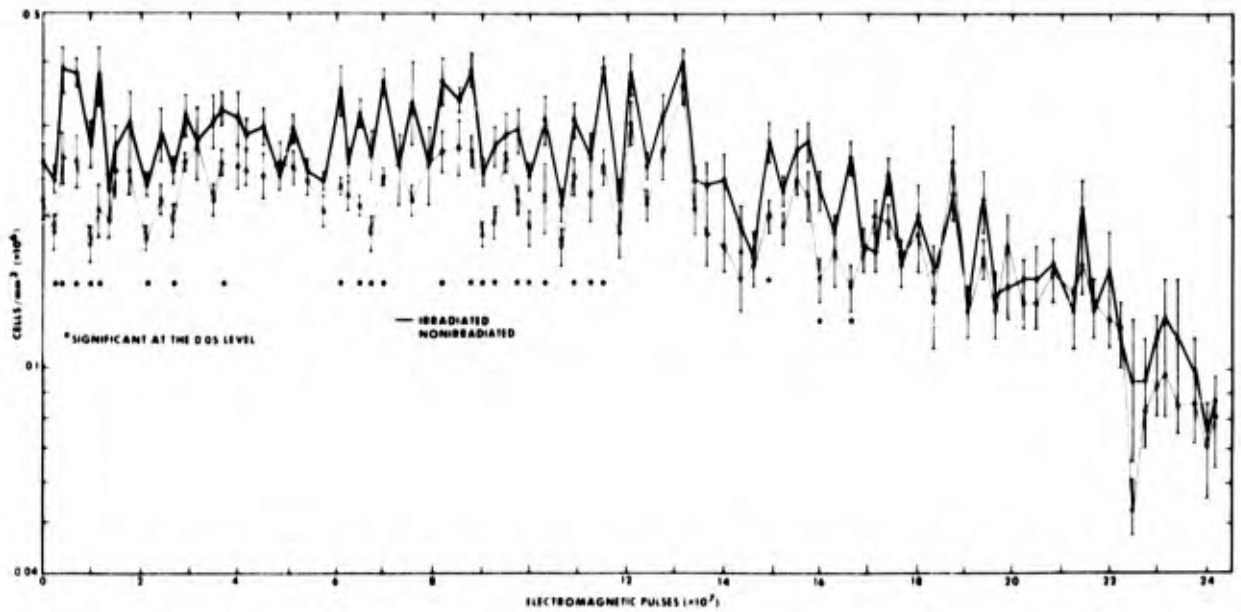


**Figure 1. Reticulocytes in peripheral blood from rats during 90 weeks of EMP exposure.**  
Each point shows a mean value with the associated standard error.

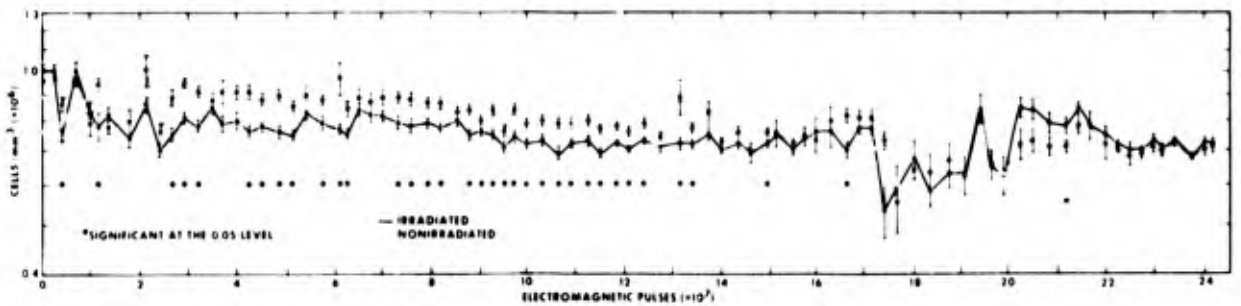


**Figure 2. Platelets in peripheral blood from rats during 90 weeks of EMP exposure.**  
Each point shows a mean value with the associated standard error.

Table I. Summary after  $2.4 \times 10^8$  Pulses during 90 Weeks of Chronic Electromagnetic Pulse Irradiation

Experiment	Animal species	Biological effect	
		FY73*	FY74*
Blood chemistry	rats	none	--
Blood count	rats	variable	none
Bone marrow	rats	none	none
Chromosomal aberration	rats	none	none
$^{59}\text{Fe}$ uptake	rats	none	--
Embryology	rats	none	none
Fertility	rats	--	none
Histology	rats	none	none
Leukemia	mice	none	--
Mammary tumors	rats	none	none
Other late effects	rats	--	none

\*  $10^8$  pulses during 34 weeks of exposure

\*  $2.4 \times 10^8$  pulses during 90 weeks of exposure



## EXPERIMENTAL COMMUNICATING HYDROCEPHALUS IN THE PRIMATE: ULTRASTRUCTURAL AND PATHOPHYSIOLOGICAL STUDIES

**Principal Investigator:** W. J. Flor

**Collaborators:** J. S. Stevenson, AFRR; A. E. James, Jr., Johns Hopkins Medical Institutions; J. Fenstermacher, National Institutes of Health; and B. L. Rish, Neurosurgical Associates, Norfolk, Virginia

**Technical Assistance:** J. L. Parker, W. G. Ewald, E. L. Barron, J. K. Warrenfeltz, M. E. Flynn, N. L. Fleming, G. L. Dunson, M. K. Mellor and J. Jozsa

The objective of this research was to produce a model of communicating hydrocephalus in the primate to study the development of the pathology and pathophysiology of this disease and to investigate countermeasures to the disease processes.

We have continued to implant monkeys with Silastic for the production of communicating hydrocephalus,<sup>2</sup> and have continued to monitor these (and previously implanted) animals by regular cisternography with 1.0 mCi  $^{99\text{m}}\text{Tc}$ -Sn-albumin.<sup>1</sup> The earliest signs of ventricular entry of radiopharmaceutical (characteristic of communicating hydrocephalus) continue to be observed about 30 to 40 days after implantation in some

animals. In others, 10 to 12 months have elapsed before initial ventricular entry has been observed. In several animals that have been observed over a period of 18 to 24 months, a clinical pattern of disease progression quite similar to that in the human has been observed; that is, (1) delay between the "injury" and the development of positive findings on cisternography (initial ventricular entry on the order of 1 to 3 months postimplantation), (2) a period of ventricular entry with stasis (retention of radiopharmaceutical within the ventricles on delayed studies) accompanied by ventricular enlargement and neurological signs including motor deficit (3 to 8 months), and (3) a period of ventricular entry with clearing (resolution of the cisternographic pattern on delayed studies) accompanied clinically by an accommodation or compensation, with some improvement in motor function and apparent slowing or cessation of the process of ventricular enlargement.

There is, of course, a range of responses in the implanted animals. Some have not yet demonstrated clear-cut ventricular entry after 18 months of observation. Some have followed a more acute course, deteriorating rapidly over a period of 2 to 3 months after the initial observation of ventricular entry and presenting extremely enlarged ventricles upon gross brain cutting.

We tried an alternative approach to our standard implantation several times, using an open posterior fossa neurosurgical approach, with some success. Also, several transcortical homograft vein shunts were attempted prophylactically in animals implanted 1 month previously with Silastic.

Pilot studies into the use of ultrastructural markers to label possible alternative pathways of CSF reabsorption have begun. A control animal has been successfully cisternogrammed with the  $^{99m}\text{Tc}$ -Sn-albumin-horseradish (HRP) mixture, and reaction product representing the presence of HRP was found in numerous places in this normal brain, which are being cataloged for comparison with future experimental animals. Two experimental hydrocephalics have also been injected by this technique, but technical difficulties were experienced.

We have selected animals which demonstrate unequivocal ventricular entry of radiopharmaceutical with stasis by 90 days postimplantation for initial studies of CSF-brain permeability changes and CSF production. Three such animals have been studied to date by ventriculocisternal perfusion. Preliminary results indicate that CSF production in these animals was within the normal range, implying no long-term compensatory shutdown of choroid plexus secretion. Brain extracellular space to all markers used appeared to be within normal limits at depths of greater than 0.8 mm. In the first two 0.4-mm slices, space often appeared qualitatively to be increased over usual figures, but the first slice must be disregarded for statistical purposes because of irregular surface geometry, and the second slice data alone showed no consistent pattern. Studies of brain periventricular extracellular space are being designed, but must address new problems of data collection in this limited tissue thickness.



Histological and ultrastructural studies are continuing. Ventricular enlargement, patency of the foramina of Luschka and Magendie, and localization of the implanted Silastic to the anterior basal cisterns have been demonstrated by gross pathological examination. Because of the chronic nature of this model, the long-term hydrocephalic animals have demonstrated secondary neuropathological deficits in motor and sensory cortex, in corticospinal tracts and in other locations which could clearly be the type of underlying cellular changes responsible for the clinically observed motor deficits in humans. These changes are being compared to human autopsy for correlation. Plans are being formulated for histological examination of specimens from earlier times during the development of the disease process, in order to determine the initial locations and types of central nervous system injury.

In summary, we have produced a reliable primate model of chronic communicating hydrocephalus and have demonstrated its similarity to the human disease process in a number of physiologically significant aspects. Studies of the developmental stages of the pathology and pathophysiology are in progress to determine alterations in CSF production, flow and reabsorption, early structural and anatomical changes in the brain parenchyma, and other parameters. Studies of these early changes will direct future efforts to evaluate countermeasures to this disease process.

#### REFERENCES

1. Flor, W. J., Stevenson, J. S., Ghaed, N. and James, A. E., Jr. Cisternograms in the primate Macaca mulatta. *Neurology* 24:266-270, 1974.
2. James, A. E., Jr., Flor, W. J., Bush, M., Merz, T. and Rish, B. L. An experimental model for chronic communicating hydrocephalus. *J. Neurosurg.* 41: 32-37, 1974.



#### A TECHNIQUE FOR THYMECTOMY IN THE ADULT RAT

Principal Investigators: C. L. Cloud and G. D. Ledney

Technical Assistance: N. A. Eaton

Thymectomy of the adult laboratory animal is a useful adjunct to the study of certain immunological processes, such as cell-mediated immunity and graft rejection. Techniques for thymectomizing adult mice, hamsters and rats have appeared in the

literature. However, a detailed description of thymectomy in the adult rat is not available. Thymectomy of the adult rat is difficult to perform due to the close association of the thymus with surrounding connective tissue.

Commonly used anesthetic agents such as Nembutal or ether have been associated with high mortality rates because of difficulties in dosage regulation of Nembutal and impaired respiration due to hypersecretion of mucus following ether anesthesia. Therefore, we sought a fast acting substitute which would assure a quick recovery and obviate undesirable side effects. Innovar-Vet (Pitman-Moore, Inc., Washington Crossing, New Jersey), an analgesic marketed for dogs and recently used in several other species, causes negligible mortality and does not have the side effects of ether or Nembutal. This report details a technique for thymectomy of adult rats using Innovar-Vet.<sup>1</sup>

Lewis rats (Lew/f Mai), free of chronic murine respiratory virus (CMRV) and weighing 125-150 g, were given subcutaneous injections of 0.04 mg/kg of atropine sulfate (Eli Lilly and Company, Indianapolis, Indiana) 10 min prior to an intramuscular injection of 0.1 ml/kg of Innovar-Vet. This compound is marketed as an analgesic; however, it produces a state of anesthesia which develops within 10 min after injection and lasts about 2 hours.

The thoracic and submandibular areas were shaved with animal clippers. A depilatory was not required. The animal was placed in a supine position upon a dissecting board with its head toward the operator. The rat was restrained as shown in Figure 3. The neck and chest were moistened with 70 percent ethanol. A longitudinal midline incision was made to the left of the midline through the skin and superficial fascia from the level of the angle of the mandible to the fourth rib.



Figure 3. Aspiration of the thymus

Blunt forceps (12 cm) were used to free the skin from the underlying muscle for ease in closure. The pectoralis muscle was transected to the left of the midline starting just below the clavicle and proceeding no further than the second rib. An incision of this size and at this level facilitated closure and avoided damage to the major blood vessels. The second and third ribs were visualized, clipped and reflected exposing the thymus, which appeared as a glistening organ anterior to the heart. A suction tube was immediately inserted into the chest cavity to aspirate the thymus. Aspiration was assisted by using a toothless iris forceps to divide all areolar tissue connections between the intact gland and the surrounding tissue (Figure 3). Approximately 45 sec were available for aspiration of the thymus. If the thoracic cavity was open for longer than 60 sec, fatal pneumothorax inevitably occurred. If the suction procedure required longer than 45 sec at any particular time, the cavity was closed manually or with 12-cm toothed forceps until the animal resumed normal breathing. A rubber bulb fitted with a two-way valve and a 4-inch piece of Tygon tubing served as a respirator for use in those animals suffering respiratory distress.

Care was taken to avoid injury to the right and left superior vena cava. Some bleeding was expected and was not overly detrimental to recovery. After visual inspection ascertained that no thymic remnants were present, air was expressed from the thoracic cavity by massage directed from the diaphragm toward the head. The thoracic walls were apposed with two 12-cm dressing forceps by the assistant while the operator closed the chest with 4-0 surgical gut medium chromic sutures and a 3/8 circle taper needle. The skin was closed with 9-mm stainless steel wound clips. The animals were then allowed to recover in a cage under a heat lamp at 35°C for 1-2 hours. Within 30 min after closure, the animals regained their normal motor control; the anesthetic effect of the Innovar-Vet subsided completely after 2 hours. Wound clips were removed 14 days after surgery.

The vacuum necessary for aspiration of the thymus was provided by a suction flask attached to a pump or other source capable of providing a pressure equivalent to 16 inches of mercury. Aspiration of the thymus was done with a glass tube which allowed visualization of the organ as it was withdrawn. The glass tube was 16 cm long with an o.d. of 6 mm and an i.d. of 4 mm. A 150° elbow bend was made at the midpoint to facilitate handling, and the ends were fire-polished to avoid trauma. When this procedure was followed precisely as described above, a survival rate of 80 percent was obtained.

#### REFERENCE

1. Cloud, C. L. and Ledney, G. D. A technique for thymectomy in the adult rat. Bethesda, Maryland, Armed Forces Radiobiology Research Institute Technical Note TN73-20, 1973.

♦♦♦♦♦♦♦♦♦♦

# SUPPRESSION OF SECONDARY DISEASE BY IN VITRO EXPOSURE OF MIXTURES OF LYMPHOID AND STEM CELLS TO PURIFIED ANTILYMPHOCYTE ANTIBODY

Principal Investigators: G. D. Ledney, E. D. Exum, R. M. Crawford,  
C. B. Galley and R. I. Walker

The objective of this research was to develop a technique for the suppression of graft versus host disease by in vitro exposure of mixtures of hematopoietic cells to antibodies prepared against lymphoid cells.

A murine model for the primate type of graft versus host disease (GVHD) (acute secondary disease) exists whereby agents or techniques found to obviate rodent GVHD can be employed in trials designed to prevent primate-type GVHD.<sup>1</sup> GVHD is usually a lethal consequence of bone marrow transplantation in humans who are engrafted because of hematopoietic dysfunctions.

Major problems in the therapy and management of animals or man undergoing treatment of GVHD are (1) drug toxicity with potential to elicit malignancies and (2) lack of specificity or selectivity for immune competent cells as compared to stem cells. Circumvention of these problems was somewhat attained by treatment of the prospective graft in vitro with antithymocyte globulin (ATG).

Presented in Table II are the survival data of mice from GVHD, the T-cell response to PHA stimulation and the spleen nodule potential of CBA mouse spleen cells

Table II. Correlation of Survival with PHA Responses and Spleen Nodule Formation in Irradiated Mice Grafted with Allogeneic Spleen Cells\*

Incubation agent	Concentration ( $\mu$ g) / $10^7$ spleen cells	Survival (percent)	Splenic nodules/ $10^6$ nucleated cells	PHA response <sup>+</sup> (percent)
ATG	1000	65	< 1	3
ATG	500	100	< 1	3
ATG	250	85	2	3
ATG	125	16	< 1	3
NRG	1000	100	6	28
NaCl	0.9%	0	10	100
900 rads				
x ray control	--	0	0	N. D.

\* Survival percentage and spleen nodule formation are based on data obtained from 6 to 10 mice per group. In all experiments B6CBF<sub>1</sub> mice were given 900 rads and either  $5 \times 10^6$  CBA spleen cells to "induce" GVHD or  $5 \times 10^5$  CBA spleen cells to test for colony forming units.

<sup>+</sup> PHA responses are expressed as a percentage of the response obtained when spleen cells incubated in NaCl were stimulated with 1  $\mu$ g PHA. Incorporation of <sup>3</sup>H-TdR in the control stimulated culture resulted in 35,000 CPM. Background uptake of isotope amounted to 1000 CPM in all non-PHA stimulated culture conditions.

after incubation in various agents including ATG. Increases in survival from GVHD correlated well with the reduced T-cell responses to PHA in all but one group of ATG treated cells. All mice that died did so with the symptoms of gram-negative bacterial sepsis. It is of interest to note that normal rabbit globulin (NRG), at the concentration used, reduced T-cell responses as measured by  $^3\text{H}$ -TdR uptake and survival from GVHD. The reduced spleen nodule formation does not correlate in a positive manner with the survival presented in Table II; the former observation is positively correlated when death results from hematopoietic insufficiency. The reason for this discrepancy is unknown and is undergoing further investigation.

## REFERENCE

1. Ledney, G. D. Secondary disease in mice after in vitro exposure of hematopoietic cells to concanavalin A. *Transplantation* 14:671-682, 1972.



## INDUCTION OF SPECIFIC IMMUNOLOGIC UNRESPONSIVENESS IN RATS USING ANTIGENIC STIMULATION AND CYTOXAN

**Principal Investigators:** *M. P. Fink, C. L. Cloud and G. D. Ledney*

Drug-induced tolerance to antigens capable of provoking a humoral immune response is a well-established phenomenon. The principles of drug-induced tolerance were applied in experiments where the objective was to abrogate the graft versus host disease (GVHD) by inducing specific immunotolerance toward allogeneic histocompatibility antigens. This was done by first establishing a model of GVHD in rats whereby 100 percent mortality could be obtained within a discrete period of time. These data are presented in Figure 4. Thus all LBN rats given 1000 rads  $^{60}\text{Co}$  gamma radiation and  $5 \times 10^7$  spleen and marrow cells derived from Lewis (L) rats died with a mean survival time (MST) of about 18 days. In subsequent experiments, L rats to be used as donors were sensitized with an I.V. injection of  $2 \times 10^8$  viable LBN spleen cells. Sensitization was done on days -5, -2, -1, 0, +1 and +5 in relationship to the injection of rats with cyclophosphamide (CY) which was given in a dose of 100 mg/kg body weight on day 0. Bone marrow and spleen cells for transplantation were obtained from these animals 7 days after CY treatment. The data presented in Table III support the idea that the severity of the GVHD was diminished by such treatment and that the magnitude of the suppressed immune competence was dependent on the interval between sensitization and the treatment with CY. Maximum suppression, as measured by a twofold

increase in MST of animals dying within the observation period as compared to controls (42 days versus 18 days) and a survival percentage of 50, was obtained when donor L rats received CY on day 0 and LBN spleen cells on day +1. Surviving animals did not have the symptomatology of GVHD. The observed immunosuppression was shown to be antigen specific (Table IV) and to result from the synergistic action of CY and cells bearing the alloantigens of recipient animals.<sup>1</sup>

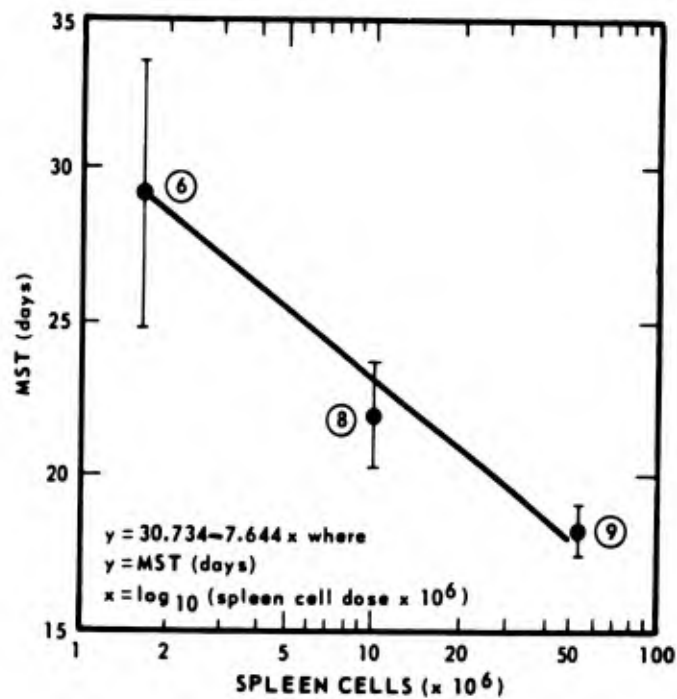


Figure 4. Survival of LBN rats given 1000 rads and  $5 \times 10^7$  L marrow and various quantities of L spleen cells. The ordinate represents the MST in days while the abscissa represents the log of the number of transplanted spleen cells. Each point represents the geometric mean ( $\pm 1$  SE) of the number of animals indicated within the circle adjacent to each point.

**Table III. Survival of LBN Rats Given 1000 Rads and  $5 \times 10^7$  Spleen and  $5 \times 10^7$  Marrow Cells Obtained from L Donors Previously Injected with CY and Sensitized with  $2 \times 10^8$  LBN Spleen Cells**

Group number	Donor treatment*	Day of antigen treatment*	Number of animals in group	MST data			Mortality data	
				MST $\pm$ SE (days)	P value cf. group 1	P value cf. group 2	Percent	P value cf. groups 1 and 2
1	None	--	9	18.22 $\pm$ 0.80	--	--	100	NS
2	CY	--	8	24.50 $\pm$ 1.28	< .001	--	100	--
3	LBN + CY	-5	9	27.00 $\pm$ 2.53	< .01	NS	100	NS
4	LBN + CY	-2	7	38.00 $\pm$ 3.61	< .001	< .001	100	NS
5	LBN + CY	-1	10	38.57 $\pm$ 4.77	< .001	< .01	70	< .05
6	CY + LBN	0	8	36.88 $\pm$ 3.83	< .001	< .01	100	NS
7	CY + LBN	+1	12	42.83 $\pm$ 3.33	< .001	< .001	50	< .025
8	CY + LBN	+5	17	26.59 $\pm$ 1.69	< .005	NS	100	NS

\* All donor rats were sacrificed on day +7 after CY treatment

\* All animals that received CY were injected with the drug on day 0

**Table IV. Survival of LBN Rats Given 1000 Rads and  $5 \times 10^7$  Spleen and  $5 \times 10^7$  Marrow Cells Obtained from L Donors Injected Either with CY and  $2 \times 10^8$  LBN Spleen Cells or Only with  $2 \times 10^8$  LBN Spleen Cells**

Group number	Donor treatment*	Day of antigen treatment*	Number of animals in group	MST data			Mortality data	
				MST $\pm$ SE (days)	P value cf. group 1	P value cf. group 2	Percent	P value cf. groups 1 and 2
9	CY + LBN	-1	11	23.36 $\pm$ 1.36	< .01	NS	100	NS
10	LBN	-1	8	22.63 $\pm$ 2.04	NS	NS	100	NS

\* All donor rats were sacrificed on day +7 after CY treatment

\* All animals that received CY were injected with the drug on day 0

## REFERENCE

1. Fink, M. P. and Cloud, C. L. Graft versus host disease in rats after donor treatment with cyclophosphamide and spleen cells of host origin. Bethesda, Maryland, Armed Forces Radiobiology Research Institute Scientific Report SR74-4, 1974.



## ENDOTOXIN EFFECTS ON MOUSE LIVER ADENYL CYCLASE

Principal Investigators: *M. A. Donlon and R. I. Walker*

The objective of this research was to abrogate the graft versus host disease (GVHD) by inducing specific immunotolerance toward allogeneic histocompatibility antigens and to investigate the role of adenylyl cyclase activity in GVHD.

Endotoxin, a lipopolysaccharide (LPS) extracted from gram-negative bacteria, has an affinity for the phospholipid portion of cell membranes. In the liver, the interaction of endotoxin with cell membrane phospholipids could interfere with the synthesis of adenosine 3',5'-monophosphate (cyclic-AMP), a compound essential for glycogenolysis. Interference with the production of this compound could contribute to death from endotoxin-induced shock. To determine if endotoxin altered the amount of liver cell adenylyl cyclase, the amount of that substance was ascertained after conversion from  $^{14}\text{C}$  adenosine labeled ATP to  $^{14}\text{C}$  labeled cyclic-AMP by adenylyl cyclase. Additionally, the modifying action of LPS on epinephrine activation of adenylyl cyclase was measured.

The cyclic-AMP formation in the presence of epinephrine and endotoxin in whole liver cells and purified mouse liver plasma membranes is presented in Figure 5. Incubation of the cells with either LPS or epinephrine stimulated twofold and threefold increases respectively in cyclic-AMP formation. Endotoxin inhibited the epinephrine stimulation of adenylyl cyclase.

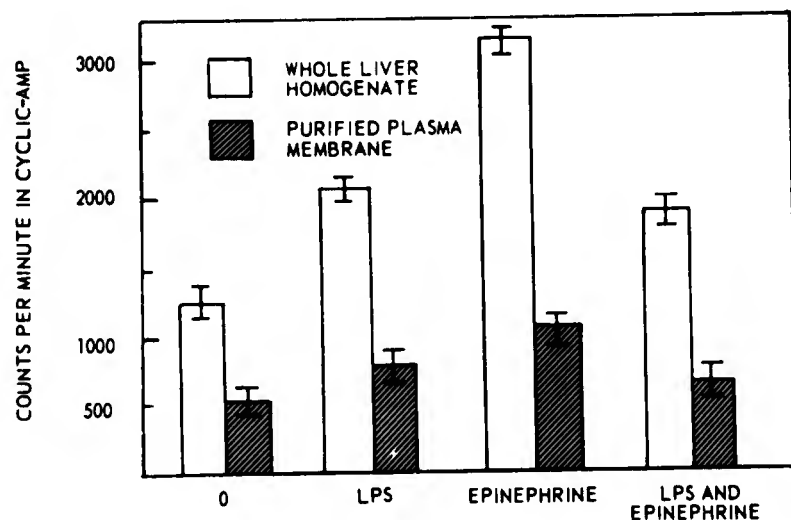


Figure 5. Cyclic-AMP formation in the presence of epinephrine and endotoxin in whole liver homogenate and purified mouse liver plasma membrane



With purified plasma membranes, the cyclic-AMP levels were reduced but similarities in responses relative to each other, as compared to that with whole cells, were seen. The epinephrine response of purified membranes was reduced threefold as compared to that of the whole cell response. This supports the contention that the epinephrine receptor is partially inactivated during the purification procedure.

Mice undergoing GVHD subsequent to irradiation and grafting with allogeneic spleen cells are sensitive to endotoxin. Preliminary studies were conducted to determine if this sensitivity involved abnormal endotoxin-membrane reactions. Two livers taken from mice on the 6th day of GVHD (death occurs by day 7) were tested and their responses obtained and compared to those found for livers taken from normal mice. Liver cell membranes from animals undergoing GVHD responded to endotoxin in a manner similar to that of membranes from normal animals.

Support for the argument that endotoxin interacts with the phospholipid segment (transducer) of the membrane-enzyme complex comes from our study of endotoxin activation of adenylyl cyclase by sodium fluoride. Preincubation of purified liver membranes in the presence of NaF prior to enzyme assay resulted in an enzyme activation curve (Figure 6) similar to that reported by others. Endotoxin interfered with the NaF activation of purified mouse liver plasma membranes. After 45 minutes of incubation with endotoxin, NaF activation was only 60 percent of that seen in preparations to which endotoxin was not added. Since endotoxin interfered with the NaF activation of purified mouse liver plasma membranes, it is probable that LPS acts at the transducer level. The epinephrine stimulation of adenylyl cyclase activity, however, was inhibited by endotoxin. In this way liver glycogenolysis may be impaired by endotoxin poisoning.

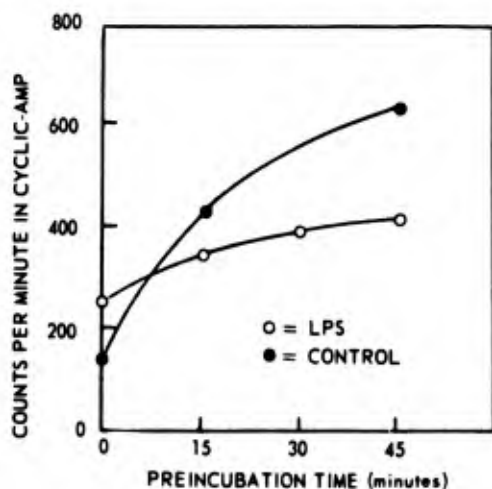


Figure 6. Adenylyl cyclase activity in purified liver cell plasma membranes incubated with or without LPS in the presence of NaF

◆◆◆◆◆◆◆◆◆◆

## HEMATOPOIETIC STEM CELL RENEWAL IN THE POSTIRRADIATED ANIMAL

Principal Investigator: K. F. McCarthy

The objective of this research was to stimulate hematopoietic stem cell renewal in the postirradiated animal.

The cellular parameters characterizing peripheral blood hematopoietic stem cells (CFU) are distinctly different from those characterizing marrow and splenic CFU and it has been suggested that peripheral blood CFU are representative of some sort of distinct CFU subpopulation. The function of this particular cellular subpopulation is not entirely understood. Outside of the fact that peripheral blood CFU play an important role in the regeneration of bone marrow following severe local irradiation damage, little is known of their physiological role, origin or ultimate fate. It has been suggested that these cells might emigrate from the marrow, enter the circulation and seed the spleen, thymus, lymph nodes and other hematopoietic organs incapable of supporting their own endogenous CFU populations. However, this view has been criticized on the grounds that peripheral blood CFU possess a low self-renewal capacity, a cellular parameter inconsistent with a multipotent role for circulating CFU, and more consistent with the presence of unipotent stem cells.

An approach to this particular problem, whether circulating CFU are multipotent or unipotent stem cells, is suggested by the recent finding that the hematopoietic organs of anemic  $S1/S1^d$  mice are deficient in erythrocytic committed CFU. Apparently, the  $S1/S1^d$  defect disrupts the flow of multipotent hematopoietic stem cells to the erythroid cellular line of differentiation. Therefore, if circulating CFU originate from unipotent or committed stem cell compartments, a deficiency of erythrocytic committed CFU in the blood of  $S1/S1^d$  mice would be expected. Alternatively, if multipotent CFU are released directly into the circulation, then  $S1/S1^d$  blood cells should, upon transplantation into irradiated recipient mice, generate the expected number of erythrocytic colonies in the spleens of these recipient mice.

The ratios of erythrocytic colonies to granulocytic colonies (E/G ratio) generated in the spleen of irradiated recipient mice receiving blood cells from both  $S1/S1^d$  mice and their normal congenic littermates (+/+) are presented in Table V. They are similar to those previously reported for their respective marrow CFU and contrast with those reported for their splenic CFU. Specifically, CFU from the marrow, blood and spleens of normal mice generate E/G ratios of 3.4, 3.7 and 35.1, while CFU from the marrow, blood and spleen of  $S1/S1^d$  mice generate E/G ratios of 2.4, 1.7 and 8.6. Thus, the  $S1/S1^d$  defect does not alter the suggested marrow origin of blood CFU; only their numbers.

Table V. Spleen Colony Types Formed in Normal Recipients of + + and S1/S1<sup>d</sup> Blood Cells Before and After B. pertussis Vaccine Treatment

Interval	Number of recipients	Donor* genotype	Dose (ml)	Mean microscopic colony counts from center sections only*†					
				E	G	M	Meg	Total	E/G ratio
Control	6	+ +	0.1	4.5 ± .8	1.2 ± .6	1.8 ± .4	1.2 ± .2	7.7 ± .8	3.74
Control	5	S1/S1 <sup>d</sup>	0.1	2.0 ± .3	1.2 ± .4	1.6 ± .4	1.4 ± .2	4.0 ± .8	1.66
Significance of difference				P = .05	N.S.	P = .10	N.S.	P < .005	
76 hours	6	+ +	0.05	5.0 ± .5	2.7 ± .7	3.3 ± .6	1.2 ± .2	11.2 ± .8	1.85
76 hours	5	S1/S1 <sup>d</sup>	0.05	1.0 ± .7	2.2 ± .6	1.4 ± .2	1.8 ± .5	4.4 ± 1.1	.45
Significance of difference				P = .005	N.S.	P = .005	P = .4	P = .001	

Colonies were counted microscopically in center sections. However, colonies counted in subserial sections gave approximately the same E/G ratios.

\* Only S1/S1<sup>d</sup> mice and their normal congenenic littermates were used in these experiments. Two donor mice were used for each donor blood cell preparation.

† E = erythrocytic, G = granulocytic, M = mixed type, Meg = megakaryocytic, E/G ratio = total number E colonies / total number G colonies in a given group of recipient spleens

\* Mean ± S.E.M.

As seen in Table VI, there are approximately twice as many peripheral blood CFU in normal mice as there are in S1/S1<sup>d</sup> mice. The "missing" CFU are apparently those CFU which generate only erythrocytic and mixed colonies. As was expected, the concentrations of CFU in the blood of S1/S1<sup>d</sup> mice which generate either granulocytic or megakaryocytic colonies are normal. Since it has previously been reported that in the spleen and marrow of S1/S1<sup>d</sup> mice there is no deficiency of CFU giving rise to mixed colonies, the significance of the reduced number of these cells in the peripheral blood is, at present, not clear.

The nature of the emigration of erythrocytic committed CFU from the marrow was investigated by challenging both S1/S1<sup>d</sup> mice and their normal congenenic littermates with a single injection of 20 x 10<sup>9</sup> heat killed Bordetella pertussis organisms. This treatment effects a sharp increase in the number of peripheral blood CFU. There was a 6.5-fold increase in +/+ mice, while in S1/S1<sup>d</sup> mice there was only a 2.4-fold increase (Table VI). The increase in S1/S1<sup>d</sup> mice was due entirely to an increase in the number of granulocytic and megakaryocytic committed CFU. There was no observed increase in the number of erythrocytic committed CFU, nor CFU giving rise to mixed colonies (Table V). Apparently, the former are released into the peripheral blood independently of the latter.

It is not immediately obvious why approximately 33 percent of the total peripheral blood CFU population should consist of erythrocytic committed CFU. The reduced concentration of CFU capable of giving rise to mixed colonies in the blood and not in the spleen or marrow of S1/S1<sup>d</sup> mice might indicate that stem cell migration is an important factor in the reversibility of commitment of individual stem cells. Perhaps the bulk of stem cells in situ are lodged within a specific microenvironment in such a manner that commitment may be possible to only a specific cell line. Reversibility of commitment would imply stem cells migrating to new and different microenvironments.

Thus, an erythrocytic committed CFU lodging in a granulocytic microenvironment might be expected to give rise to both erythrocytic and granulocytic progeny and therefore generate a mixed colony. However, this is speculative and awaits further experimentation.

Table VI. Blood Cellularity and CFU Number of +/+ and S1/S1<sup>d</sup> Mice Following a Single Injection of B. pertussis Vaccine

Interval	Blood cellularity (x 10 <sup>-6</sup> /ml)	CFU/10 <sup>5</sup> cells	CFU ml of blood
+/+ mice			
Control	5.9 ± 1.9*	9.0 ± 1.2	50 ± 12
28 hours	2.2 ± 0.6	12.8 ± 2.2	28 ± 4
76 hours	10.4 ± 1.4	31.3 ± 4.4‡	325 ± 51§
158 hours	7.0†	18.2	131
S1/S1 <sup>d</sup> mice			
Control	7.4 ± 1.8	3.6 ± 1.1	26 ± 10
28 hours	--	--	--
76 hours	6.2 ± 1.1	10.9 ± 1.9**	62 ± 5††
158 hours	--	--	--

\* Mean ± S.E.M. of two to four determinations performed on two animals

† One determination on two animals  
Significantly different from control at

‡ P < .005

§ P < .010

\*\* P < .025

†† P < .050



## FEEDBACK MECHANISMS BETWEEN INFLAMMATORY AREAS AND THE GRANULOPOIETIC MICROENVIRONMENT

Principal Investigators: *D. E. Wyant and S. J. Baum*

Technical Assistance: *R. T. Brandenburg*

The objective of this research was to determine the possible feedback mechanisms between inflammatory areas and the granulopoietic microenvironment.

The specific process by which leukocytes are stimulated to replace themselves in the progenitor compartment is not clear. However, it has been demonstrated that a small fraction of the leukocytes in an inflammatory exudate have stem cell capabilities, and it is possible that these cells after being primed in the exudate return to hematopoietic centers and initiate granulopoiesis. Research was directed at exploring this possibility.

No existing experimental model of acute inflammation was sufficient for this research. Hence, a new in vivo model which can measure dynamic exudate cell migration during acute inflammation was developed. This model simulates more closely cellular inflammation. It involves a subcutaneously implanted plastic cup which can easily be used in both normal and irradiated rats and mice to assess exudate cell migration quantitatively. The implantation of the cup was accomplished as follows. A 3-cm longitudinal, paravertebral, full-thickness skin incision was made. A subcutaneous pouch was produced by a blunt dissection with a hemostat, and a 15-mm round, 0.2-ml capacity acrylic cup filled with bacteria free Hanks' balanced salt solution was inserted into the pouch at a 2-cm distance from the incision. The incision was then closed with a stainless steel wound clip. The cup was removed at various time intervals following implantation to study qualitatively and quantitatively the exudate cells which collect in the fluid.

An early polymorphonuclear cell predominance was noted and the exudate cellular profile reveals a later mononuclear cell predominance (Figure 7). The profile also reveals that the number of mononuclear cells vacillates considerably from one sampling time to another, an observation which has not previously been reported probably because most other models only sample a small portion of inflamed tissue whereas this one samples the entire skin section above the subcutaneous cup.

The mononuclear cells in irradiated animals were significantly reduced ( $p < 0.001$ ) from nonirradiated control values for all sampling times from 20 to 75 hours (Figure 8).

Granulocyte numbers were below control values at all sampling times for rats that received either 250 or 500 rads. However, granulocyte values for the 750-rad group exceeded control values on the 1st and 3rd day (Table VII). Lymphocytes were

drastically reduced in many samples and totally absent from others for all doses of radiation (Table VII).

This model is presently being used to test the migration behavior and hematopoietic potential of the leukocytes found in exudate.

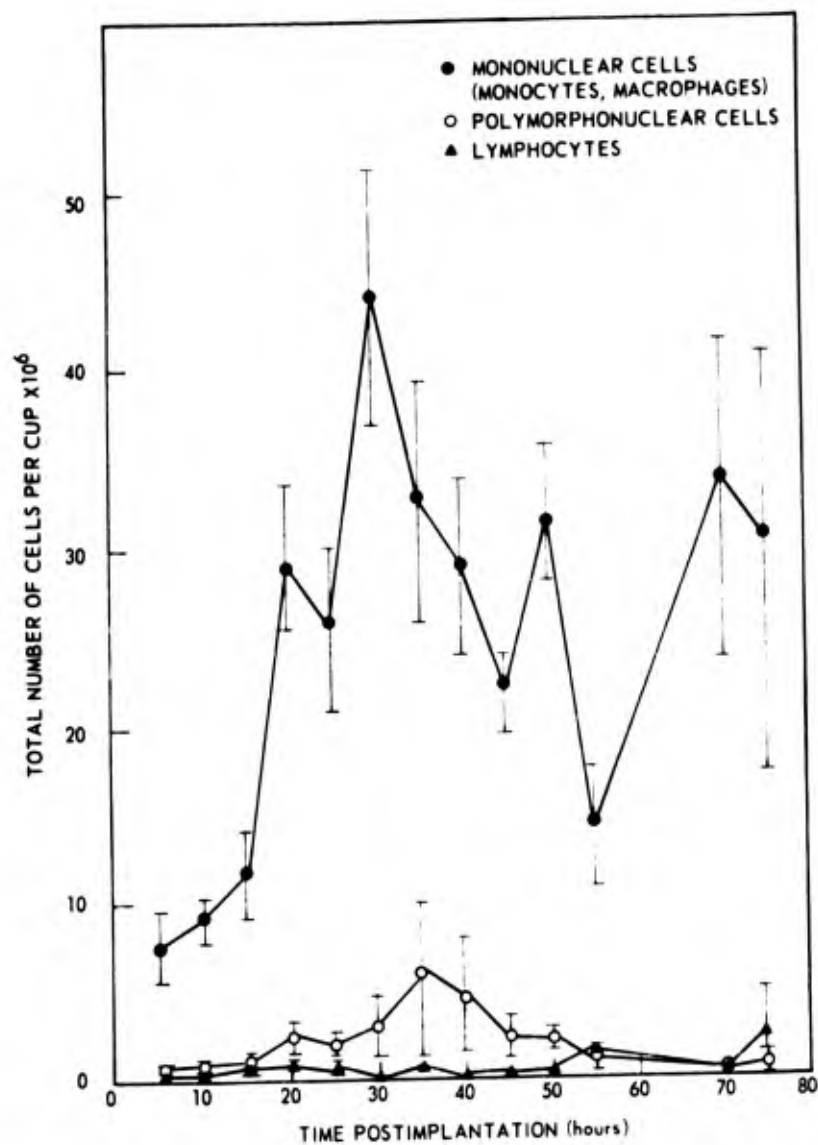


Figure 7. Inflammatory cellular response in rats following cup implantation

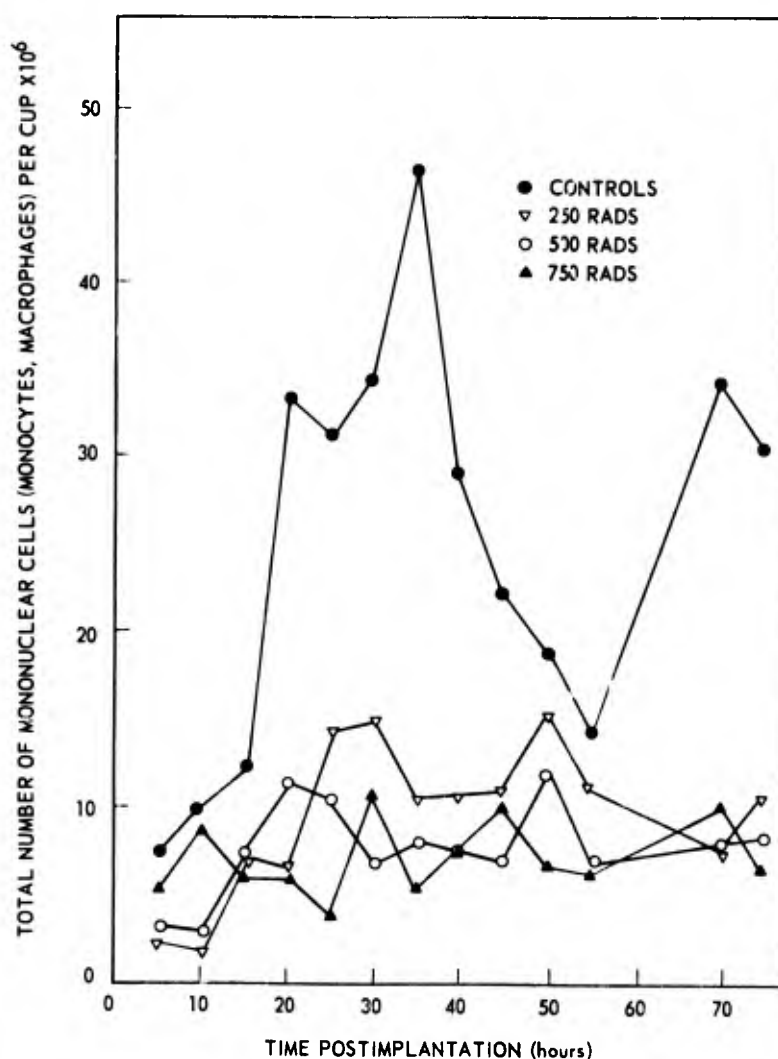


Figure 8. Inflammatory mononuclear cell response following cup implantation in rats exposed to 250, 500 or 750 rads of gamma radiation

Table VII. Granulocyte and Lymphocyte Response (mean number per cup) in Rats Following Cup Implantation

		Rads	Time postimplantation (hours)											
			5	10	15	20	25	30	35	40	45	50	55	70
Granulocytes	0	47.74	46.97	101.86	467.65	292.16	402.35	1043.38	390.68	179.03	195.14	76.54	37.69	52.16
	250	10.36	7.59	11.65	24.60	51.48	173.40	18.26	27.38	60.72	63.25	41.14	18.26	44.66
	500	28.93	19.47	69.76	10.92	55.33	20.13	177.87	165.70	123.51	193.27	73.70	22.76	9.68
	750	118.47	66.44	202.75	274.23	570.02	264.55	218.35	333.76	535.04	640.97	309.88	225.17	86.68
Lymphocytes	0	28.63	19.44	50.20	20.46	23.53	3.22	20.11	0.0	4.57	13.76	25.96	46.30	64.49
	250	0.18	0.88	0.0	3.08	16.50	1.45	0.88	0.0	0.0	0.0	0.0	11.22	0.0
	500	3.63	0.0	.44	1.54	10.89	0.0	2.86	2.35	3.85	1.10	0.33	37.95	28.05
	750	5.61	2.53	2.61	1.65	12.54	3.08	2.75	0.0	0.0	4.84	0.0	37.93	0.88

•••••

## DEVELOPMENT OF CLINICAL APPROACHES FOR THE TREATMENT OF RADIATION SICKNESS AND GRAFT VERSUS HOST DISEASE THROUGH MANAGEMENT OF THE INTESTINAL FLORA

Principal Investigators: *R. I. Walker and G. D. Ledney*

Collaborators: *P. E. Ewald, M. E. Ekstrom and C. B. Galley*

The objective of this research was to increase survival following lethal irradiation by the proper selection of radiation dose and dose rate designed to eradicate immune capability against allogeneic donor blood cells used in conjunction with antibiotic therapy.

Endotoxemia of intestinal origin may alter physiologic and immunologic functions in individuals subjected to high doses of either ionizing radiation or radiation followed by transplants of foreign immune competent cells capable of producing graft versus host disease (GVHD). The results of the following studies support the contention that aseptic endotoxemia may be due to failure to clear endotoxin from the circulation and detoxify it in the liver of immunosuppressed animals.

To determine if intestinal endotoxin may contribute to pathogenesis in immunosuppressed individuals, B6CBF<sub>1</sub> mice were exposed to 850 rads of x rays, and transplanted with allogeneic CBA spleen cells. Aseptic endotoxemia, detected with the limulus lysate assay, was found at 24 and 72 hours postirradiation in livers of mice irradiated only (Figure 9). Contrary to this, endotoxin was not found in mice on days 5, 7 and 8 after x irradiation. Mice died between 11 and 13 days after radiation exposure at which time bacteria and endotoxin were detected in the liver.

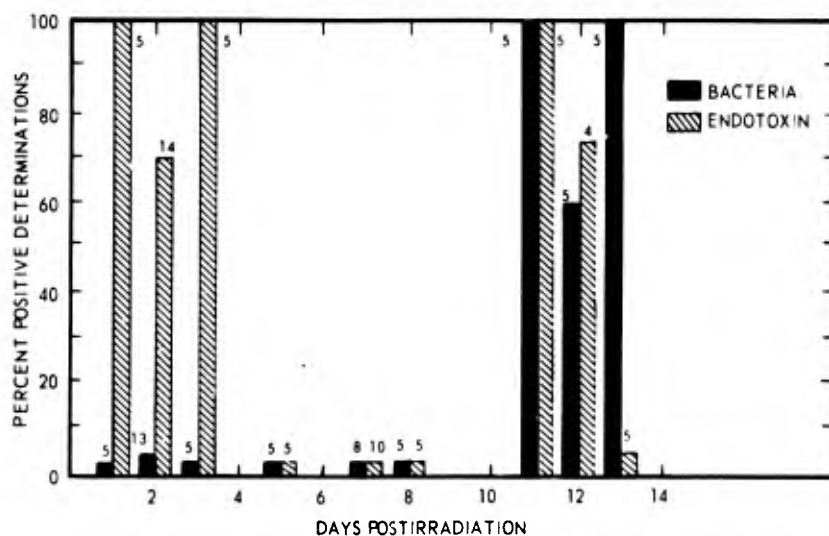


Figure 9. Endotoxin and bacteria detected in livers of mice receiving 850 rads x radiation. Numbers associated with individual bars denote number of samples tested.



In contrast endotoxin was demonstrable on days 1 and 5 in mice undergoing GVHD (Figure 10). Mice receiving allogeneic grafts after 850 rads survived only 7 days, while gram-negative organisms were detected frequently in liver fragments from 24 hours to day 7.

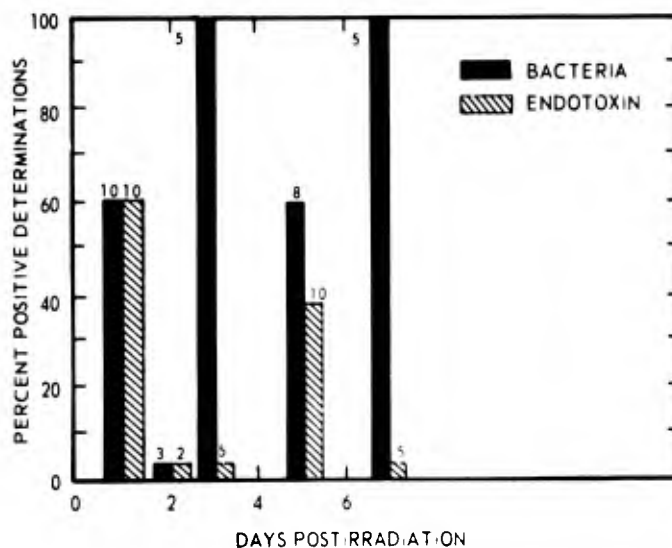


Figure 10. Endotoxin and bacteria detected in livers of mice grafted with  $5 \times 10^6$  allogeneic spleen cells immediately after receiving 850 rads x radiation. Numbers associated with individual bars denote the number of samples tested.

By day 4, hepatosplenic localization of I.V. injected  $^{51}\text{Cr}$  endotoxin was reduced 50 percent in animals undergoing GVHD and twofold to threefold increases in endotoxin levels were found in lung, kidney, heart and brain. Hepatosplenic endotoxin concentration was also depressed in mice receiving radiation alone, reaching a low between days 12-14. Endotoxin levels in other organs were not altered.

Immunosuppressed animals used in this work were more sensitive than normal animals to challenge with endotoxin. As shown above, reticuloendothelial organs from these animals do not sequester endotoxin as efficiently as normal animals and this process may contribute to increased sensitivity. Intestinal antibiotic decontamination prior to irradiation or GVHD exacerbates impairments of endotoxin uptake. Furthermore, although hepatic uptake of living bacteria injected I.V. remains normal in these immunosuppressed mice, intestinal decontamination reduces the intracellular bactericidal activity. Impaired elimination of bacterial cells makes possible accumulation of higher levels of endotoxin-producing gram-negative organisms in immunosuppressed animals.

•••••

## THE PHARMACOKINETICS OF SODIUM NITRITE AND ITS RELATIONSHIP TO METHEMOGLOBINEMIA IN SELECTED MAMMALS

Principal Investigator: N. R. Schneider

The objective of this research was to study the pharmacokinetics of nitrite for a more complete understanding of the toxic syndrome of nitrite toxicosis, as well as for the development of better diagnostic procedures in nitrite-nitrate toxicity, and improved therapy for cyanide poisoning.

Nitrite and nitrate have become increasingly significant environmental chemicals in recent years. The nitrite ion is of toxicological interest both as an environmental toxicant and as a drug. The role of the nitrite ion in the formation of methemoglobin is well known. However, little is known about the biological pathways of the nitrite ion or its oxidized form, nitrate. Although nitrite is thought of primarily as a toxicant, knowledge of the pharmacokinetics of intravenously injected nitrite will provide information to enable a more precise calculation of nitrite dosage in the regimen of therapy for cyanide poisoning, both in domestic animals and man. Predictable plasma kinetics of nitrite and nitrate also provide a valuable laboratory aid for the diagnosis, treatment and prevention of nitrite-nitrate toxicoses.

Previously initiated comparative studies in domestic animals<sup>2</sup> indicated that the canine was the best animal model for the determination of nitrite pharmacokinetics. Consequently, two dogs were administered a known sublethal dosage of sodium nitrite (20 mg  $\text{NaNO}_2$ /kg I.V.) in a series of experiments. Serial blood samples were collected at specific timed intervals after injection, and tissues were obtained at the time of euthanasia. Analytical methods for methemoglobin, total hemoglobin, nitrite, and nitrate were refined and perfected. Methemoglobin concentrations in whole blood were measured according to a modification of the method described by Hainline.<sup>1</sup> Total hemoglobin was determined by the cyanmethemoglobin method.\* Nitrite and nitrate concentrations in biological material were quantitated colorimetrically according to the method of Schneider and Yeary.<sup>3</sup> Plasma protein binding was ascertained in vitro using equilibrium dialysis chambers.

The data indicate that the nitrite ion follows first-order disappearance in the canine and is not present in biologically significant amounts ( $<1 \mu\text{g NO}_2^-/\text{ml}$  plasma) in the blood later than 2 hours after injection. Nitrite concentrations in the plasma ranged from 14.5 to 16.5  $\mu\text{g NO}_2^-/\text{ml}$  at 1 minute after injection. Peak methemoglobinemia development was slightly over 30 percent of total hemoglobin. Nitrate plasma levels maintained a slowly declining plateau. Nitrate was still present in the plasma 24 hours

---

\* HYCEL Cyanmethemoglobin Standard, HYCEL, Inc., Houston, Texas

after injection at concentrations ranging from 16 to 46  $\mu\text{g NO}_3^-/\text{ml}$ , which approximated one-third to one-half of the peak concentrations reached after nitrite injection. Tissue assays suggest that no apparent specific target organs are responsible for sequestration or retention of nitrate (Table VIII).

Table VIII. Tissue Distribution of Nitrate (micrograms  $\text{NO}_3^-$  per gram)

	Brain	Heart	Liver	Kidney cortex	Kidney medulla
Canine #1	N. D.	N. D.	12.0	23.2	34.9
Canine #2	37.1	12.9	14.0	15.3	15.0

N. D. = Not determined

In vitro studies of protein binding in canine plasma were carried out. Although the use of phosphate buffer was initially attempted in the dialysis procedure, Bis-Tris buffer provided the most reproducible results when used in conjunction with equilibrium dialysis chambers. The results of the study of nitrite binding to plasma protein in the canine are summarized in Table IX. Instead of exhibiting a degree of binding inversely proportional to concentration as do many drugs, nitrite was found to bind to plasma proteins directly proportional to concentration at levels of 5 to 25  $\mu\text{g NO}_2^-/\text{ml}$  (4.5 to 13.6 percent bound). However, as concentrations were increased to 50 to 100  $\mu\text{g NO}_2^-/\text{ml}$ , the extent of binding became inversely proportional to concentration (9.8 to 8.8 percent bound). This phenomenon may have resulted from the nitration (nitrosation) of plasma proteins by nitrite at low concentration, the nitrite ion thus having been irreversibly bound and not in equilibrium. At higher concentrations, these irreversible binding sites could have been saturated, which would then have permitted the nitrite to become associated with the reversible binding sites inversely proportional to concentration. Protein binding studies in vitro of nitrate in canine plasma were also conducted similar to those of nitrite, using equimolar concentrations of nitrate. In these studies, no appreciable extent of protein binding by nitrate was exhibited at any of the concentrations utilized.

Nitrite concentration at equilibrium in Bis-Tris buffer ( $\mu\text{g}/\text{ml}$ )	Percent bound ( $\bar{x} \pm \text{S. E. M.}$ )
5	4.5 $\pm$ 0.5
10	5.1 $\pm$ 0.9
25	13.6 $\pm$ 2.6
50	9.8 $\pm$ 0.2
100	8.8 $\pm$ 0.3

Table IX. Nitrite-Plasma Protein Binding In Vitro in the Canine

## REFERENCES

1. Hainline, A., Jr. Methemoglobin. In: Standard Methods of Clinical Chemistry, Vol. 5, pp. 143-157, Meites, S., editor. New York, N. Y., Academic Press, 1965.
2. Schneider, N. R. The pharmacokinetics of sodium nitrite and its relationship to methemoglobinemia in the canine, ovine, and equine. M.Sc. Thesis, Columbus, Ohio, The Ohio State University, 1972.
3. Schneider, N. R. and Yeary, R. A. Measurement of nitrite and nitrate in blood. Am. J. Vet. Res. 34:133-135, 1973.



## CONTROL OF WHITE CELL POPULATION IN THE POSTIRRADIATED ANIMAL

**Principal Investigators:** T. J. MacVittie, K. F. McCarthy and S. J. Baum

The objective of this research was to improve postirradiation production of granulocytes by accelerating primitive progenitor recovery.

The in vivo diffusion chamber (DC) technique for mouse marrow culture was used to determine the effect of a granulocyte inhibitor (chalone) on the proliferation of the pluripotent stem cell (CFU-S) and the granulocyte progenitor cell (CFU-C). The DC's were each inoculated with a normal mouse marrow suspension and then implanted into host mice exposed 4 hours previously to 900 rads  $^{60}\text{Co}$   $\gamma$ -radiation. Granulocyte inhibitor (chalone) containing solution was collected as the 20-hour incubation media of rat granulocytes previously obtained by peritoneal lavage.

The granulocytic inhibitor was injected intraperitoneally in 1.5-ml aliquots into chamber-bearing mice at 5, 20, 24, 28, 44 and 48 hours after implantation. This regimen resulted in a significantly reduced number of granulocytic progeny formed within the DC's while there was no growth inhibition of mouse fibroblasts cultured under identical conditions (Figure 11). The reduced cell production was due in part to a significant reduction in the self-renewal rate of the CFU-C while no apparent direct effect was observed upon the growth of the CFU-S within the same cultures (Figures 12 and 13).

These data suggest that the granulocytic inhibitor (chalone) acted to reduce the active growth fraction of the CFU-C and precursor populations and thereby reduced the amplification potential inherent in the initial cell inoculum.

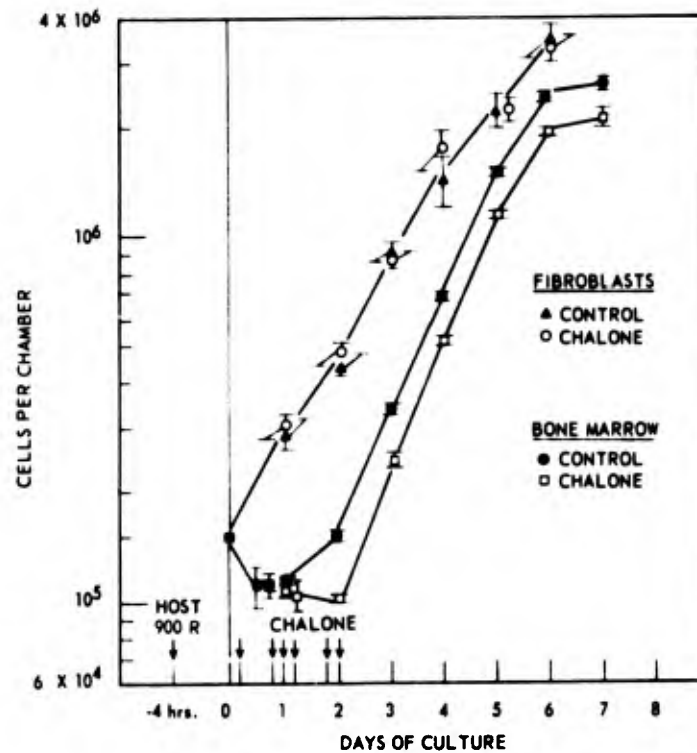


Figure 11. The effect of granulocyte chalone injections on the growth of mouse fibroblasts (L-929) inoculated at  $10^5$  per chamber after removal from monolayer culture and of nucleated cells (granulocytes and macrophages) inoculated at a concentration of  $1.5 \times 10^5$  normal bone marrow cells per chamber. Host animals were exposed to 900 rads of whole-body gamma radiation 4 hours prior to implantation. Mean values ( $\pm$  SEM) are results of six replicate experiments and observed differences are significant at  $p < 0.001$  level.

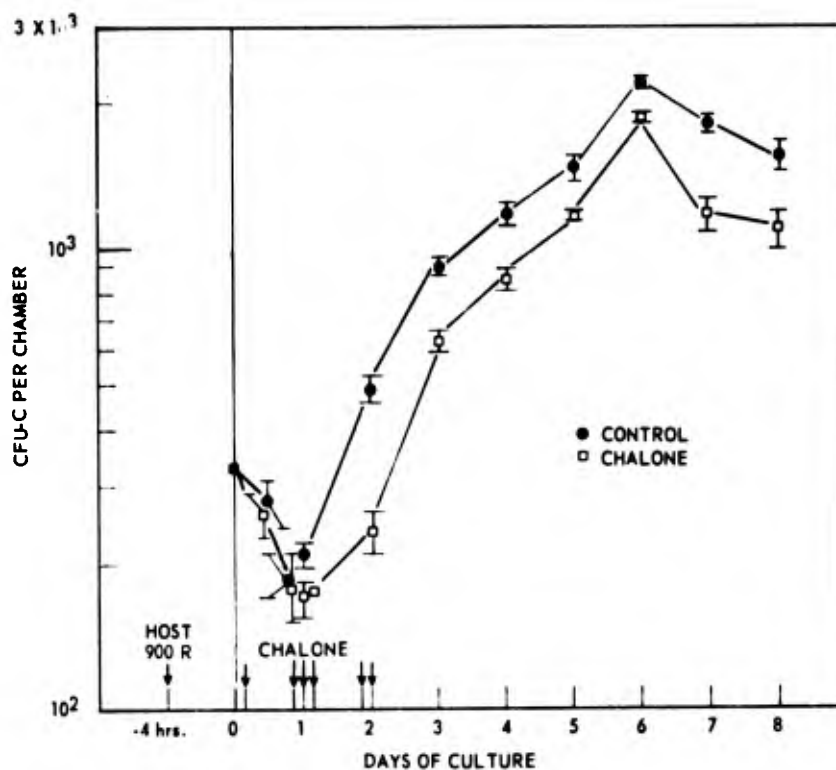


Figure 12. The effect of granulocyte chalone on the growth of *in vitro* colony forming units (CFU-C) in diffusion chambers inoculated with  $1.5 \times 10^5$  normal bone marrow cells and implanted into whole-body gamma irradiated (900 rads) hosts. Values ( $\pm$ SEM) are results of at least four replicate experiments in which chamber cells were pooled and used to inoculate four agar plates per point.

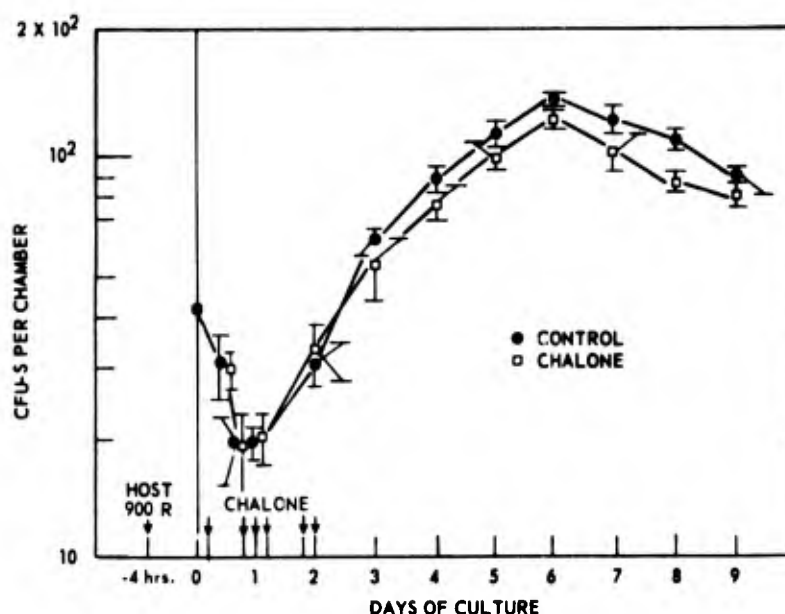


Figure 13. The effect of granulocyte chalone on the growth of *in vivo* colony forming units (CFU-S) in diffusion chambers implanted into whole-body gamma irradiated (900 rads) hosts. Chambers were inoculated with  $1.5 \times 10^5$  normal bone marrow cells. Values ( $\pm$ SEM) are results of at least four replicate experiments in which chamber cells were pooled and used to inject 8- to 10-assay mice per point.

\*\*\*\*\*

## EVALUATION OF THE BIOLOGIC ACTIVITY OF ATTENUATED ENDOTOXIN

**Principal Investigators:** C. B. Galley, R. I. Walker, G. D. Ledney and M. R. Gambrill

The objective of this research was to evaluate the biologic properties of normal and attenuated endotoxin in conventional and antibiotic decontaminated mice.

Endotoxin-induced lethality was significantly reduced in conventional and antibiotic decontaminated mice by treatment of the lipopolysaccharide molecule of endotoxin with  $\text{FeCl}_3$  before inoculation (Table X). Although less lethal than normal (untreated) endotoxin, the attenuated preparation was a more effective B-lymphocyte mitogen (Figure 14). Injection of B6CBF<sub>1</sub> mice with 25  $\mu\text{g}$  of either endotoxin preparation 24 hours prior to 850 rads of x rays resulted in similar numbers (75 percent) of 30-day survivors. Therapeutic treatment of irradiated mice and those undergoing graft versus host

disease (GVHD) was impractical as these mice died within 24 hours after an I. P. injection of 25  $\mu\text{g}$  of either normal or attenuated endotoxin. Antibiotic decontaminated mice given 850 rads of x rays did not die when challenged with either endotoxin preparation.

Table X. Survival Fraction\* of Mice Treated either with Normal *S. typhosa* Endotoxin or with Endotoxin Treated with Ferric Chloride†

Microbiologic status	Normal endotoxin			Attenuated endotoxin		
	0.5 mg	0.75 mg	1.0 mg	1 mg	FeCl <sub>3</sub>	Saline
Conventional	4/5	0/5	0/20	29/34	10/10	10/10
Decontaminated	ND	ND	0/10	9/10	ND	ND

\* Number survivors/number treated

† Mice were injected I. P. with the endotoxin preparation or the equivalent amount of saline or FeCl<sub>3</sub> present in a 1-mg injection of endotoxin. Survival was monitored over a 72-hour period.

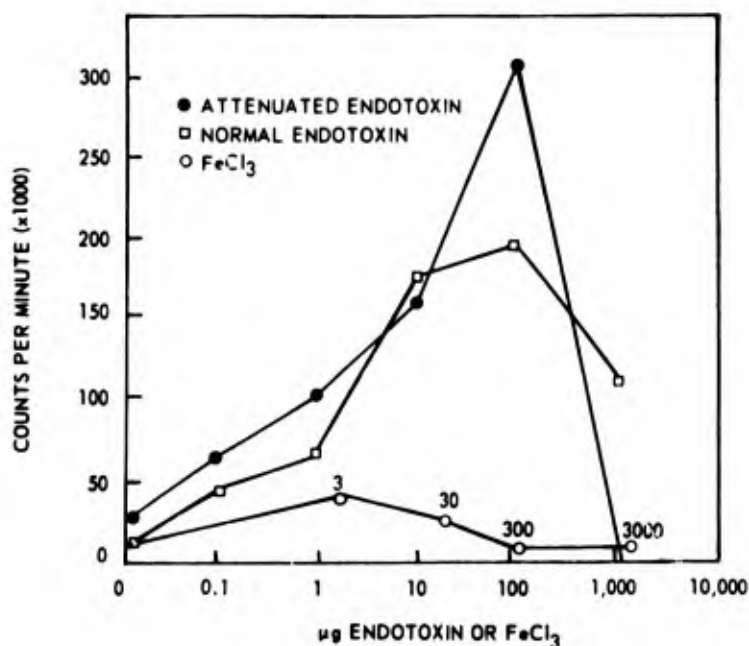


Figure 14. B-lymphocyte mitogenicity as measured by <sup>3</sup>H-TdR uptake. Each point represents five determinations.

reference to either untreated or attenuated endotoxin was achieved by giving seven consecutive daily (spaced) I. P. injections of 30  $\mu\text{g}$  of those substances to CBA mice. Graftment of spleen cells from such mice into irradiated conventional B6CBF<sub>1</sub> mice did not significantly prolong survival from acute GVHD. However, all decontaminated



mice receiving cells from animals made tolerant to either endotoxin preparation survived for more than 30 days. At this time the animals were normal in appearance. Thus, the combination of the two treatments, decontaminated hosts and cells from endotoxin tolerant donors, was effective in promoting survival from acute GVHD. Neither treatment alone could achieve the effectiveness of the two used together.



## PROTEIN-BOUND CARBOHYDRATES AS BIOCHEMICAL CRITERIA IN DIAGNOSIS AND PROGNOSIS OF MALIGNANT NEOPLASIA

**Principal Investigator:** A. S. Evans

**Collaborators:** M. F. Dolan, W. J. Fouty, National Naval Medical Center;  
J. D. Lamberg, T. C. Pomeroy, National Institutes of Health;  
and W. E. Jackson III, AFRRI

**Technical Assistance:** M. J. Ryan, G. E. Routzahn and P. W. Jones III

The present study is a continuation of the investigation of the utility of the glycoprotein profile system as an objective diagnostic and prognostic tool to aid the physician in in-hospital management and outpatient follow-up of patients with, or suspected of having, malignant neoplasia.

During this period, 994 serum specimens were examined. One hundred fifty-six of these samples were from patients in (or outpatients of) the National Naval Medical Center, Bethesda, Maryland, and 765 from the cancer therapy group, National Institutes of Health (NIH) Clinical Center, Bethesda, Maryland. In addition to the above human patients, sera from 73 rats were received from P. Z. Sobocinski of the AFRRI. Combined with previous periods, a total of 2,114 samples have been received for processing.

The test battery consisted of total protein, total serum globulins, protein-bound neutral hexoses, hexosamines, sialic acid, and fucose. From these analytical data, a number of additional parameters were derived: ratios of the various carbohydrates to the total protein (mg CHO/dg protein), carbohydrate to globulin ratios (mg CHO/dg globulin), and mole-fraction ratios of the various carbohydrates. The glycoprotein profile consisted of the graphical representation of these analytical and derived data.

The glycoprotein profile system continues to exhibit excellent correlation with clinical data for presurgical estimation of malignant tumor extension or activity<sup>2,3</sup> and postsurgical evaluation of therapeutic efficacy.<sup>1</sup>

Preliminary computerization of the data by discriminant analyses of a 27 x 27 matrix indicates that the site of the tumor process exercises a large influence on the glycoprotein response of the patient. Thus, when only first samples on each patient were considered -- without regard for the individual's clinical status, response to therapy, or the cell-type of the tumor -- 91.7 percent of buccal cavity and pharyngeal tumors, 83.9 percent of breast tumors, 82.1 percent of tumors of the digestive organs and peritoneum, and 63.0 percent of tumors of the respiratory system were correctly selected by the computer as to tumor locale. In the respiratory tumors, which showed the poorest selectivity, 8 of 10 of the "misclassifications" gave the correct site of the primary lesion as a strong second choice with the first choice being sites of metastases.

#### REFERENCES

1. Dolan, M. F. Patterns of specific glycoprotein response in the course of malignant disease and variations in specific carbohydrate components. In: Proceedings of 1st Invitational Symposium on the Serodiagnosis of Cancer, pp. 143-156. Bethesda, Maryland, Armed Forces Radiobiology Research Institute Special Publication SP74-1, 1974.
2. Evans, A. S. Serum protein-bound neutral hexoses and L-fucose as an index of metastatic disease and efficacy of therapy. In: Proceedings of 1st Invitational Symposium on the Serodiagnosis of Cancer, pp. 129-142. Bethesda, Maryland, Armed Forces Radiobiology Research Institute Special Publication SP74-1, 1974.
3. Evans, A. S., Dolan, M. F., Sobocinski, P. Z. and Quinn, F. A. Utility of serum protein-bound neutral hexoses and L-fucose for estimation of malignant tumor extension and evaluation of efficacy of therapy. Bethesda, Maryland, Armed Forces Radiobiology Research Institute Scientific Report SR73-20, 1973. Cancer Res. 34:538-542, 1974.



## ALTERATIONS OF SERUM SIALIC ACID LEVELS IN MINIATURE SWINE AFTER SPLIT DOSE EXPOSURE TO $^{60}\text{Co}$ RADIATION

**Principal Investigators:** *P. Z. Sobocinski and J. F. Taylor*

**Collaborators:** *W. J. Canterbury and N. S. Mathewson*

The prognostic significance of serum levels of various protein-bound carbohydrates has been previously reported from this laboratory. The purpose of the present investigation was to determine whether the alterations in serum levels of one of these carbohydrate residues, sialic acid (N-acetylneuraminic acid), would provide information useful in assessing the clinical status of the irradiated animal. Thirteen miniature swine received an initial exposure to 150 rads of  $^{60}\text{Co}$  radiation followed 28 days later by an exposure to 550 rads. Sera, obtained at weekly intervals, were assayed for neuraminidase-labile sialic acid and protein-bound neutral hexose levels. Elevated sialic acid levels were observed in survivors and decedents. However, these elevations were transient in the six animals which survived for 30 days after the second exposure. Alterations in neutral hexose levels were similar to those observed for sialic acid levels. Results indicate that the serum sialic acid level, which is easily and rapidly determined by an automated method, may provide some information useful in the initiation of therapy in radiation injury.



## AUTOMATED DETERMINATIONS FOR SERUM SIALIC ACIDS AND HEXOSAMINES

**Principal Investigators:** *N. S. Mathewson and P. Z. Sobocinski*

**Technical Assistance:** *W. J. Canterbury, K. M. Hartley and M. L. Nelson*

The objective of this research was to provide automated methods for determining serum sialic acids and hexosamines. The present method of choice for determining sialic acids, the thiobarbituric acid method (TBA) of Aminoff,<sup>1</sup> requires an organic phase separation of the chromogen and a 1-hour acid hydrolysis of the sample. Serum hexosamines are determined by the method of Winzler<sup>5</sup> requiring a 4-hour hydrolysis of serum samples.

A fully automated method for determining serum sialic acid concentrations has been developed which (1) analyzes 20 samples per hour (1:2), (2) employs neuraminidase (E.C.3.2.1.18) to release bound sialic acids, and (3) utilizes a dialysis step to prevent serum protein-bound substances from interfering with the automated TBA

analysis. The replicate precision of standards and samples yields a coefficient of 0.02 or less. Optical density is a linear function of sialic acid up to 200 mg/dl. Figure 15 demonstrates that normal as well as one and one-half and two times the normal level of serum bound sialic acids are essentially completely released during the 30-minute incubation time employed by this method.

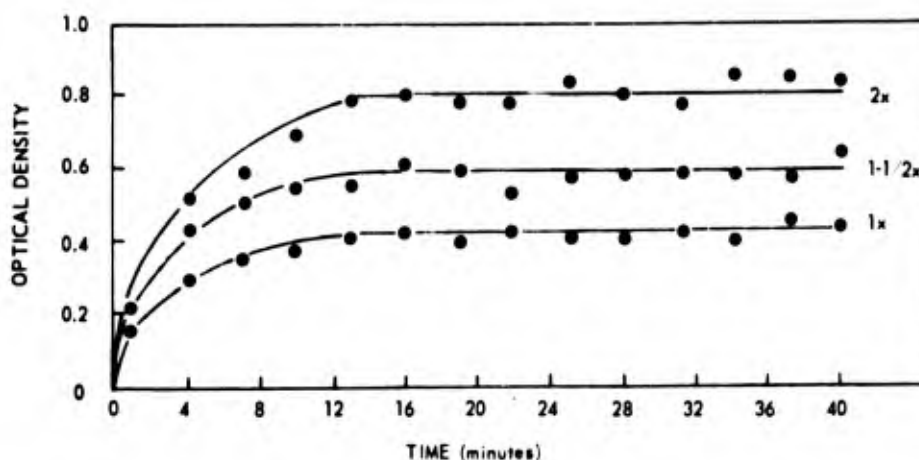


Figure 15. Release of sialic acid by automated serum-enzyme mixture. Optical density due to only free sialic acid as measured by the method of Aminoff.<sup>1</sup> The serum-enzyme mixture is buffered and diluted in the same proportions used by the automated method with one, one and one-half and two times (shown as 1x, 1-1/2x and 2x, respectively) the normal amount of bound sialic acid.

Due to the large variability found in literature values for a normal human serum sialic acid, ranging from 4.2 to 86 mg/dl, the following four methods are compared with the proposed procedure: (1) a modification of the acetic-sulfuric method,<sup>3</sup> (2) the TBA method of Aminoff<sup>1</sup> employing acid hydrolysis. (3) the periodate-resorcinol method,<sup>4</sup> and (4) the diphenylamine reaction.<sup>2</sup> Linear regression of the acetic-sulfuric sialic acid values against the automated values for 112 serum samples showed a high degree of linear correlation with a correlation coefficient of 0.967. Similarly, linear regression of the periodate-resorcinol sialic acid values against the automated method's values for 107 serum samples showed a high degree of correlation with a regression coefficient of 0.975.

Normal levels for human serum sialic acids were obtained by the different methods on healthy human adults and are summarized in Table XI. To clearly distinguish the apparent differences among these methods, a commercial control serum was repeatedly analyzed by one person using the same set of standards. The sialic acid levels obtained by using each method are shown in Table XII. These different sialic acid concentrations serve to illustrate that each method is interfered with by various serum constituents in quantitatively different ways and that a "true" sialic acid level for serum is not easily defined. By using the high specificity of neuraminidase to release only

sialic acid from serum it is felt that the automated sialic acid value is subject to a minimum of serum interference and therefore represents an accurate lower limit to the true serum sialic acid concentration.

Table XI. Normal Serum Sialic Acid Concentrations

Method	Sialic acid (mg/dl)*
Automated	65.5 $\pm$ 9.1 (38)
Acetic-sulfuric	71.0 $\pm$ 11.7 (36)
Periodate-resorcinol	72.9 $\pm$ 10.5 (39)
Diphenylamine	89.6 $\pm$ 14.5 (36)

\* Concentration measured as N-acetylneuraminic acid, mean  $\pm$  S. D. (number of individual serums)

Table XII. Replicate Analyses of a Commercial Control Serum

Method	Sialic acid (mg/dl)*
Automated	61.9 $\pm$ 1.7 (6)
Acetic-sulfuric	66.7 $\pm$ 2.0 (15)
Periodate-resorcinol	69.1 $\pm$ 3.5 (10)
Aminoff-TBA (ref. 1)*	69.4 $\pm$ 2.5 (20)
Diphenylamine	85.1 $\pm$ 6.5 (15)

\* Concentration measured as N-acetylneuraminic acid, mean  $\pm$  S. D. (number of replications)

\* Because this method measures only unbound sialic acid, acid hydrolysis (0.1 N H<sub>2</sub>SO<sub>4</sub>) is employed for 60 minutes at 80°C

The hexosamine method is a semiautomated method using modified Elson-Morgan reagents which minimize the known interference produced by lysine and neutral hexoses. This procedure utilizes a 15-minute hydrolysis in a standard clinical autoclave rather than the standard hydrolysis of 4 hours thus effecting a considerable savings in analysis time. This method operates at 20 samples per hour (1:2) and the chromogen can be quantitated by its optical extinction at 530 nm or by fluorescence emission at 490 nm when excited at 410 nm.

Linear regression of hexosamine levels obtained with 30 human serum samples assayed by the proposed automated method and by the manual method described by Winzler<sup>5</sup> yielded a correlation coefficient of 0.96. Replicate analyses of a commercial control serum by both methods are presented in Table XIII and the difference between these methods is not of practical significance.

Table XIII. Replicate Analyses of a Commercial Control Serum Performed by Automated and Manual Methods

Method	Hexosamine (mg/dl)*
Automated	92.5 ± 5.6 (31)
Manual†	87.6 ± 8.7 (51)

\* Hexosamine measured as glucosamine, mean ± S. D. (number of analyses)

† Manual method refers to that described by Winzler<sup>5</sup>

## REFERENCES

1. Aminoff, D. Methods for the quantitative estimation of N-acetylneuraminic acid and their application to hydrolysates of sialomucoids. *Biochem. J.* 81:384-392, 1961.
2. Ayala, W., Moore, L. V. and Hess, E. L. The purple color reaction given by diphenylamine reagent. I. With normal and rheumatic fever sera. *J. Clin. Invest.* 30:781-785, 1951.
3. Hess, E. L., Coburn, A. F., Bates, R. C. and Murphy, P. A new method for measuring sialic acid levels in serum and its application to rheumatic fever. *J. Clin. Invest.* 36:449-455, 1957.
4. Jourdian, G. W., Dean, L. and Roseman, S. The sialic acids. XI. A periodate-resorcinol method for the quantitative estimation of free sialic acids and their glycosides. *J. Biol. Chem.* 246:430-435, 1971.
5. Winzler, R. J. Determination of serum glycoproteins. *Methods Biochem. Anal.* 2:279-311, 1955.



## GLYCOPROTEINS IN DIABETES

**Principal Investigators:** *R. J. O. Woods and P. Z. Sobocinski*

**Technical Assistance:** *M. L. Nelson and W. J. Canterbury*

This study was performed to determine whether alloxan treatment of rats alters levels of the terminal carbohydrate residues, L-fucose and sialic acid, of serum glycoproteins. Results indicate that in the uncompensated diabetic animal a chronic depression of serum sialic acid level occurred with no apparent alteration in the level of L-fucose. The depression in sialic acid level may be attributed in part to decreased activities of hepatic enzymes involved in sialic acid synthesis similar to those observed by others after treatment of rats with the diabetogenic agent, streptozotocin. The lack of any significant alteration in the level of L-fucose fails to confirm, in the experimental diabetic animal, the increased protein-bound fucose levels reported in human diabetics. Administration of insulin was not effective in modifying the sialic acid response after alloxan treatment.



## EXPERIMENTAL INDUCTION OF NEUROGENIC TUMORS IN MINIATURE SWINE (NEUROGENIC TUMOR MODEL)

**Principal Investigator:** *M. E. Ekstrom*

**Collaborators:** *W. G. Shain, Jr., J. E. West and J. S. Stevenson*

**Technical Assistance:** *J. E. Egan, W. W. Wolfe, P. E. Haynesworth and G. D. Lee*

The purpose of this study is to induce neurogenic tumors in miniature swine using the potent chemical carcinogen, 1-ethyl-1-nitrosourea (ENU). These tumors will be used as models for studying diagnostic, therapeutic, and pathophysiologic aspects of comparable neoplasms which occur in humans. Transplantation studies will be initiated with tumors that develop.

The etiology and pathogenesis is still basically unknown for the majority of naturally occurring primary neurogenic tumors found in man and animals. The glial tumors are the most common intracranial tumors in man and apparently in most animal species. With few exceptions treatment of glial tumors is only palliative and not curative. Recently ENU and certain other N-nitrosourea compounds have generally been shown to cause the selective induction of neurogenic tumors in rats, rabbits, and dogs;

the tumors have in most respects been comparable to those that occur in man. The development of similar tumors in a large animal species like miniature swine which have a size like that of man is needed.

To achieve the objectives of this study two groups of miniature swine were exposed to intravenously administered ENU. Exposures began in the prenatal period when a gilt was injected with a 10-mg/kg dose at biweekly intervals during the last trimester of two pregnancies. After birth one litter (Group 1) received 15-20 mg/kg at monthly intervals until the age of 1 year. Group 1 consisted of five pigs, two of which were controls. Group 2, consisting of eight pigs, two of which were controls, received this same dose at biweekly intervals until the age of 6 months. The pigs have been monitored for tumor development by the following methods: (1) evaluation of clinical signs; (2) quantitative and qualitative hematologic analyses; (3) determination of serum creatine phosphokinase, glycoproteins and other selected chemistries; and (4) brain scans with a gamma camera using  $^{99m}\text{Tc}$  pertechnetate as a scanning agent.

Tumors have not been detected to date. ENU exposed pigs in group 1 have a mean weight of 32 kg versus 25 kg for controls. No differences in other physiologic parameters have been detected. The absolute latent period for neurogenic tumors which may arise in the miniature pig is not known. Experimental animals will continue to be observed and evaluated for evidence of tumor development.



## DEVELOPMENT OF A HYPOTHROMBOGENIC BLOOD OXYGENATOR MEMBRANE

**Principal Investigator:** *P. K. Weathersby*

**Collaborators:** *T. Kolobow, E. W. Stool and F. Hayano,  
National Institutes of Health*

The objectives of this study were: (1) to determine the thrombogenicity of a pure polydimethylsiloxane (PDMS) rubber compared to standard medical grade silicone rubber (PDMS plus silica filler, peroxide catalyst and residues and other additives), and (2) to develop and test a practical method of using a pure PDMS surface in a full-scale membrane oxygenator.

An early pilot study demonstrated that a layer of PDMS substantially prolongs the in vitro whole blood clotting time.<sup>1</sup> Subsequent work has shown that this effect is much more sensitive to the removal of silica fillers than to the presence of oxidation products. The extension of these studies to ex vivo testing is underway.



Filler-free silicone rubber is very fragile. This lack of strength has been overcome by a system for casting reliable composite fabric reinforced membranes. Entire membrane oxygenator perfusion circuits have been constructed of surfaces free of silica (but not of oxidation products). These surfaces have been shown in full-scale animal testing to be hematologically superior to standard medical grade silicone rubber.

#### REFERENCE

1. Weathersby, P. K., Kolobow, T. and Stool, E. W. Polydimethylsiloxane: a feasibility study of a thromboresistant biomaterial. Bethesda, Maryland, Armed Forces Radiobiology Research Institute Technical Note TN74-5, 1974.



#### TECHNETIUM-99m PHOSPHATE BONE IMAGING: A METHOD FOR ASSESSING BONE GRAFT HEALING

**Principal Investigators:** *J. S. Stevenson, AFRRRI; R. W. Bright, Naval Medical Research Institute; G. L. Dunson, AFRRRI; and F. R. Nelson, National Naval Medical Center*

Although autologous bone has long been recognized as the best material for bone grafting, large osseous defects resulting from trauma or surgical resection often preclude their use. Allograft and xenograft bone substitutes, which are fresh, frozen, freeze-dried, irradiated, decalcified or gas autoclaved, have been utilized in attempts to solve this significant medical problem. Early evaluation of the healing process of nonautologous grafts is very important in patient management. Roentgenography, though of some value late in the healing phase, does not meet this need.

Technetium-99m polyphosphate ( $^{99m}\text{Tc PP}$ ) and technetium-99m diphosphonate ( $^{99m}\text{Tc DP}$ ) are ideal bone scanning radiopharmaceuticals since they encompass the easily collimated and imaged 140 keV gamma emission of  $^{99m}\text{Tc}$  coupled with the bone localizing properties of phosphorous compounds. In addition,  $^{99m}\text{Tc}$  has a low cost, continuous availability from commercial  $^{99}\text{Mo}$ - $^{99m}\text{Tc}$  nuclide generators, and gives a low patient radiation dose.

The new technetium-99m phosphate bone scanning radiopharmaceuticals now allow the development of highly efficacious methods of nuclear bone imaging which can be used to evaluate a wide variety of bone disorders. One of which is the evaluation of bone healing after fractures and grafting. This study reports on a nuclear bone imaging method for assessing bone healing and for comparing freeze-dried autologous grafts and freeze-dried cortical segmental allografts.<sup>2</sup>

The autografts (Group 1) and the allografts (Group 2) were transplanted into surgically created 2-cm defects in the distal ulnas of adult dogs, according to the method of Heiple.<sup>1</sup> One ulna always received fresh autologous bone as a control graft, while the opposite ulna received the experimental bone graft. Fourteen Group 1 grafts were used to evaluate autologous bone graft healing, while fourteen Group 2 allografts were transplanted to study the graft material usually provided clinically by the Naval Medical Research Institute Tissue Bank.

Nuclear bone imaging procedures suitable for patient use were performed. <sup>99m</sup>Tc PP or <sup>99m</sup>Tc DP was administered (0.5  $\mu$ Ci/kg) as a single bolus intravenously. Approximately 3 hours after the injection the dogs were anesthetized and each leg was imaged using a Nuclear-Chicago high performance scintillation camera with both the pinhole and the high resolution collimators. Roentgenograms of the respective graft area were obtained on the same day. Photographic records of the nuclear bone imaging data were stored on magnetic tapes for subsequent computer retrieval and quantification. Comparisons were made of scintiphotographs and radiographs. Each graft area was studied sequentially at 2, 4, 6, 8, 12, 18, and 24 weeks postgrafting.

Technetium-99m polyphosphate and technetium-99m diphosphonate appear to localize in areas of active bone formation, but the exact mechanism of bone uptake is not yet known. Three general patterns of graft healing were demonstrated during the 24-week period of serial evaluation. First, both the roentgenogram and bone imaging revealed nonhealing of the graft site. Second, both the x-ray and bone imaging techniques revealed progressive healing of the graft site. Finally, the bone imaging data revealed either healing or nonhealing when the roentgenograms were inconclusive (Figure 16).

The longitudinal profile of each scan was evaluated with the MED-II Nuclear Data Computer (Figure 17). Each graft area was always compared to the control data recorded from the opposite limb of the same dog. In those grafts which showed progressive healing, the two areas of activity at the graft-host junctional site showed progressive coalescence into one peak. This provided a dynamic measure of the rate of bone healing (Figure 18).

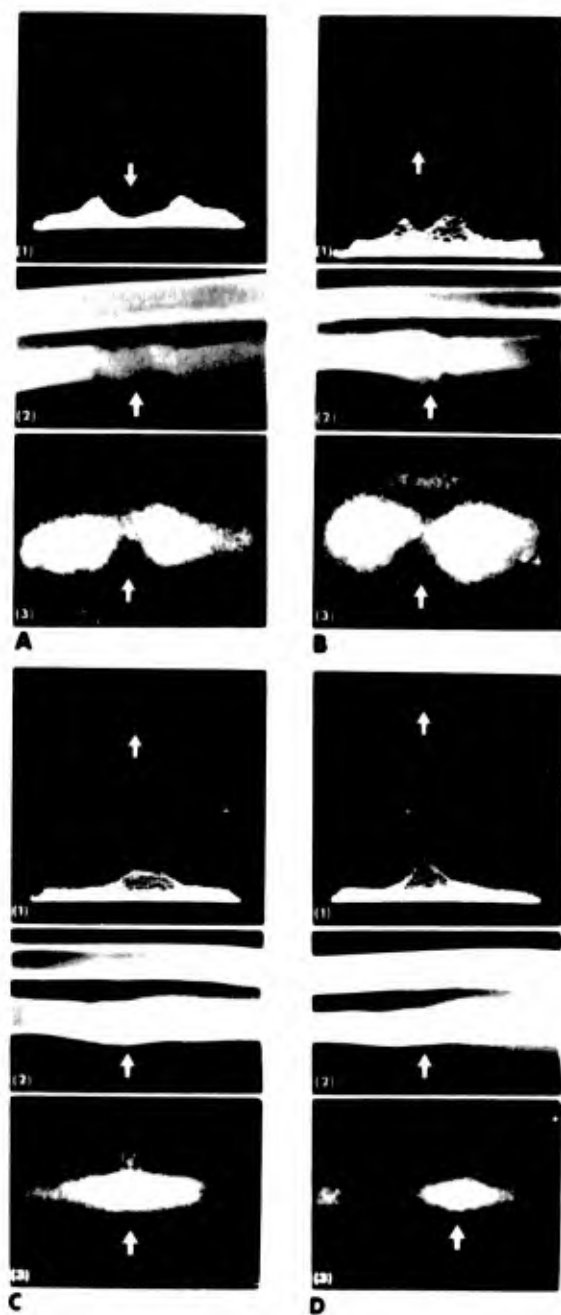


Figure 16. Radiographic and radioisotope computer and scan analysis of a healing bone graft. Initially (A), the graft is minimally viable. The scan A3 reveals little activity of the graft (arrow) which on the computer display is represented by a valley (A1, arrow). As healing progresses, the areas of junctional activity on the scan coalesce (B3, C3, D3) into one "hot spot." The computer display (B1 and C1) reveals coalescing of the two peaks into one, which later narrows (D1).

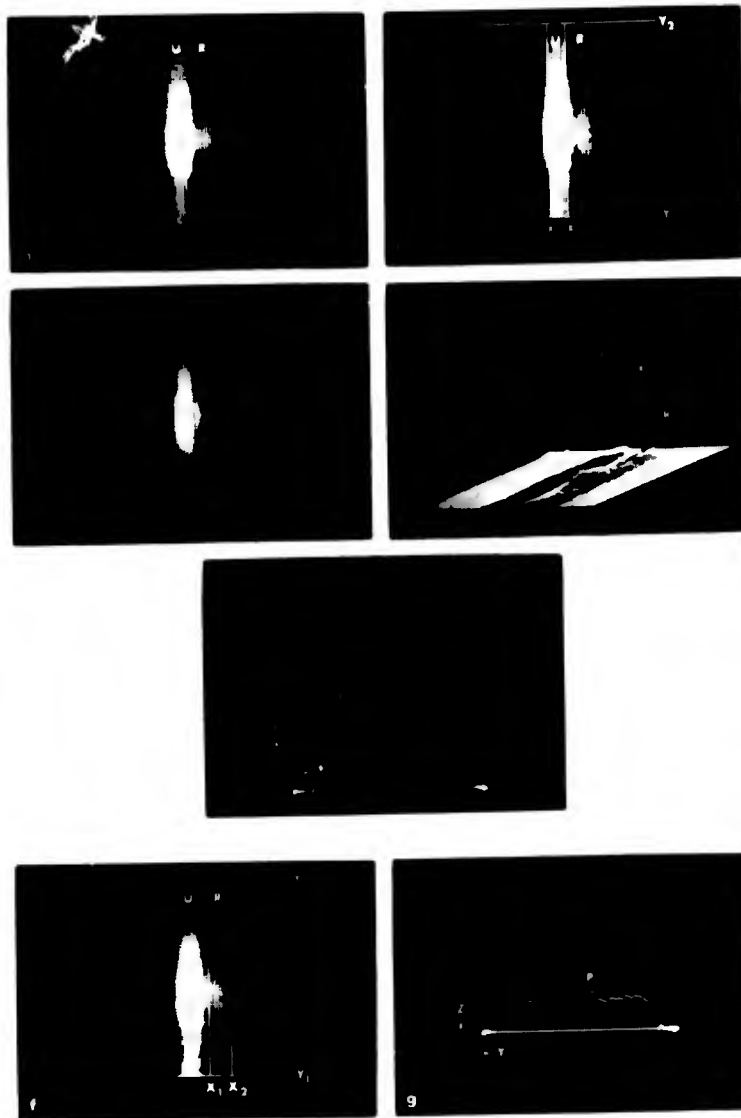


Figure 17. Data processing by the computer (image a) is accomplished by framing the ulna (U, image b) and storing the sum of each seven channels between  $X_1$  and  $X_2$  in the corresponding first channel of the profile at the far left (P, image c). This integrated profile may be displayed isometrically (image d) and separately (image e) for analysis and teletype output. Similarly, the radius is also framed (R, image f) to give an integrated profile (image g).

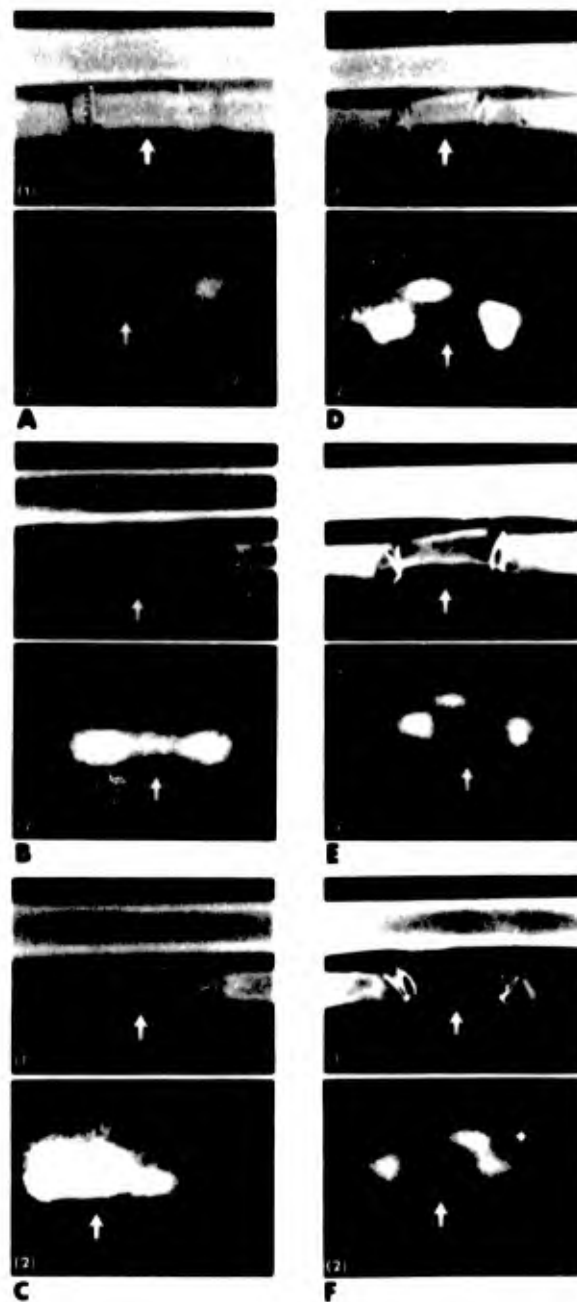


Figure 18. Two cancellous grafts. Two weeks after surgery, A1 and D1 show reabsorption radiographically: B1 and E1 by 6 weeks. By scan however, one of the grafts (E2) reveals minimal viability while the other (B2) shows excellent viability. Sixteen weeks later, the graft in E1 which showed poor healing by scan (E2) has been completely reabsorbed radiographically (F1) and shows no viability by scanning (F2). However, the graft in B1 which showed viability via scanning (B2) has progressively healed radiographically (C1).

Occasionally, the grafts failed to incorporate the radiopharmaceutical; and, with associated resorption, a residual osseous defect was evident. In these dogs, peripheral peaks of the radioactivity never coalesced at the center of the graft. The roentgenograms of the bone grafts eventually showed complete resorption of the graft. The lack of peak coalescence recorded by sequential imaging and by the MED-II computer foretold the eventual fate of that graft as early as 4 to 6 weeks before identifiable graft resorption was evident radiographically (Figure 18). This new dimension of being able to predict bone graft healing was an unexpected bonus.

## REFERENCES

1. Heiple, K. G., Chase, S. W. and Herndon, C. H. A comparative study of the healing process following different types of bone transplantation. *J. Bone Joint Surg.* 45A:1593-1616, 1963.
2. Stevenson, J. S., Bright, R. W., Dunson, G. L., Nelson, F. R., Barron, E. L. and Merriman, M. L. Technetium-99m polyphosphate bone imaging: a quantitative method for assessing bone healing. Bethesda, Maryland, Armed Forces Radiobiology Research Institute Scientific Report SR73-11, 1973.



## TECHNETIUM-99m PYROPHOSPHATE: COMPARISON OF ED<sub>50</sub> FOR TETANY AND ACIDOSIS WITH ACUTE LD<sub>50</sub>

**Principal Investigators:** J. S. Stevenson, AFRRRI; W. C. Eckelman, Washington Hospital Center; P. Z. Sobocinski, E. L. Barron and S. G. Levin, AFRRRI

The clinical symptomatology occurring acutely after toxic doses of technetium-99m-Sn-pyrophosphate are administered is consistent with tetany and metabolic acidosis. To evaluate each of these phenomena, measurements of serum calcium and PCO<sub>2</sub> were made after administering technetium-99m-Sn-pyrophosphate intravenously, as a single bolus, to Sprague-Dawley rats on a milligram per kilogram body weight basis. The LD<sub>50/5</sub> minutes for pyrophosphate was 41.0 mg/kg with 95 percent confidence limits of 39.4 to 42.7 mg/kg body weight. The LD<sub>50/5</sub> minutes for polyphosphate was 29.4 mg/kg with 95 percent confidence limits of 27.4 to 31.5 mg/kg body weight (Figure 19). Plots evaluating the slopes of the two compounds showed no significant statistical difference. Polyphosphate was 1.4 times as toxic as the pyrophosphate agent on an LD<sub>50/5</sub> minutes basis.<sup>1</sup>

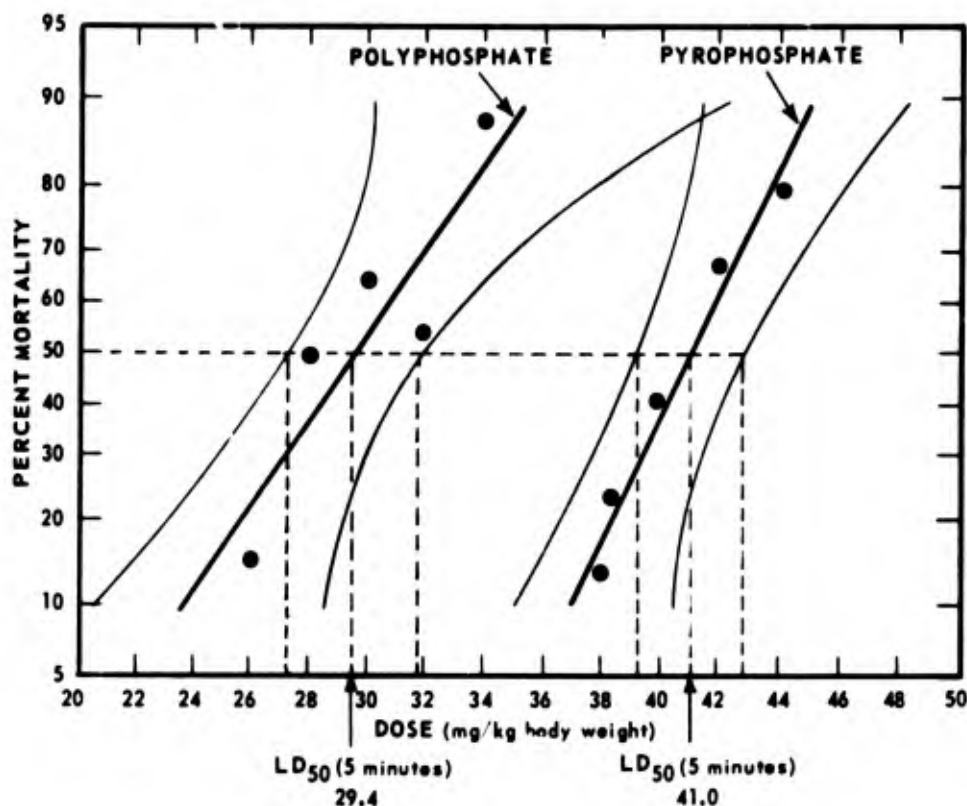
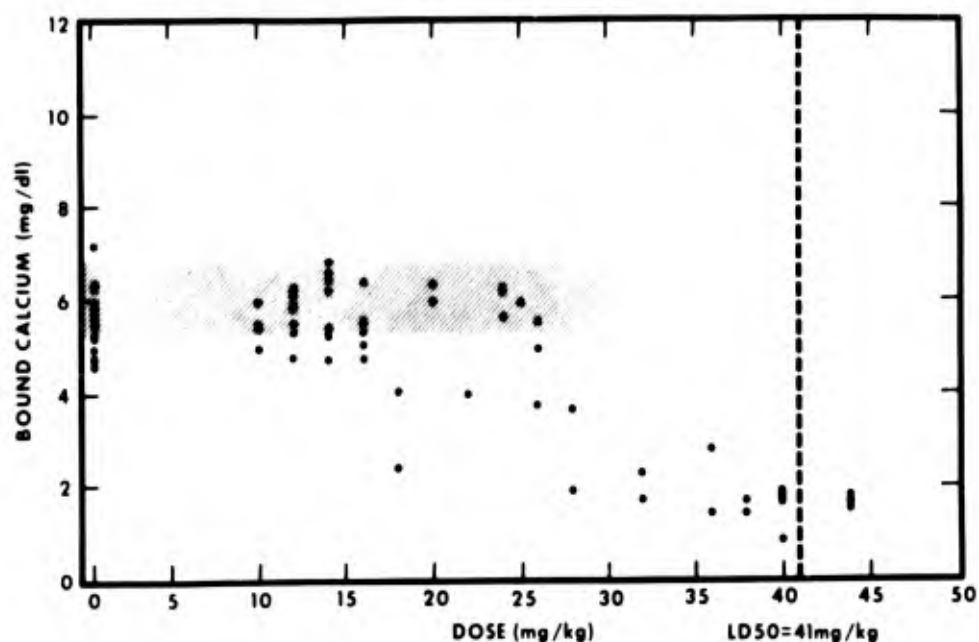


Figure 19. Plot of acute mortality (5 minutes) of Sprague-Dawley rats receiving intravenous injections of polyphosphate or pyrophosphate. Time of death is within 5 minutes after injection. Each point represents the percent mortality of 7 to 14 animals.

Acidity measurements revealed that the plasma serum  $\text{PCO}_2$  level remained between 30 and 40 torr until doses of pyrophosphate exceeded 35 mg/kg body weight, after which it fell sharply. Serum calcium levels were measured by atomic absorption spectroscopy and electrocardiography. Both techniques revealed a significant drop in the values of ionizing and bound calcium beginning at a dosage of 12 mg/kg or greater. The clinical symptomatology consistent with hypocalcemia did not manifest itself, however, until the dosage of 22 mg/kg body weight of the pyrophosphate compound was reached (Figure 20). It is therefore concluded that determination of toxic effects of phosphate agents should not be based on the  $\text{LD}_{50}$  alone, but on dosages which produce hypocalcemia and metabolic acidosis.



**Figure 20.** Serum-bound calcium concentrations 5 minutes following intravenous injection of pyrophosphate. Each point represents the mean of 2 to 10 animals. Hatched area represents normal range ( $\bar{x} + 2$  S.D.) of control rats.

## REFERENCE

1. Stevenson, J. S., Eckelman, W. C., Sobocinski, P. Z., Barron, E. L., Levin, S. G. and Reba, R. C. Technetium-99m pyrophosphate: comparison of ED<sub>50</sub> for tetany and acidosis with acute LD<sub>50</sub>. Bethesda, Maryland, Armed Forces Radiobiology Research Institute Scientific Report SR74-5, 1974.



## TECHNETIUM-99m PYROPHOSPHATE FOR BONE IMAGING

**Principal Investigators:** W. C. Eckelman, Washington Hospital Center; R. C. Reba, H. Kubota, George Washington University; and J. S. Stevenson, AFRRl

Of the various  $^{99m}\text{Tc}$  phosphates suggested for bone imaging,  $^{99m}\text{Tc}$  pyrophosphate appears to have the desirable characteristics of commercial availability of



sodium pyrophosphate and analytical controls available to assure the quality of the final product. Systematic variations of the parameters of the  $^{99m}\text{Tc}$  tin pyrophosphate preparations were evaluated by gamma camera images in miniature swine. Table XIV lists the factors studied and the scan quality obtained. All studies were done in duplicate. Scan quality was based on a scale of 1 to 4 with 4 indicating high bone concentration of  $^{99m}\text{Tc}$  and low interference from its concentration in other organs. These studies indicated that the best bone distribution is obtained by adding 1.75 ml of 0.1 M sodium pyrophosphate at pH 10 to 0.25 ml of 1 mg/ml stannous chloride followed by 1.50 ml  $^{99m}\text{TcO}_4^-$ .<sup>1</sup> In vivo organ distribution indicated the importance of normalizing doses on a per weight basis for comparative animal studies. Data reported for  $^{99m}\text{Tc}$  phosphates without consideration of the dose on a weight basis can be misleading. If the optimal dose of pyrophosphate is used,  $^{99m}\text{Tc}$  pyrophosphate results in high quality bone images in animals and humans. Easily prepared and assayed  $^{99m}\text{Tc}$  phosphates are now considered to be the agents of choice for bone imaging.

Table XIV. Comparison of Gamma Camera Images in Swine for  $^{99m}\text{Tc}$  Pyrophosphate

Factors studied	Scan quality	Factors studied	Scan quality
pH of pyrophosphate solution before addition to tin chloride solution		Concentration of chloride before mixing with pyrophosphate ( $\mu\text{g/ml}$ )	
3.5	2	1000	4
5.5	2	1500	4
10.0	4	2000	3
Molar concentration of pyrophosphate solution before addition to tin chloride		Reproducibility of optimal product	
0.20	3	Scan #1	4
0.10	4	Scan #2	4
0.05	1	Scan #3	4
0.02	1		
Final pH of solution after mix of all components			
5.9	3		
6.3	4		
6.6	4		
7.7	3		
11.8	1		
12.6	1		

## REFERENCE

1. Eckelman, W. C., Reba, R. C., Kubota, H. and Stevenson, J. S. Technetium-99m pyrophosphate for bone imaging. Bethesda, Maryland, Armed Forces Radiobiology Research Institute Technical Note TN74-3, 1974.



## EVALUATION OF HEALING OF MANDIBULAR BONE GRAFTS IN DOGS BY QUANTITATIVE TECHNETIUM-99m POLYPHOSPHATE BONE IMAGING

**Principal Investigators:** J. F. Kelly, J. D. Cagle, *Naval Medical Research Institute;*  
J. S. Stevenson and G. J. Adler, *AFRRI*

The following graft systems have been studied in the mandibles of 24 dogs: (1) lyophilized allografts with autogenous particulate cancellous marrow, (2) lyophilized allografts with allograft destructured cortical bone, and (3) allograft destructured cortical bone with a Millipore filter system.

During the periods of healing the following sequential studies were performed for interval analysis: appropriate radiographic examination,  $^{99m}\text{Tc}$  diphosphonate bone imaging to determine the progress of osteogenic activity, and procion #8BS administered intraperitoneally at 2-week intervals for labeling bone to determine apposition rates.

An equal number of animals with each graft system were carried to 21 and 42 days, euthanatized and the specimens recovered. Data have been reviewed. Osteogenic activity in graft system 1 as determined by  $^{99m}\text{Tc}$  studies was equivalent to the controls at both 21 and 42 days. In system 2 osteogenic activity was less than controls at 21 days but equivalent at 42 days. In system 3 osteogenic activity at 21 days was inconsistent compared to controls while at 42 days this activity was definitely less than the controls.

It was found that  $^{99m}\text{Tc}$  bone imaging was a noninvasive, nondestructive method of evaluating the progress of osteogenic activity in mandibular bone grafts.

A long term study has been initiated in which 10 dogs had graft systems 1 and 2 applied to their mandibles. These animals will be followed for 6 months during which the same sequential and end point analyses will be performed. In addition, sequential analysis of bone mineral content using an americium gamma source will be performed.

$^{99m}\text{Tc}$  images will be correlated with americium images in an attempt to more precisely define the biologic interval at which graft repair has approached functional activity.

During this same period the  $^{99m}\text{Tc}$  mandibular bone imaging techniques were refined allowing for accurate and reproducible positional and quantitative analysis.



## CORRELATION OF GAMMA CAMERA AND FLOWMETER DETERMINED RENAL BLOOD FLOW MEASUREMENTS

**Principal Investigators:** *P. T. Kirchner, National Naval Medical Center; F. C. Gray,  
D. B. Short, AFRRI; and R. S. Filo, National Naval Medical Center*

Gamma camera flow curves are widely used for estimating renal blood flow. We have developed a technique for analyzing renal blood flow curves that shows good correlation with simultaneously obtained electromagnetic flowmeter determinations.

In six dogs an electromagnetic flowmeter was attached to the left renal artery following splenectomy. During steady-state renal artery flow, 5 mCi of  $^{99m}\text{Tc}$  sulfur colloid were injected intravenously in a 0.5-ml bolus. The first transit of tracer through aorta and kidneys was recorded on magnetic tape for analysis with an on-line computer. Following hepatic clearance of the colloid from the circulation, second and third injections in the same dog were similarly recorded for different renal blood flow levels induced by mechanical renal artery constriction. The first transit of tracer through the kidney and through a short (constant size) section of aorta was quantitated for each injection as the integral of the respective time activity curve or as the slope of a linear least squares fit to the curve. Internal standardization for variations in dose and injection technique was achieved by expressing renal blood flow as the ratio of quantitated renal flow curve to quantitated aortic flow curve, each reduced to unit time.

In 11 of 14 measurements the gamma camera determined, renal flow quantitation produced a linear correlation with the flowmeter readings for either mode of curve analysis. In each of the three instances of poor correlation the aortic flow curve was of poor quality.

Our results suggest that noninvasive quantitation of individual renal blood flow can be obtained from analysis of gamma camera derived renal flow curves. For us the most useful clinical application of this technique has been the evaluation of renal transplant function and viability.



## TECHNETIUM-99m METHOTREXATE STUDIES

**Principal Investigator:** *P. T. Kirchner, National Naval Medical Center*

**Collaborators:** *R. H. Adams, L. L. Heck, J. W. Duley, National Naval Medical Center; D. B. Short and G. L. Dunson, AFRRI*

The normal migration rates of selective radioactive tracers in the cerebral spinal fluid system of the body have been studied and much is known about them. However, the migration rates of chemotherapeutic agents used for the therapeutic purposes of diseases involving the cerebral spinal cord such as leukemia involvement of the spinal cord have received little attention. Our laboratory evaluated both radioactive labelled and nonlabelled methotrexate migration rates from the lumbar subarachnoid injection site to the basal cistern looking at not only the migration rates but also the quantity which migrated with reference to time. The study was monitored in 40 Sprague-Dawley rats and 40 rhesus monkeys. The migration rates were determined to develop a measure of a time required for the labelled methotrexate to arrive in the cerebral area, thus giving a quantitative indication of the amount that reaches the cerebral cortex for therapeutic purposes.

A correction factor was developed for the relative external detection efficiencies of radioactivity in the cerebral spinal fluid space of the head versus the cerebral spinal fluid compartment in the subarachnoid area. This required the construction of appropriate spine and head phantoms, monitoring animals and patients, as well as companion radioactive tracer studies including indium-111-DTPA to acquire data on both the range and average amounts of the agent reaching the cerebral spinal fluid space.

This study also determined the LD<sub>50</sub> of radiolabelled methotrexate which was found to be approximately 15 mm/kg, a value which is in fair agreement with the published data on the toxicity of nonlabelled methotrexate. Suppression of bone marrow activity was found to be comparable with both the labelled and nonlabelled methotrexate compounds. In all instances the radioactive tracers moved at a rate which paralleled the migration rate of nonlabelled methotrexate. The technetium-99m methotrexate migrated at a rate almost identical with that of the nonlabelled pharmacological grade

methotrexate. Similar results were found with the indium-111-DTPA agent although a one to one correspondence of migration rates was not quite as exact. In all of the animals evaluated the peak activity of the radiolabelled methotrexate compound in the cisterna magna was exactly the same as for the quantity of pharmacological grade methotrexate over the same period of time.

Our conclusions from the study are that both the technetium-99m methotrexate and the indium-111-DTPA can be used as quantitative indicators of the ascent of methotrexate from the lumbar subarachnoid injection site to the basal cisterns in the head.



## A QUALITATIVE AND QUANTITATIVE COMPARATIVE ANALYSIS OF SCINTILLATION CAMERA TOMOGRAPHY WITH THE LATEST CONVENTIONAL IMAGING TECHNIQUES

**Principal Investigators:** *V. L. McManaman, M. D. Sinclair and J. S. Stevenson*

The rapid growth rate of the field of nuclear medicine over the past several years can be attributed almost exclusively to the development of the scintillation camera for generating images of radionuclides distributed throughout the organs of the body. Prior to that the rectilinear scanner which is much slower and considerably less versatile was the only practical imaging device. With the development of the scintillation camera have come many modifications and adaptations to meet a plethora of various clinical requirements. Two such new devices, a tomographic unit and a DIVCON collimator recently acquired by the AFRRI, have been comparatively evaluated with respect to well-established imaging instruments including the pinhole collimator, the high resolution collimator, the high sensitivity collimator, the rectilinear scanner and computer processed images. The tomography attachment (Tomocamera) to the scintillation camera allows the generation of five images simultaneously where each image is effectively focused at a different depth within the organ under consideration. According to the degree of focus, the depths of tumors or other defects may then be determined without the need for acquiring additional views (i.e., lateral, posterior-anterior, etc.). The major advantages of the tomographic unit are speed and possibly increased resolving power. The DIVCON collimator is essentially a combination high resolution-high sensitivity magnifying collimator designed to combine the advantages of the high resolution and high sensitivity collimators.

Through the use of special head and tumor phantoms designed to challenge the detection limits of all the systems mentioned, qualitative comparisons were performed

using the film images. They reveal the following order of performance in decreasing sequence; rectilinear scanner, pinhole collimator, DIVCON collimator, high resolution collimator and Tomocamera. Computer images for all the camera systems were comparable in quality to those of the rectilinear scanner. Quantitative data (viz., resolution indices and modulation transfer functions) for the scintillation camera systems were obtained from computer images of a uniform line source of activity. These demonstrate the following responses in decreasing order: DIVCON collimator, high resolution collimator, Tomocamera and high sensitivity collimator. These quantitative data show a wider margin of difference in response of the systems thereby supporting the need for their use as more sensitive criteria for evaluating imaging systems.

Although the quantitative data are complete and rigorous, considerable phantom and patient data are still required for a more thorough applied or clinical evaluation of these systems. Particular emphasis should be given to cases where the tissue surrounding the tumor or defect has a higher radionuclide specific activity than the tumor itself.

\*\*\*\*\*

## TECHNETIUM-99m POLYPHOSPHATE RENAL IMAGING

**Principal Investigators:** *M. D. Sinclair and J. S. Stevenson*

**Collaborators:** *V. L. McManaman, G. L. Dunson and D. B. Short*

Patients undergoing  $^{99m}\text{Tc}$  polyphosphate bone scanning at the National Naval Medical Center have been found to have renal pathology, confirmed by surgery or biopsy. This suggests that renal lesions can be easily detected on the bone scan.

A collaborative study with the National Naval Medical Center was undertaken to determine what abnormal renal lesions could be identified by this technique. The renal lesions detected included displacement of kidney, unilateral poorly functioning kidney, nonfunctioning kidney, hydronephrosis, hydroureter, renal cyst, hypernephroma, hydrocele, benign ovarian cyst, and metastasis to the renal parenchyma. The study concluded that extraosseous genitourinary lesions could be demonstrated adequately by this technique.

The radiation dose to the kidneys was calculated to be 890 mR/10 mCi  $^{99m}\text{Tc}$  phosphate administered, assuming 50 percent of the injected dose in the kidneys, the rest disappearing by physical decay alone. For decreased radiation dose to kidneys

and bladder, hydration and frequent voiding are recommended. It is hoped that these results will alert others to the full diagnostic possibilities of  $^{99m}\text{Tc}$  polyphosphate bone scans.



## INSTRUCTION IN NUCLEAR MEDICINE

**Principal Investigator:** *J. S. Stevenson*

Rapidly becoming a major medical discipline, nuclear medicine is currently being introduced into medical school curricula throughout the country. During the past several years we have begun instruction in nuclear medicine including lectures at the Medical Officers' Course at the National Naval Medical Center Program and the Health Physics Board Certification Course. This study describes our current methods of instruction.

The instruction in nuclear medicine includes an integral part of both basic science courses and research and clinical materials. The integration of the basic sciences with the research and clinical data is as follows:

Basic science. (1) Integration of the following specialties: anatomy, biochemistry and physiology; and (2) laboratory problem solving exercises.

Introduction to clinical medicine. (1) Lectures on major nuclear medicine procedures and techniques and (2) touring of research and clinical facilities.

Clinical medicine. (1) Three 1/2-day rotations through clinical laboratories for in vitro analyses, (2) attendance at monthly disciplinary conferences, (3) day to day consultation concerning patient studies being obtained from nuclear medicine laboratories, and (4) elective clinical rotations.

Research medicine. (1) Schedule three 1/2-day rotations through the research laboratories, (2) attendance at monthly disciplinary conferences related to research and various basic science and clinical medical fields, (3) day to day consultation concerning research in the field of nuclear medicine, and (4) elective research rotations (3 to 10 weeks).

Integration of nuclear medicine throughout the entire course in medical education appears optimal in teaching all personnel dealing with nuclear medicine this discipline

and can be effectively obtained through both the clinical and research facilities used in the diagnosis and treatment of patients as well as development of new and better nuclear medicine radiopharmaceuticals and techniques. This was accomplished during the past year with active participation of both the AFRRI staff and the staff at the National Naval Medical Center in developing a program to allow fellows and residents in nuclear medicine to receive training at both facilities. In addition, teaching carousels were developed on renal diseases and on the use of nuclear medicine techniques for diagnosis and treatment, and brain and lung evaluations. In addition, a study on the feasibility of placing a teaching carrel not only for nuclear medicine but for the other disciplinary areas at AFRRI was undertaken and found that such should be obtained.

To be successful in teaching nuclear medicine as well as other fields the study concluded the following: (1) practical nuclear medicine should be taught in the context of general medicine, (2) courses or rotations should be organized so that the student's time will not be wasted and so that he encounters both clinical laboratory studies as well as research studies, (3) each student should have clearly stated what is expected of him and should be kept apprised of his progress through appropriate evaluating methods, and (4) subjects of both the research aspects and clinical aspects should be presented enthusiastically and honestly.

During the past year the following projects have been offered through the facilities of the nuclear medicine and radiopharmacy research program at AFRRI: (1) the distribution of different radiopharmaceuticals labelled with radioactive materials including technetium-99m, bleomycin labelled with  $^{125}\text{I}$ , and  $^{57}\text{Co}$ , (2) the evaluation of the usefulness of these compounds for imaging various organ systems, (3) the assessment of the development of different radiopharmaceuticals for imaging lung, brain, blood pool, and bone, and (4) an ongoing teaching program for the Armed Services in the field of radiopharmacy with the students rotating through on a set program being administered by the chief radiopharmacist.

These projects have been well received and topics such as these will continue in the future. The aim of these topics was and has been to orient the students in such areas as the function and operation of equipment, counting statistics, and the handling and development of radiopharmaceuticals. The program is conducted in such a manner that it maximizes the students developing sufficient skills to conduct their projects with minimal supervision following an indoctrination period with faculty available for consultation and assistance as required. Each project was assigned so that it was manageable in the time allotted, allowed considerable student participation, and, where applicable, was clinically relevant. It was well noted that success or failure, however, was probably directly related to the degree of interest and enthusiasm of the faculty involved as well as the students.

At the conclusion of each project, the data are compiled and analyzed. After discussion with each project coordinator, the data are presented by the student to the



entire staff. This permits students to gain experience not only in organizing, developing, and executing the project, but also in presenting the results from that project to the entire group.

We in no way imply that the approach we have developed here at AFRRI in coordination with the National Naval Medical Center is the one which should be followed in all nuclear medicine teaching. It has worked effectively in our institutions to date. The integration of the nuclear medicine research and clinical facilities is an excellent way to not only expand the skills and knowledge of the faculty, but also to develop a continuing education program for those interested in the field of nuclear medicine.

♦♦♦♦♦♦♦♦♦♦

## **LEAD SHIELD TO IMPROVE DETECTION OF HIGH-ENERGY PHOTONS BY SCINTILLATION CAMERAS**

**Principal Investigator: J. S. Stevenson**

With the recent surge of interest in myocardial imaging using annihilation photons of 511-keV energies, a method for detecting these photons using the presently available scintillation cameras is needed. Positron cameras are available; however, these are costly and difficult to obtain. Therefore, a simple shield was developed for the readily available pinhole collimator for the Nuclear-Chicago HP scintillation camera in our laboratory. This report describes the construction of such a collimator and discusses the specific aspects of the collimator design for improving the imaging of annihilation photons.

Following several routine examinations of the pinhole collimator, using potassium-38 as a 5-keV annihilation photon emitter, it was found that the design of the present pinhole collimator had several disadvantages. First, by holding the radiation source in the field of view of the collimator and moving the source laterally around the sides of the collimator, it was noted that large amounts of the emitted photons penetrated its walls and interacted with the 1.3-cm thick NaI(Tl) crystal of the camera, i.e., reflected by little change in count rate. It was especially evident that a large amount of the emitted radiation leaked through at the junction between the camera head and the collimator.

Anger and Davis previously showed that the probability of photopeak interaction with the 1.3-cm thick NaI(Tl) crystal of the Anger camera is approximately 17 percent.<sup>1</sup> Therefore, since a small amount of the emitted photons interact with the crystal, and since a large amount of the emitted photons penetrate the pinhole collimator, a lead

shield was designed to cover the collimator to prevent photon penetration. The design of this lead shield had to take into consideration the fact that potassium-38 decays by emitting 2.68 MeV (maximum) positrons with a 7.7 min  $T_{1/2}$  (half-life), and that 200 percent of the 511-keV annihilation  $\pm$  gamma rays are available for imaging. The shield covering the crystal needed to be thick enough to absorb not only the penetrating 511-keV energy radiation, but also the 2.68 MeV positrons. In addition, since it was found that a significant amount of photon leak occurred at the collimator-scintillation camera head junction, the lead shield had to be designed to cover that portion of the collimator. A large amount of lead, calculated to be approximately 4 cm thick, was needed since the calculated half-thicknesses for these annihilation radiations from potassium-38 are approximately 4.3 cm for NaI, 7.2 cm for water and 0.42 cm for lead. The weight of the shield itself would therefore be extremely heavy and thus construction of a movable cart to hold the collimator was necessary. Figure 21 shows the complete design of the shielding apparatus, including its carrying cart.



Figure 21. Pinhole collimator with lead shield and carrying cart

Our initial experiments with  $^{38}\text{K}$  have shown that the collimator does an adequate job of absorbing the unwanted radiation and, therefore, the myocardial area can be visualized.

#### REFERENCE

1. Anger, H. O. and Davis, D. H. Gamma-ray detection efficiency and image resolution in sodium iodide. *Rev. Sci. Instrum.* 35:693-697, 1964.

\*\*\*\*\*

## MEASUREMENT OF CATHEPSIN D ACTIVITY ON BIOLOGICAL SAMPLES OBTAINED FROM IRRADIATED RATS

Principal Investigators: S. L. Snyder and P. Z. Sobocinski

The objective of this study is to measure and evaluate the possible significance of cathepsin release from cell lysosomes induced by exposure to ionizing radiation. Since present techniques available for measuring cathepsin activity are crude and tedious a number of new potential techniques for measuring cathepsin activity have been investigated. We have found that a partially purified cathepsin preparation obtained from bovine uterus hydrolyzes certain N,N-dimethyl proteins (N,N-dimethyl hemoglobin and bovine serum albumin). These substrates are prepared by reductive methylation of their amino groups with formaldehyde and  $\text{NaBH}_4$ . The cathepsin-catalyzed hydrolysis of these modified proteins (whose amino groups have been "blocked") can be measured quantitatively by spectrophotometry at 420 nm using trinitrobenzenesulfonic acid (TNBS) reagent.<sup>1</sup> A new procedure employing TNBS for the quantitative determination of amino groups has been developed. This procedure eliminates quenching steps employed by previous investigators,<sup>1</sup> reduces background absorbance and increases the sensitivity of the method by a factor of about threefold.

### REFERENCE

1. Mokrasch, L. C. Use of 2,4,6-trinitrobenzenesulfonic acid for the coestimation of amines, amino acids, and proteins in mixtures. *Anal. Biochem.* 18:64-71, 1967.

♦♦♦♦♦♦♦♦♦♦

## A CRITICAL EVALUATION OF 1,10-PHENANTHROLINE AS A REAGENT FOR SIALIC ACID DETERMINATIONS

Principal Investigators: S. L. Snyder, N. S. Mathewson and P. Z. Sobocinski

The use of o-phenanthroline as a reagent for the quantitative determination of sialic acids has been proposed by a previous investigator.<sup>1</sup> This method was based on an increase in absorbance at 307 nm that occurred when solutions of o-phenanthroline and various sialic acids were mixed. It was postulated that the increase in absorbance resulted from the formation of specific complexes. We have found, however, that the

results obtained from the o-phenanthroline method are spurious in that the increase in absorbance at 307 nm associated with increasing concentrations of N-acetylneuraminic acid (NeuNAc) in the presence of o-phenanthroline results not from the formation of a specific complex, but rather from a shift in the pH of the medium, causing a concomitant increase in the protonated form of o-phenanthroline.<sup>4</sup>

Figure 22 shows the relationship between absorbance at 307 nm and NeuNAc concentration. These results are in substantial agreement with those of Dimitrov.<sup>1</sup> However, we have noted on this figure that increasing the NeuNAc concentration also causes substantial increases in the acidity of the medium.

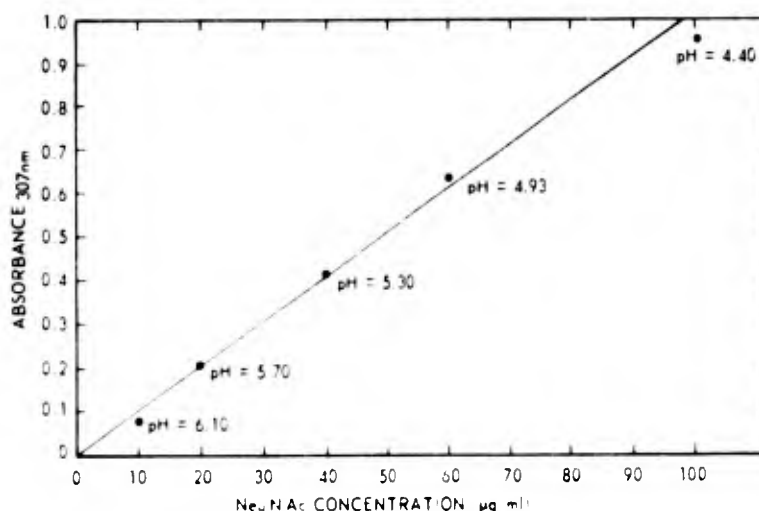


Figure 22. Absorbance at 307 nm versus NeuNAc concentration. The blank is 0.005 percent o-phenanthroline in 0.05 M NaCl at pH 7.4 (absorbance = 0.27).

These results show that the change in absorbance at 307 nm observed when NeuNAc is mixed with aqueous solutions of o-phenanthroline does not result from the formation of a NeuNAc-o-phenanthroline complex. Rather, what is observed in the spectrophotometer is the titration of the weak base o-phenanthroline (B) by NeuNAc (HA):



Since  $BH^+$  has a greater absorbance than B, increasing the concentration of NeuNAc (HA) shifts the equilibrium (equation 1) to the right and an increase in absorbance is observed. Such a phenomenon would result when any acid having a  $pK_a$  below that of  $BH^+$  was mixed with o-phenanthroline.

Employing the data presented in Figure 22 we have estimated the  $pK_a$  of the o-phenanthroline ion through the application of equation 2:

$$pK_a = pH + \log \frac{\text{Absorbance}_{\text{observed}} - \text{Absorbance}_B}{\text{Absorbance}_{BH^+} - \text{Absorbance}_{\text{observed}}} \quad (2)$$

The value obtained from our experiments of  $pK_a = 5.06$  is in close agreement with the value previously reported by Krumholz<sup>3</sup> ( $pK_a \cong 4.92$ ).

The o-phenanthroline method has been cited in a recent review article concerning the chemistry of serum glycoproteins.<sup>2</sup> On the basis of our results we recommend not using this method in experiments where there is any possibility of the presence of other acids or in experiments performed at a fixed pH. The use of o-phenanthroline as originally proposed, therefore, cannot be recommended.

#### REFERENCES

1. Dimitrov, G. D. A spectrophotometric method for qualitative and quantitative determination of sialic acid in glycoproteins and glycopeptides. Hoppe Seylers Z. Physiol. Chem. 354:121-124, 1973.
2. Heide, K. and Schwick, H.-G. Chemistry and significance of the carbohydrate moieties of human serum glycoproteins. Angew. Chem. (Engl.) 12:721-733, 1973.
3. Krumholz, P. Structural studies on polynuclear pyridine compounds. J. Am. Chem. Soc. 73:3487-3492, 1951.
4. Snyder, S. L., Mathewson, N. S. and Sobocinski, P. Z. A critical evaluation of 1,10-phenanthroline as a reagent for sialic acid determinations. Bethesda, Maryland, Armed Forces Radiobiology Research Institute Technical Note TN74-7, 1974.

◆◆◆◆◆◆◆◆◆◆

## TECHNETIUM-99m METHOD OF HIP SCANNING TO DETECT EARLY ASEPTIC NECROSIS

**Principal Investigators:** *J. S. Stevenson, AFRRl; and F. R. Nelson,  
National Naval Medical Center*

To date, ten National Naval Medical Center patients have had bilateral tomographic hip technetium scans performed.<sup>1</sup> These patients were selected by history as having a high probability of early aseptic necrosis of the hip. Their ages ranged from 20 to 62.

Technetium-99m on a sodium polyphosphate carrier was injected between 2 and 3 hours prior to the scanning procedure. The gamma camera was centered over the hip and tomographic "cuts" were then made to approximately 500,000 counts. The urinary bladder contained the greatest activity in most cases, and usually required the patient to void prior to scanning.

Once the tomographic level of interest was ascertained, it was used for both hips in identical fashion. The data were then acquired on a MED-II computer. This equipment allows for the projection of a picture on a 64 x 64 point grid, giving a total of 4096 points, from which a mathematical histogram computation can be performed for areas of interest (Figure 23). In the case of the hip scan, the areas of interest would be any point of decreased uptake of material in the presence of a surrounding area of increased uptake. It was felt that this would reflect an area of decreased bone metabolism (aseptic necrosis) surrounded by an area of increased accretion (increased bone turnover).

Of the ten patients, there were four true positives, four true negatives, and one each false negative and false positive. Although this series of patients is too small to draw any definite conclusions as to the accuracy of the method, it is apparent that it is a potentially good means of detecting the presence of aseptic necrosis prior to radiographic changes.

### REFERENCE

1. Stevenson, J. S., Nelson, F. R. and McManaman, V. L. Technetium-99m diphosphonate scintigraphy to detect early avascular necrosis of the hip. Bethesda, Maryland, Armed Forces Radiobiology Research Institute Technical Note TN74-6, 1974.

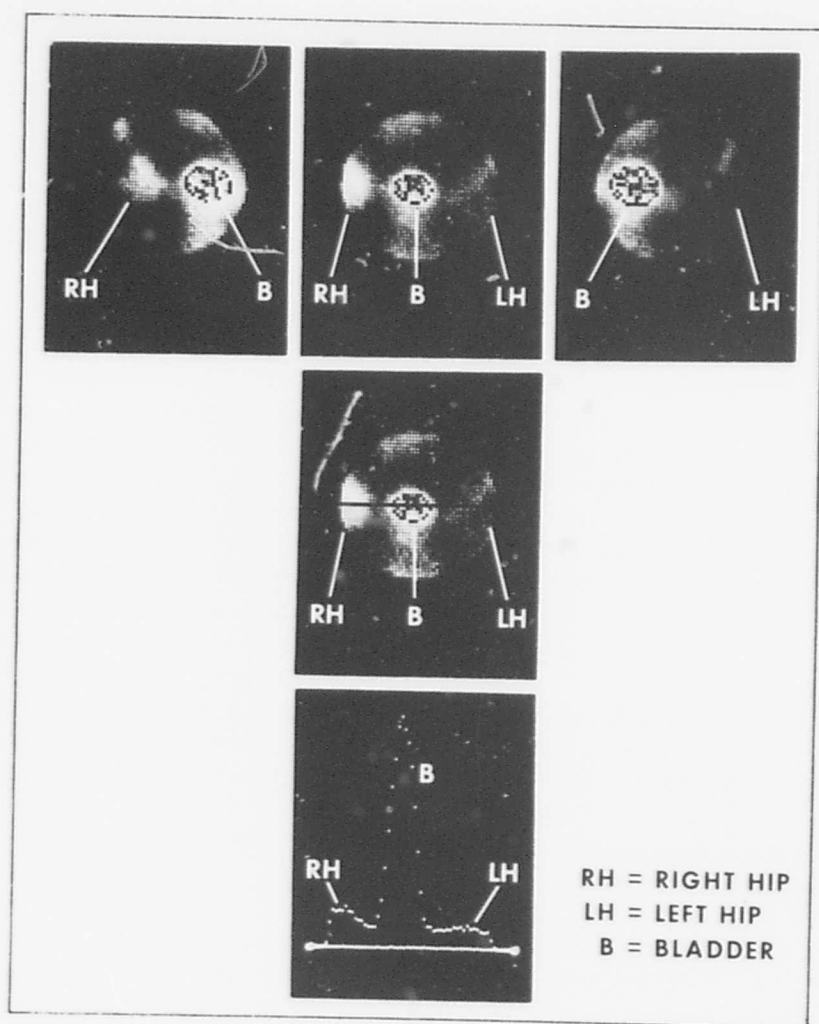


Figure 23. Computer cathode-ray tube images of both the right hip and left hip were obtained. An area of interest was chosen (linear black line in middle figure) and a histogram generated (lower figure) revealing decreased activity in the LH area as compared to the RH (the center peak on the histogram represents bladder activity) consistent with RH avascularity and the patient's response in attempting to revascularize the area.

\*\*\*\*\*

## RADIONUCLIDE ANGIOCARDIOGRAPHY

**Principal Investigators:** *V. L. McManaman and J. S. Stevenson*

**Technical Assistance:** *E. L. Barron, N. L. Fleming, M. E. Flynn  
and J. K. Warrenfeltz*

A system was developed to interface the MED-II Nuclear Data computer with the Nuclear-Chicago high performance scintillation camera with video tape store unit in order to study the passage of radioactive material through the vascular system of the brain and heart. The system consisted of the marking and selecting areas of interest on the computer cathode-ray tube with either a light pen or by utilizing a framing technique. This study to evaluate cardiac activity was accomplished by interfacing the above described equipment with an electrocardiogram such that a precise area of interest could be marked, and correlated with the electrocardiogram, allowing fast response counting rate recordings which could be used to determine the ejection fraction from the heart, not only from the entire cardiac area but from each chamber of the heart, particularly the left ventricle. From the data obtained the cardiac output was determined and recorded. In the absence of vascular insufficiency the end diastolic volume of the ventricular areas could be computed. Comparisons of the end diastolic volume obtained from the radionuclide technique and end diastolic volume determined by other techniques such as dye solution techniques, radiographic contrast media injection techniques were found to be quite similar. The main advantage of the radionuclide technique is that it is a noninvasive technique requiring only the simple intravenous injection of a radionuclide which stays in the blood vascular pool, such as technetium-labelled MAA, or technetium-99m pertechnetate, then following the passage of the radiopharmaceutical through each of the cardiac chambers with the scintillation camera and MED-II computer systems.

Clinical application of these techniques has already been demonstrated by previous authors and the ability of both radioisotope cardiography and radioisotope cerebral angiography has been found to provide a large amount of information not obtainable by other simple techniques, such as contrast media angiography. It is likely that this method will prove useful in situations requiring serial studies such as in the management of intensive care patients who have sustained cardiac abnormalities such as myocardial infarctions.

\*\*\*\*\*



## CEREBRAL AND CAROTID RADIOANGIOGRAPHY

**Principal Investigators:** *V. L. McManaman, J. S. Stevenson, AFRRl;  
and J. H. Thrall, Walter Reed General Hospital*

**Collaborator:** *M. D. Sinclair*

Utilizing the MED-II Nuclear Data computer interfaced with the Nuclear-Chicago high performance scintillation camera a quantitative imaging technique was developed to measure the rates of activity of injected intravenous radionuclides as they pass through the cerebral vascular system. Specific regions of interest over the cerebral cortex could be selected with the computer and from the data obtained the time from the initial intravenous injection of technetium pertechnetate to the time of arrival of peak activity of the radionuclide in the area of interest could be determined. By analyzing the initial slope of the curves, which described the rate of arrival of the tracer at various regions of the cortex as well as the rate of washout, and comparing them between corresponding regions over each cerebral hemisphere, a technique which has previously been described by Moses et al.,<sup>1</sup> reveal that in persons tested without evidence of cerebral vascular disease the right to left ratios of the cerebral hemispheres measured  $1.00 \pm 0.10$  (1 S.D.). Of patients studied who showed evidence clinically of cerebral vascular accidents their right to left ratios were found to be beyond the two standard deviations. This study was done in conjunction with both animal experiments and patients at the Walter Reed General Hospital, Nuclear Medicine Department. It was concluded that sensitivity of this method increases the day to day evaluation of those patients with cerebral and carotid vascular diseases, especially those sustaining cerebral vascular accidents and those with carotid arterial plaque lesions which decrease the blood flow to the cerebral hemispheres.

The studies we have done validate Moses et al.'s method. In addition, in those patients with carotid atherosclerotic disease associated with partial or complete vascular occlusion, one can determine, by evaluating them preoperatively and postoperatively, improved results in those patients undergoing repair for carotid arterial narrowing. We have shown this to be of extreme value, and have validated the impressions of Moses et al. that by interfacing a small general purpose computer and a gamma scintillation camera, additional meaningful information can be obtained on cerebral blood flow, over the routine viewing of static images, which is the routine method used in most nuclear medicine clinics today. It is hoped that with further scientific evaluations of these techniques it will become a routine procedure in clinical nuclear medicine laboratories.

## REFERENCE

1. Moses, D. C., Natarajan, T. K. and Wagner, H. N., Jr. Quantitative criteria for the interpretation of pertechnetate cerebral transit studies. *J. Nucl. Med.* 13:455 (Abstract), 1972.



## A COMPUTER SERVICE FOR ANALYZING CLINICAL SCINTIGRAPHIC DATA

**Principal Investigators:** *V. L. McManaman and J. S. Stevenson*

The advantages of a computer for the analysis of scintigraphic data have been amply demonstrated by data quantitation studies, dynamic function studies, and other general data manipulations. However, the expense of small dedicated computers prohibits most hospital clinics from having their own. Other less expensive means of analyzing scintigraphic data are usually too slow or too cumbersome for the already time-limited clinician.

As part of our developing program in nuclear medicine, a system has been assembled whereby scintigraphic data which are recorded at local hospitals may be entered into a small computer which is dedicated to clinical and research studies in nuclear medicine.<sup>1</sup> The clinical data are recorded onto videotape which is then brought to the AFRRI and replayed on a Nuclear-Chicago videotape unit which is coupled to a Nuclear Data MED-II computer system through a Nuclear-Chicago high performance scintillation camera. The data are transferred to the computer in real time, as originally recorded onto the videotape. However, once the data are stored by the computer, analysis may be done conveniently and rapidly in computer time.

Scintigraphic data may be recorded by the videotape unit, by the computer, or by both at the option of the user. The videotape unit serves not only to replay clinical data for storage by the computer but also allows the computer to be processing data off-line while the videotape unit is storing data from the scintillation camera. Although the transcription of such videotape data will employ both the scintillation camera and the computer, it can be performed by a technician during slack periods or after the normal working schedule. This arrangement provides a much more efficient use of the entire system in contrast to the situation where the scintillation camera and the computer are simultaneously engaged by one study during peak demand hours.

This totally integrated assembly consisting of the scintillation camera system and the computer system provides the capability for conducting state of the art research and for supporting a plethora of clinical studies. Once the data have been stored in the computer, the necessary analysis can be quickly performed using simple and easy to learn two-letter mnemonic instructions. The simplicity of the total assembly is such that a technician is able to operate the scintillation camera, transfer videotape data to the computer and perform all the standard computer operations. However, should he desire, the physician may personally operate the computer and perform his own data analysis. This may be done conveniently and quickly since little preparation is required to become proficient with the computer and since data analysis is done in computer time, in contrast to real time, with the videotape unit.

In addition to basic clinical and research applications, this type of integrated operation is well suited for other purposes. For example, a compendium of interesting or unusual research and clinical data can be catalogued at a central computer location for use in training programs. This gives a capability for wider dissemination and use of pertinent educational information. Physicians having a need for computer processing of clinical laboratory data from nonambulatory patients can use this system to particular advantage. Such studies may be conveniently performed within the scheduled routine of the clinic by storing the data on videotape and subsequently sending it to the computer facility for transcription and analysis.

#### REFERENCE

1. McManaman, V. L. and Stevenson, J. S. A computer service for analyzing clinical scintigraphic data. Bethesda, Maryland, Armed Forces Radiobiology Research Institute Technical Note TN73-4, 1973.



#### FACTORS AFFECTING THE DIAGNOSTIC RELIABILITY OF SCINTILLATION CAMERA FILM IMAGES

**Principal Investigators:** *V. L. McManaman, J. S. Stevenson and M. D. Sinclair*

Most data from scintillation cameras are recorded on standard Polaroid and/or 35-mm films. Without some type of data handling device, it is not possible to obtain maximum information from film data without repeating the imaging procedure. The

purpose of this work<sup>1</sup> was to demonstrate several potential weaknesses of film data which are commonly neglected and which may lead to the loss of data of significant diagnostic value.

Data were obtained using an Alderson head and skull phantom with a volume of 3500 cm<sup>3</sup> and containing a hollow ovoid shaped pseudotumor with a volume of 6 cm<sup>3</sup>. The tumor and head were filled with water and <sup>99m</sup>Tc pertechnetate (<sup>99m</sup>TcO<sub>4</sub><sup>-</sup>) at such a tumor-tissue volume normalized activity ratio (4:1) to produce a barely discernible image of the tumor on 35-mm film. Images of this phantom were recorded on 35-mm film and by the computer using the high resolution collimator and Tomocamera. In addition, a flat field flood phantom was also used to demonstrate the camera uniformity response over the surface of the detector for the pinhole and the high resolution collimators.

The 35-mm film image (Figure 24A) of the field flood phantom using the high resolution collimator reveals an obvious nonuniform response over the detector surface. These variations are made much more obvious by computer displays (Figure 24B,C) of the same image. Quantitative visualizations of vertical and horizontal profiles (Figure 24E,F) taken across the original computer image (Figure 24D) verify that these variations are clinically and statistically unacceptable. Although the 35-mm film image (Figure 24A) clearly shows a detuned camera, it would not be very difficult, solely on the basis of the 35-mm film data, in this and other less severe cases to delay tuning the camera because of the effort and time involved.

The 35-mm film image (Figure 25A) taken with a pinhole collimator and a well tuned camera reveals a slightly brighter central region due to the inverse square effect of the distance from the source to the crystal. However, the apparent difference between the central light region and the peripheral dark region does not appear to be very significant. The computer display of the same image (Figure 25B) dramatically reveals the wide count differential between these regions. A plot (Figure 25D) of the number of counts as a function of distance for a horizontal profile across the image (Figure 25C) again verifies statistically significant variations.

As a more practical consideration, the Alderson head phantom and pseudotumor were imaged with the high resolution collimator. The pseudotumor which is at a depth of 2-1/2" beneath the surface of the head is poorly visualized on 35-mm film (Figure 26A). However, the computer display of the same image (Figure 26B) clearly shows the pseudotumor well differentiated from the background activity. Using the tomography attachment to the camera<sup>2</sup> and the same phantom arrangement, the pseudotumor, which is not in a plane of focus, is again barely perceptible on the film output (Figure 26C) and yet clearly visualized on the computer display (Figure 26D).

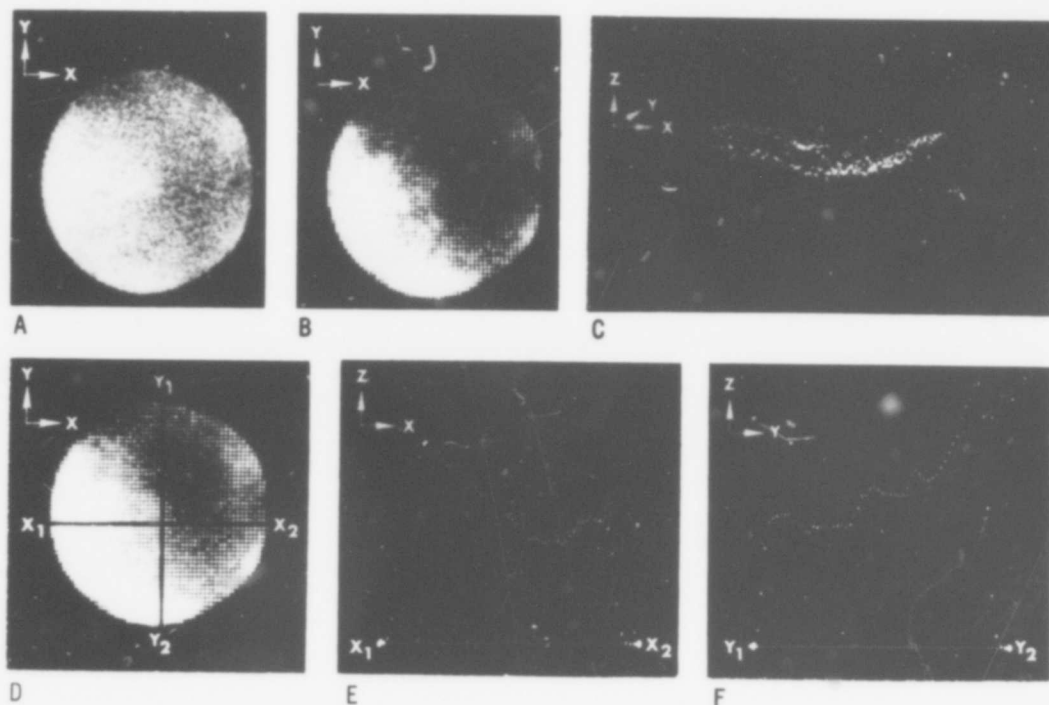


Figure 24. Field uniformity variations of flood image recorded on 35-mm film (A) are dramatically revealed by planar display (B) and isometric display (C) of same image recorded by computer. Horizontal ( $X_1$ ,  $X_2$ ) and vertical ( $Y_1$ ,  $Y_2$ ) profiles across computer planar display (D) reveal statistically significant variations (E and F, respectively) after nine-point smoothing operation.

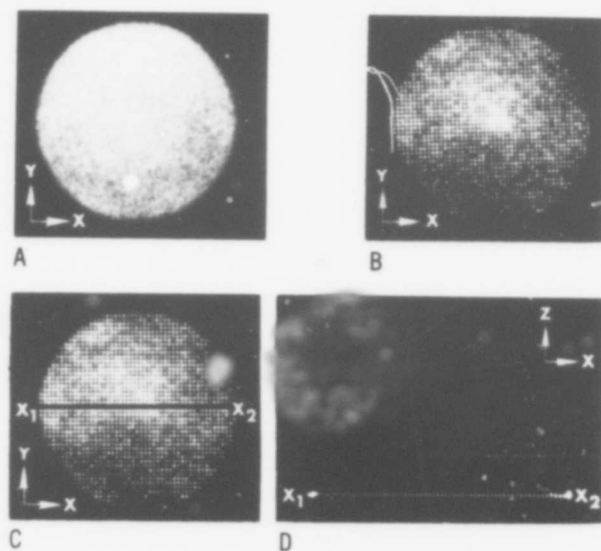


Figure 25. Field uniformity variations of flood image taken with pinhole collimator and displayed on 35-mm film (A) are more readily observed on computer planar display (B) of same image. A horizontal profile ( $X_1$ ,  $X_2$ ) across computer display (C) clearly reveals statistically significant variations (D) after nine-point smoothing operation.

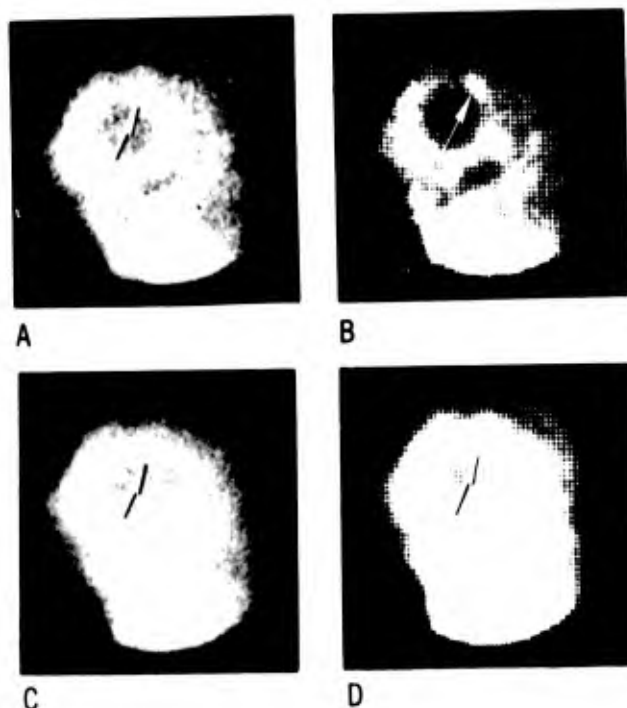


Figure 26. Image of Alderson head phantom recorded with high resolution collimator on 35-mm film (A) reveals vaguely discernible pseudotumor (↗), whereas computer display (B) provides far greater assurance of its presence (↗). Tomographic image of pseudotumor (↗) positioned at unfocused plane of interest is barely discernible on 35-mm film image (C) and clearly discernible (↗) on computer display of same image (D).

The examples presented demonstrate the potential limitations on diagnostic value when relying solely on film for displaying scintillation camera data. The advantages offered by a computer for displaying the data are clearly evident. More importantly, it is hoped that these examples serve to stress the importance of maintaining excellent quality control on imaging instrumentation particularly for those facilities which are not equipped with elaborate data handling systems. Shadows or other minor variations on field flood images which are not promptly eliminated can lead to loss in diagnostic value especially where a slightly active region of an organ is imaged at a slightly insensitive region of the detector, and vice versa. At the very least it is assured that well tuned instrumentation will provide the maximum level of diagnostic reliability, while untuned equipment alone may lead to inaccurate diagnoses.

## REFERENCES

1. McManaman, V. L., Stevenson, J. S. and Sinclair, M. D. Factors affecting the diagnostic reliability of scintillation camera film images. Bethesda, Maryland, Armed Forces Radiobiology Research Institute Technical Note TN74-1, 1974.
2. Sinclair, M. D. and McManaman, V. L. A table for quickly determining planes of focus for a scintillation Tomocamera. Bethesda, Maryland, Armed Forces Radiobiology Research Institute Technical Note TN73-19, 1973.



## EFFECTS OF IONIZING RADIATION ON PHYSICAL ACTIVITY

**Principal Investigators:** *C. R. Curran and C. G. Franz*

**Technical Assistance:** *W. R. Wiegel, C. H. Avila and L. Clark*

The objective of this study is to establish an ED<sub>50</sub> and a dose response curve for a physical activity task in a radiation field (neutron to gamma = 3.0).

Five male rhesus monkeys were irradiated at 4500 rads. All five animals exhibited an early transient incapacitation beginning 2-8 minutes postirradiation, which was consistent with observations made in prior studies. Two of the animals did not recover above 35 percent of base line during the 6-hour test period; two recovered to approximately 55 percent of base line, and one animal recovered to approximately 80 percent of base line and maintained a performance level of 70 percent of base line for the 6-hour testing period. One subject vomited 45 minutes postirradiation. Average survival time for the group was 30 hours.

An additional two animals were exposed to 2900 rads. Both animals exhibited early transient incapacitation within 6 minutes and both recovered to 90 percent of base line.



## THE INCIDENCE OF BEHAVIORAL INCAPACITATION AS A FUNCTION OF PULSED WHOLE-BODY HIGH NEUTRON RADIATION DOSE

**Principal Investigators:** *R. W. Young and G. R. Middleton*

**Technical Assistance:** *J. R. Harrison, P. Mannon, G. G. Kessell and C. A. Boward*

The objective of this study was to define the dose-response relationship for behavioral incapacitation in the monkey as a function of pulsed high neutron radiations.

Forty male monkeys, trained to a shock-avoidance visual discrimination task, were irradiated with single whole-body doses of pulsed radiations from the AFRRI-TRIGA reactor (neutron to gamma = 3.0). Ten subjects were irradiated at each of four doses: 2050, 2700, 3600, or 4500 rads midline tissue dose (MTD). The average percentage of correct responses during each minute of the 1st hour after irradiation is presented for the four groups in Figure 27.

Employing a criterion for incapacitation of 1 minute of not performing the task, the analysis of these data indicated that 30 percent of the animals were incapacitated at 2050 rads, 50 percent were incapacitated at both 2700 and 3600 rads, and 80 percent of the animals were incapacitated at 4500 rads.

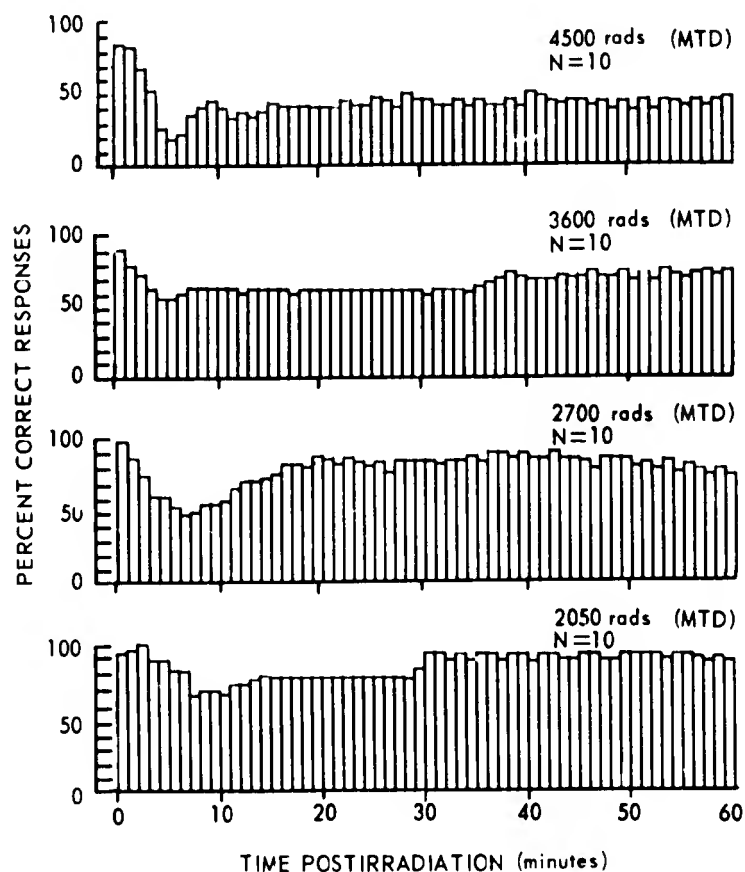


Figure 27. Mean percentage of correct responses during each minute for the 1st hour after irradiation (neutron to gamma = 3.0)

A probit analysis of these data produced an estimate of the  $ED_{50}$  equal to approximately 2700 rads (MTD). A comparison of this  $ED_{50}$ , for a field having a neutron to gamma ratio of 3.0, with the previously determined  $ED_{50}$  for a field having a neutron to gamma ratio of 0.4, strongly suggests a relative effectiveness of neutrons substantially less than 1.0 for producing behavioral incapacitation.

In addition to performance, emesis and survival time after irradiation were recorded. Thirty-six percent of the subjects vomited after exposure. With only one exception, of the 14 animals which exhibited emesis, none were incapacitated. Survival decreased as a function of increased dose. Mean survival times were 58 hours for the 2050-rad group, 16 hours for the 2700-rad group, 14 hours for the 3600-rad group and 13 hours for the 4500-rad group.

◆◆◆◆◆◆◆◆◆◆



## EMESIS FOLLOWING EXPOSURE TO IONIZING RADIATION

Principal Investigators: G. R. Middleton and R. W. Young

Technical Assistance: J. R. Harrison, P. Mannon, G. G. Kessell and C. A. Boward

Emesis has been observed in supralethally irradiated subjects shortly after exposure to ionizing radiation and again as a symptom of terminal radiation sickness prior to death. The later stage of vomiting has been described in lethality studies, but data concerning the initial phase of emesis are sparse. The purpose of this study was to determine the relationship between radiation dose and occurrence of emesis during the first 2 hours postirradiation.

One hundred and twenty-nine male rhesus monkeys (*Macaca mulatta*) were studied. The animals were trained to a simple visual discrimination behavioral paradigm and the behavioral performance data were reported previously.<sup>1</sup> The monkeys were exposed to prompt radiations (neutron to gamma = 0.4; pulse width = 50 msec) ranging from 700 to 5600 rads (midhead dose) and data collected were evaluated for incidence of emesis. The animals were fasted 18 hours preexposure and observed for incidence of vomiting for 2 hours postexposure. The percentage of animals that vomited is presented in Figure 28. For doses less than 1000 rads the number of animals that vomited increased directly with dose. Above 1000 rads, the number of animals that vomited decreased with increasing dose. The time course of the vomiting is shown in Figure 29. In all dose groups most of the emesis episodes occurred between 20 and 50 minutes postirradiation.

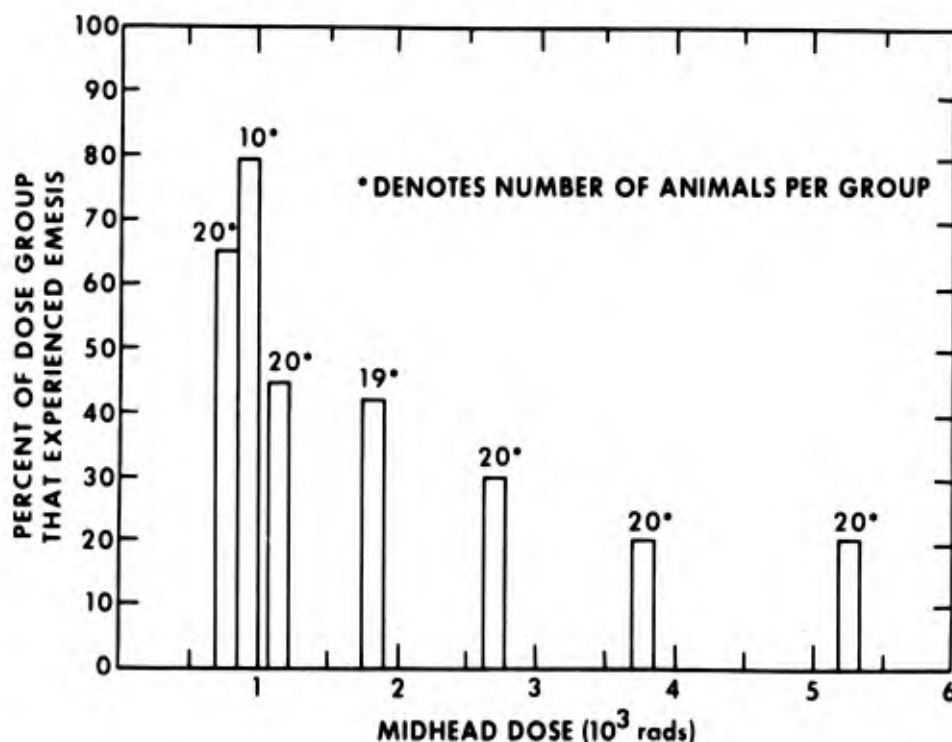


Figure 28. Incidence of emesis in the rhesus monkey after pulsed whole-body irradiation

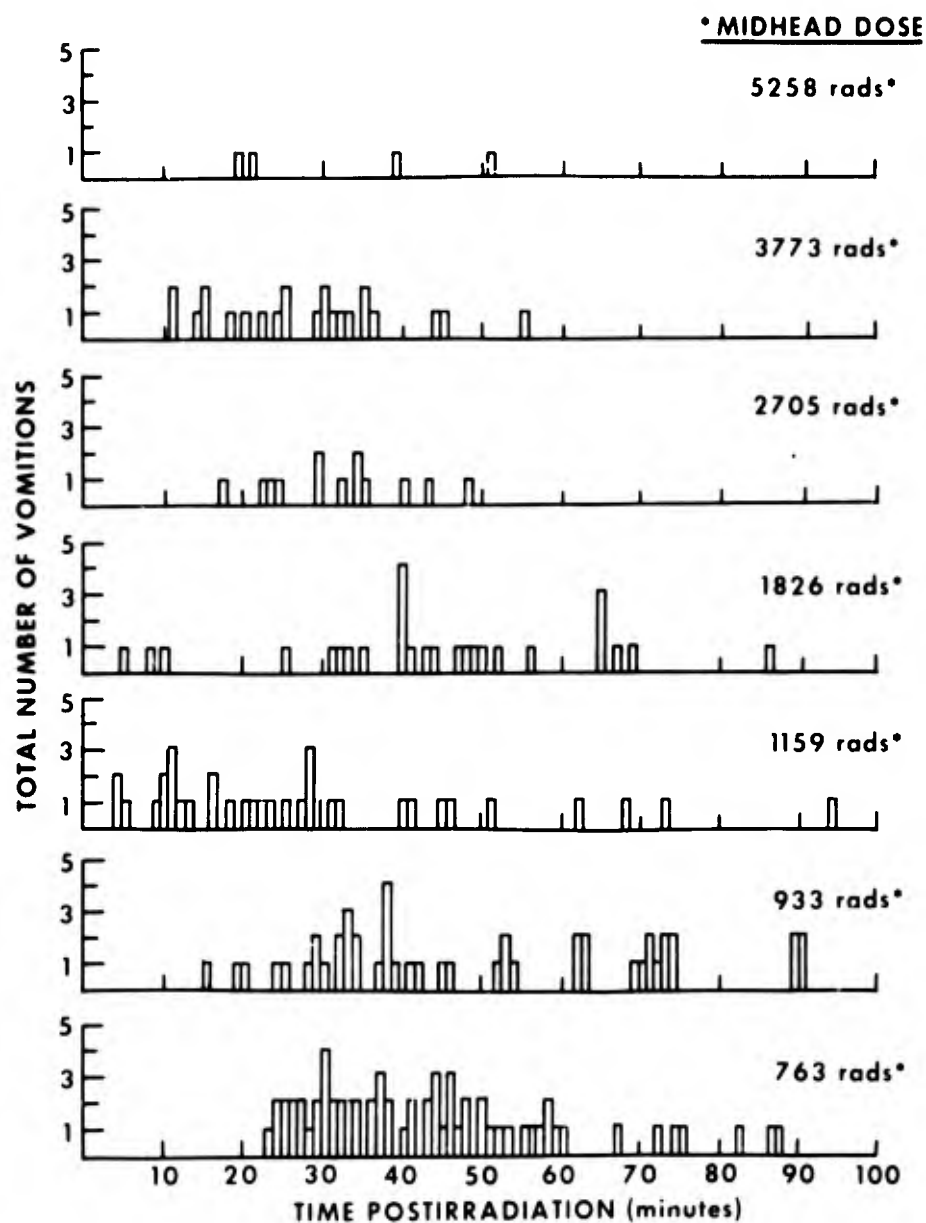


Figure 29. Time distribution of total vomition episodes in the rhesus monkey after pulsed whole-body irradiation

#### REFERENCE

1. Young, R. W. and Middleton, G. R. The incidence of behavioral incapacitation in the monkey (*Macaca mulatta*) as a function of pulsed whole-body gamma-neutron radiation dose. Bethesda, Maryland, Armed Forces Radiobiology Research Institute Annual Research Report ARR-7, 1 July 1972 - 30 June 1973.



## BEHAVIORAL TOXICOLOGY

**Principal Investigators:** *R. W. Young, G. R. Middleton, C. G. Franz and C. R. Curran*

**Collaborator:** *L. J. Jenkins, Jr., Navy Toxicology Unit*

**Technical Assistance:** *R. L. Brubaker, G. G. Kessell, AFRRl; and R. A. Jones,  
Navy Toxicology Unit*

Many current systems have as an integral part, or produce as a by-product, substances that in extremely low concentrations may significantly degrade human performance. This fact, coupled with data which indicate that significant behavioral effects may appear before clinical signs and symptoms, has led to the initiation of a study to assess the effects of possible toxic compounds on performance, using trained rhesus monkeys as a model for performance testing. The specific purpose of this study was to test the effects of chronic inhalation of three airborne contaminants on the capability of the monkey to perform a behavioral task.

Two of the compounds evaluated for possible toxicity were the dinitrates 1,2-propylene glycol dinitrate (PGDN) and triethylene glycol dinitrate (TEGDN). The third compound was an acid gas absorber, tetrahydrothiophene 1,1-dioxide (sulfolane-w).

A multiple schedule behavioral paradigm was employed to obtain the performance measures. Eight male rhesus monkeys were trained and stabilized on a discrete avoidance visual discrimination, free operant avoidance schedule. Each animal was tested for 160 consecutive days, which included 3 weeks of preexposure and 2 weeks of post-exposure testing. Six of the subjects were paired and placed in inhalation chambers where they were exposed to either PGDN, TEGDN or sulfolane for 23 hours per day for 125 consecutive days. The remaining two subjects were placed in identical inhalation chambers containing an ambient atmosphere. The free operant responding data for the control subjects are presented in Figure 30. All animals were tested for 1 hour each day for 7 days per week. A weekly blood sample was taken from each animal to permit blood-level contaminant evaluation.

One pair of subjects was exposed to successive atmospheric concentrations of TEGDN vapors at 4.5, 9.5, and 18 mg/m<sup>3</sup>. The longest exposure to a single exposure level was 91 days. Exposure to all three concentrations resulted in an increase in response latency for one of the two test monkeys on the discrete trial, cued avoidance schedule. The increase in mean response latency was not dose dependent in the range of exposures studied. Consistent with this finding was the observation that blood plasma levels of TEGDN did not change when the nominal chamber concentration of TEGDN was increased.

Two animals were exposed to successive atmospheric concentrations of PGDN vapors at 3.4, 6.8, 13.6, and 27.2 mg/m<sup>3</sup>. The longest exposure to a single concentration was 56 days. For these subjects, the plasma levels of PGDN appeared to

increase each time the chamber concentration was increased. However, avoidance behavior was not disrupted at any of the four concentrations employed in this study.

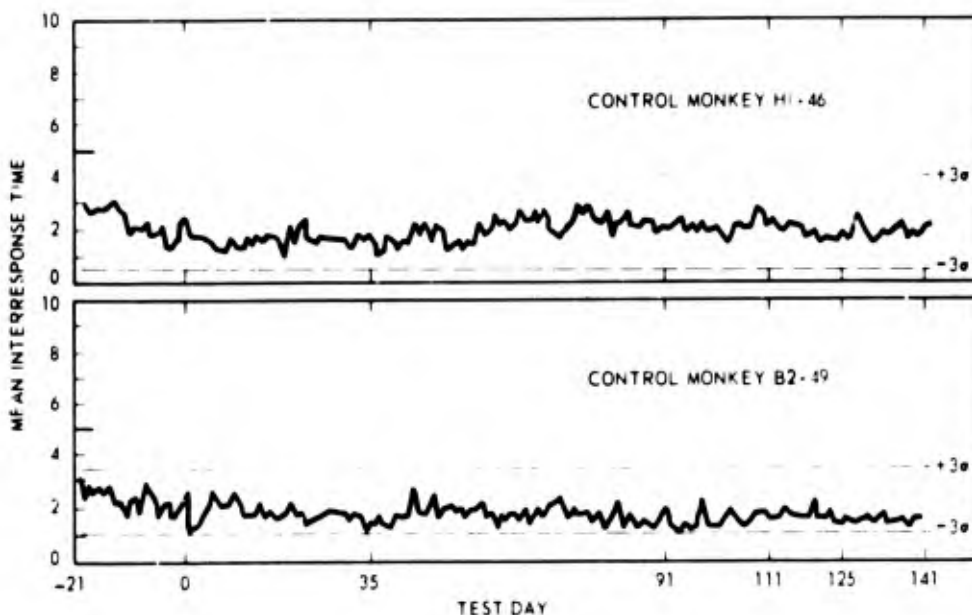


Figure 30. Free operant avoidance for control monkeys

The third pair of experimental animals employed in this study was exposed to four successive atmospheric concentrations of sulfolane vapor at 65, 130, 260, and 520 mg/m<sup>3</sup>. The free operant avoidance record for these subjects is presented in Figure 31. Exposure at 520 mg/m<sup>3</sup> resulted in significant depression of free operant responding in both subjects. A less severe, but similar, depression was also observed for both animals at a concentration of 130 mg/m<sup>3</sup>. One subject exhibited some minimum signs of behavioral effect at the lowest concentration employed (65 mg/m<sup>3</sup>). Blood plasma levels of sulfolane increased with each increment in atmospheric concentration and corresponded to the depressions observed in free operant responding. At the highest concentration (520 mg/m<sup>3</sup>), the most severe depression in operant responding was accompanied by anorexia and convulsions on one day. After this maximum excursion, neither subject exhibited further clinical signs of toxicity and both resumed more normal operant levels prior to any reduction in atmospheric sulfolane concentration. At the lower concentrations of the vapor, the effect of sulfolane inhalation appeared to be limited to a depressive influence on avoidance behavior.

Based on the profile of behavioral deviations observed in this study, the time course of the toxic manifestations would appear to be the result of a buildup of the material in the body to the point of maximum effect followed by an accommodation and dissipation process.



## THE EFFECTS OF PROPYLENE GLYCOL DINITRATE VAPORS ON VISUAL EVOKED RESPONSE AND FREE OPERANT AVOIDANCE TASK

**Technical Assistance:** *B. A. Dennison, W. N. Fry, W. R. Wiegel and C. H. Avila*

It has been reported that humans exposed to propylene glycol dinitrate at concentrations of 0.2 ppm and greater showed a disruption of the visual evoked response (VER). Higher concentrations, up to 1.5 ppm for 3 hours, caused marked impairment in balance, headaches, and eye irritation.

The objective of this research was to corroborate the human VER findings using rhesus monkeys, and to determine the VER dose effect response for propylene glycol dinitrate (PGDN).

The VER's were accomplished while the monkeys were performing a free operant avoidance task. The behavioral task minimized changes in electroencephalogram (EEG) and VER that would be due to changes in attention and alertness, and provided an objectively measured parameter other than EEG and VER.

VER's have been collected from two monkeys. One monkey was exposed to PGDN vapors at 2 ppm on three occasions, 7 ppm, and 20 ppm. Exposures lasted at least 4 hours and were separated by at least 1 week. The other monkey was exposed to PGDN vapors at 3 ppm and 10 ppm. The characteristic 3-4-5 waveform (Figure 32) of the VER's was not affected at 2 or 3 ppm. Only the 5 wave was affected at higher concentrations. Although statistically significant, the meaning of this change was unclear since the 5 wave is very vulnerable to changes in amplitude caused by changes in attention or alertness. Figure 32 shows a dramatically increased 5 wave due to covering the strobe for ten flashes before the VER was collected. Normally the strobe flashes continuously throughout the recording session. During other nontoxic manipulations of the environment, the 5 wave was again the only VER component that changed. Therefore, during PGDN vapor exposure, the 5 wave changes could not be interpreted as due to toxic CNS changes, but were probably due to the irritant effects of higher PGDN vapor concentrations.

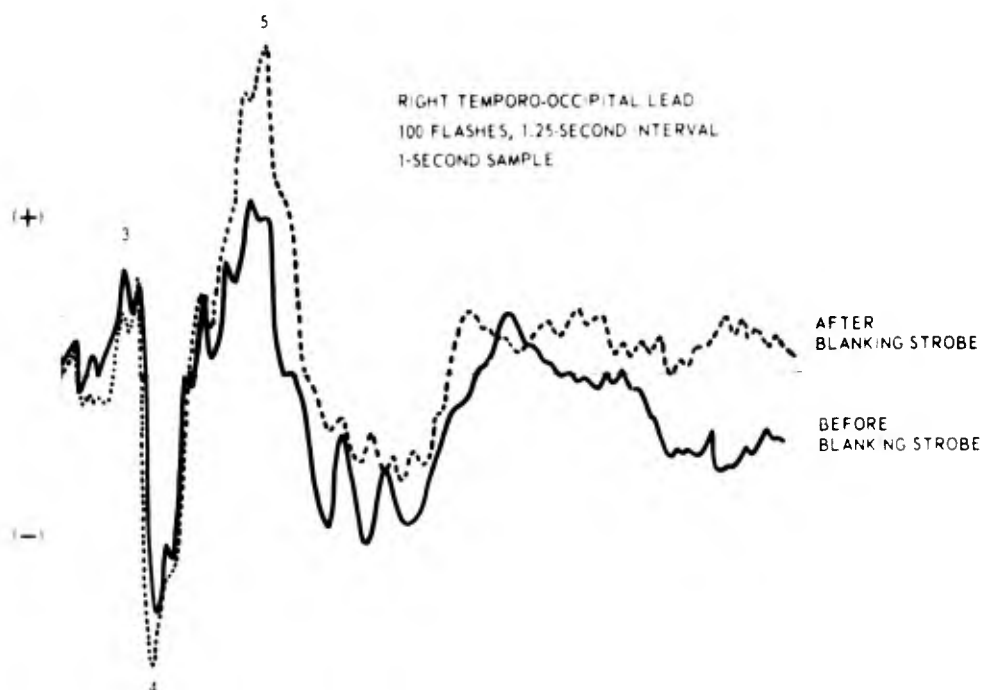


Figure 32. Visual evoked response recorded from epidural electrodes. Note the minor changes in the 3 and 4 waves, and the significant increase in the 5 wave of the VER due to increasing the monkey's interest in the strobe light by blanking the strobe just before the 100 flashes needed for the recording.

The avoidance task response rate appreciably increased at 7, 10, and 20 ppm, making it clear that both monkeys were being affected by the vapors. One monkey worked the avoidance task during his rest periods while exposed to higher fume levels, a behavior that was clearly abnormal.

Humans report eye irritation and headache during exposure to PGDN vapors, and the increased avoidance task performance of the monkeys may have been in response to comparable noxious effects of the fumes. Currently we speculate that it is the noxious effects of the fumes, rather than the neurotoxic effects, that caused changes in the 5 wave amplitude.

\*\*\*\*\*

## THE EFFECTS OF SULFOLANE ON SHOCK ELICITED AGGRESSION

**Principal Investigators:** *G. R. Middleton and R. W. Young*

**Collaborator:** *L. J. Jenkins, Jr., Navy Toxicology Unit*

**Technical Assistance:** *J. R. Harrison, AFRRl; and R. A. Jones, Navy Toxicology Unit*

Exposure to sulfolane has produced apparent aggressive behavior and convulsions in experimental animals, but reports have been based on subjective impressions and lack objective quantification. The purpose of this study was to determine quantitatively if exposure to sulfolane produces increased aggression.

Various techniques for producing aggression have been described. The procedure in this study utilized electric footshock delivered to a pair of rats, while an observer scored the number of aggressive responses. Figure 33 shows a pose of a typical aggressive response.



Figure 33.  
Pose of a typical shock-elicited  
aggressive response

Thirty male Sprague-Dawley rats were randomly paired and tested for shock-elicited aggression. Each daily session lasted 10 minutes and consisted of sixty 2-milliampere shocks of 2 seconds duration delivered at 10-second intervals. Thus, a pair of rats exhibiting 30 aggressive responses during a session received a score of 50 percent.

At the end of 2 weeks of preexposure testing, the rats were divided into a test group (nine pairs) and a control group (six pairs). The test group was exposed to sulfolane at an average concentration of  $213 \text{ mg/m}^3$  of air (standard error =  $2.0 \text{ mg/m}^3$ ) for 30 days. The only interruption in the exposure was for feeding and testing, which lasted approximately 1 hour each day. The control group was housed in an identical inhalation chamber containing an ambient atmosphere.

At the end of the 30-day exposure to sulfolane, the exposure chamber was returned to an ambient atmosphere. Testing of the control and test groups was continued for 1 week postexposure.

Previous work suggested that increased aggression would occur in the second half of the 30-day exposure. Therefore, the aggression rate data for each pair of animals were accumulated in 2-week blocks and then averaged within the control and test groups. The 2-week base-line and the 1-week postexposure testing were treated similarly (Figure 34).

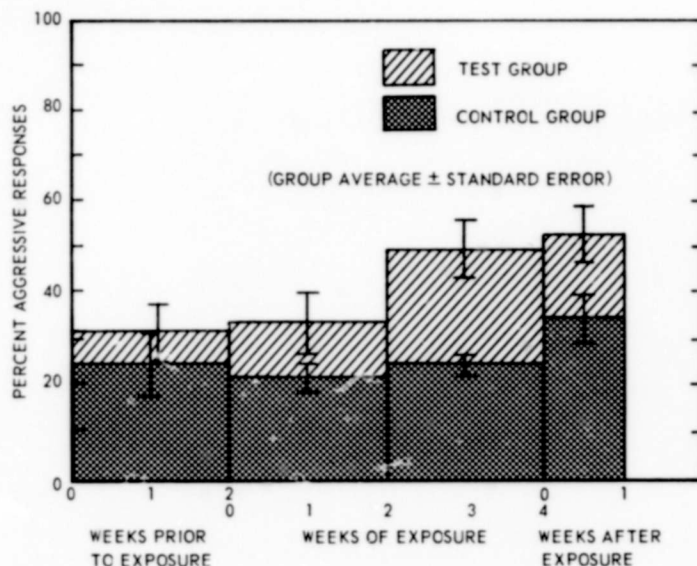


Figure 34. Aggression rate data from rats exposed to sulfolane-w



Changes observed in the aggression rate of the control group were not different from those expected from chance fluctuation at the  $p \leq .01$  level. The test group aggression rate was significantly different from its base-line level during both the second half of the exposure and the postexposure periods (paired t-test,  $p \leq .01$ ). The two groups were different from each other only during the second 2-week period of the exposure (unpaired t-test,  $p \leq .01$ ).

Additionally, in the control group during the entire study, and for the test group before and after the exposure period, aggressive responses occurred only during the period of time the rats were actually getting shocked. When an individual shock ended, the rats usually "froze" in position until the next shock was delivered and very little exploratory behavior was observed between shocks. After 10 days of exposure, one-third of the exposure group showed aggressive activity that extended beyond the duration of the shock. Fighting continued after a given shock ended, but usually stopped before the next shock occurred. This behavior was sporadic and at times during the exposure was observed in nearly one-half the test group. This extended aggressiveness was never observed in the control group, nor before or after exposure in the test group.

The observance of extended aggressions during the exposure period only and the elevated aggression rate after exposure to sulfolane strongly suggest that sulfolane may produce increased aggressiveness.



## EARLY DETECTION OF CENTRAL NERVOUS SYSTEM DAMAGE

Principal Investigators: *J. L. Mattsson and S. G. Levin*

Collaborator: *E. Miller, Food and Drug Administration*

Technical Assistance: *W. N. Fry*

At present there exists no capability of early detection of CNS damage that may be caused by contaminants such as mercury and lead in the food supply. This is a pilot effort to develop a set of parameters that will allow screening for contaminants in the food supply for early signs of CNS toxicity well in advance of overt signs of CNS poisoning.

To date, the behavioral equipment has been fabricated and tested (auditory discrimination, shock avoidance task). One dog has been surgically implanted with eight epidural electrodes, and training of the dog has begun.



## HIPPOCAMPAL BIOELECTRIC PATTERNS AND BEHAVIOR

**Principal Investigator:** *H. Teitelbaum*

**Technical Assistance:** *J. F. Lee and J. N. Johannessen*

The purpose of this study is to determine the neuroanatomical and neurochemical basis of behaviorally induced changes in hippocampal bioelectric activity.

Previous work<sup>1</sup> showed that forced movement can result in the instantaneous appearance of theta waves (6- to 8-Hz synchronous activity) recorded from the dorsal hippocampus. More recent experiments have been conducted that indicate that this behaviorally evoked response is cholinergic and is mediated by a fiber pathway originating in the medial septal nucleus. The effect of cholinergic blocking agents on this behaviorally induced bioelectric pattern is being investigated.

A biofeedback procedure has been developed whereby rats are reinforced only when 7-Hz activity monitored from the hippocampus increases at a faster rate than other frequencies in the 1 to 20-Hz range. This conditioned alteration in hippocampal EEG is cued by a light in the testing chamber.

The biofeedback procedure will be used to determine whether movement is necessary for increased generation of hippocampal theta activity, and to see if cortical theta waves can be conditioned in the absence of such bioelectric patterns in the hippocampus.

### REFERENCE

1. McFarland, W. L., Teitelbaum, H. and Hedges, E. K. Relationship between hippocampal theta activity and running speed in the rat. Bethesda, Maryland, Armed Forces Radiobiology Research Institute Scientific Report SR74-6, 1974.



## CHANGES IN BRAIN BIOELECTRICAL ACTIVITY AS A RESULT OF REPEATED MORPHINE ADMINISTRATION

**Principal Investigators:** *H. Teitelbaum, G. N. Catravas and J. C. Blosser*

**Technical Assistance:** *J. F. Lee*

EEG recording techniques and behavioral assays have been used to study the development of morphine tolerance in rats subjected to repeated systemic morphine injections.

Tolerance was manifested by a diminished EEG response at cortical and subcortical recording sites. Reversal of tolerance to morphine resulted from destruction of the medial thalamus. Lesions of the caudate nucleus and hippocampus had no effect on morphine sensitivity of tolerant rats. In a more recent experiment, it was found that lesions of the ventral tegmentum are also effective in reversing morphine tolerance. Approximately 2 months of two daily morphine injections are required for the reacquisition of drug tolerances in these animals. In another study, it has been possible to obtain morphine tolerance with direct intracerebral injections of morphine sulfate into the amygdaloid complex of the rat. Although unilateral injections of morphine caused spike and wave patterns in both amygdaloid regions, tolerance to morphine developed only at the injection site.



## MOLECULAR STUDIES OF OPIATE TOLERANCE AND DEPENDENCE IN THE MAMMALIAN BRAIN

**Principal Investigators:** G. N. Catravas, J. Takenaga and C. G. McHale

**Technical Assistance:** M. J. Iadarola

Earlier results in this laboratory<sup>1</sup> indicated morphine-induced changes in the activity of monoamine oxidase (MAO) in discrete brain regions of the rat differed depending on whether the animals exhibited tolerance syndromes (hyperactivity, gnawing, etc.) or not, shortly after the last administration of the drug. More specifically, it was found that in rats which exhibited these syndromes, MAO activity was markedly reduced with lowest values at 30 to 60 minutes after the last morphine injection, whereas in animals that did not, MAO activity was not much affected. Based on previous observations that brain mitochondria, depending on their size, contain more of the one MAO form than of the other and that these forms (A and B) have different substrate specificities, experiments have been started to separate these forms using gradient density centrifugation and to determine if and to what extent they contribute to the activity differences observed between rats showing the tolerance syndromes and animals that do not, and which form is more susceptible to morphine. Collected thus far, data of preliminary experiments are being evaluated. Previous experiments have shown that during the time the animals exhibited the tolerance syndrome (first 30 minutes after last morphine injection), choline acetyl transferase activity was markedly increased whereas no appreciable changes were observed in cholinesterase activity. Preliminary experiments with rats chronically treated with morphine and euthanatized 30 minutes after the last injection have shown increases in the levels of acetylcholine

in the cerebrum and cerebellum, brain areas which are involved in motor activity and coordination of movement, whereas hippocampal acetylcholine appeared to be decreased (Table XV).

Table XV. Acetylcholine Levels in Discrete Brain Areas of Morphine Tolerant Rats Euthanatized 30 Minutes after the Last Injection of the Drug

Brain area	Acetylcholine (nmoles/100 mg brain tissue)	
	Morphine	Controls
Cerebral cortex	4.26 $\pm$ 1.7	3.20 $\pm$ 1.5
Cerebellum	2.70 $\pm$ 0.3	1.17 $\pm$ 0.4
Hippocampus	4.03 $\pm$ 0.7	6.20 $\pm$ 0.8

Based on our earlier observations that a number of chronically morphinized rats exhibited pronounced tolerance syndromes, whereas others did not, attempts are being made to breed strains of rats sensitive and also resistant to morphine and determine the underlying macromolecular causes of these differences. A male and a female rat, both of which on becoming tolerant exhibited strong tolerance syndromes, were mated. Progeny resulted. First and second progenies are being tested for sensitivity to morphine.

Methodologies are being worked out for the development of tolerance by subcutaneous implantation of morphine pellets. To control rate of absorption of the drug and therefore development of tolerance, various materials are being tested as "carriers" and for consistency of the pellet.

#### REFERENCE

1. Catravas, G. N., McHale, C. G. and Cohan, S. L. Morphine-induced changes in the activity of enzymes involved in neurotransmitter metabolism in specific brain regions of the tolerant rat. Bethesda, Maryland, Armed Forces Radiobiology Research Institute Scientific Report SR74-9, 1974.



## NEURONAL AMINO ACID METABOLISM

**Principal Investigators:** *G. H. Zeman and G. N. Catravas*  
**Collaborator:** *P. Z. Sobocinski*

Micromethodologies are being worked out using a sensitive amino acid analyzer to assay amino acids spectrophotometrically in the picomole range. This technique will be used to measure postirradiation changes in brain amino acid patterns and determine whether brain amino acids play a role in the neurologic radiation syndrome.

Groups of male rats weighing 240 to 260 grams were exposed to 20,000 rads of ionizing radiation from the AFRRI LINAC. The irradiated animals were euthanatized by decapitation at 2, 5, 20 minutes, 1, 3 or 4 hours postexposure. Sham irradiated control rats were also decapitated. Experiments are in progress to isolate and purify the brain amino acids before assaying them in the amino acid analyzer.



## CEREBRAL BLOOD FLOW IN EXPERIMENTAL SUBARACHNOID HEMORRHAGE

**Principal Investigators:** *A. N. Martins, A. I. Kobrine, T. F. Doyle and N. Newby*  
**Technical Assistance:** *W. L. Stringfield*

It is widely assumed that when blood suddenly enters the intracranial subarachnoid space, as when a berry aneurysm ruptures, the vessels of the circle of Willis respond with spasm. This vasospasm is believed to be an important determinant of the mortality and morbidity associated with ruptured aneurysm. The vasospasm is assumed to produce ischemia in the field supplied by the spastic arteries. There is much experimental and clinical evidence to support the preceding assumptions.

The cause of the vasospasm is assumed to be a spasmogenic agent in the blood, perhaps serotonin. Since bloodborne spasmolytic agents are ineffective, we proposed to use spasmolytic agents intracisternally to reverse the spasm.<sup>1</sup>

We perfected a stereotaxic technique of injecting autologous whole blood into the chiasmatic cistern of rhesus monkeys which were prepared so that we could measure cerebral blood flow (CBF) before and after the simulated subarachnoid hemorrhage (SAH) by the hydrogen clearance technique.

We expected to be able to demonstrate a reduction in CBF, and then go on to test the effect of phentolamine, a patent alpha-adrenergic blocking agent, on CBF after

SAH. Unexpectedly, we found that in our model, after SAH, CBF did not decrease, but instead gradually increased during the 5 hours after the SAH. Control animals also showed a gradually increasing CBF, which is probably an artifact of anesthesia. Table XVI summarizes the data.

Table XVI. Effect of Subarachnoid Hemorrhage (SAH) on Cerebral Blood Flow\*

	Time (hours)					
	Before SAH	After SAH				
	1	1	2	3	4	5
Experimental (N = 8)	58 ± 13	64 ± 21	67 ± 20	71 ± 26	67 ± 25	66 ± 20
Control (No SAH) (N = 5)	56 ± 20	66 ± 12	66 ± 17	62 ± 11	61 ± 8	58 ± 9

\* All figures ml/100 g per min ± S. D.

These data suggest that although fresh blood in the subarachnoid space may indeed cause a constriction of blood vessels, this constriction is not hemodynamically significant. Perhaps other factors such as brain edema or intracranial hypertension are responsible for the spreading ischemia of a SAH. Additional experiments are underway to further define these mechanisms.

## REFERENCE

1. Martins, A. N. and Wiley, J. K. Side effects of spasmolytic agents in the monkey: intracisternal phenoxybenzamine and phentolamine. J. Neurosurg. 39:629-635, 1973.



## EXPERIMENTAL POSTIRRADIATION MYELOPATHY

**Principal Investigators:** J. M. Fein, AFRRl; and G. Di Chiro, National Institutes of Health

**Technical Assistance:** L. J. Parkhurst

While its pathophysiology remains obscure, postirradiation myelopathy remains a significant neurologic problem. To differentiate between vascular and direct parenchymal injury after spinal cord irradiation, 14 rhesus monkeys were exposed to pulsed doses of radiation, utilizing the linear accelerator, delivered every other day for a total dosage of 4,000 to 10,000 rads. Six animals were monitored by neurologic examination, preirradiation and postirradiation angiography, postmortem microangiography and histology (Table XVII).

Table XVII. Fractionation Table for Rhesus Monkeys Irradiated Through a 10 x 3 cm Portal Centered over the T11-12 Vertebral Interspace

Animal	Paraparesis	Single dose (rads)	Number of exposures	Total dose (rads)	Start-finish radiation (days)	Postirradiation interval
0617	+	1,002	10	10,026	25	132
P-547	+	1,000	10	10,000	26	213
P-183	+	399	15	5,982	38	268
0718	-	399	15	5,981	35	87
836	-	252	24	6,050	74	251
677	-	252	24	6,047	59	243

After a latency of 6-8 months, sensory-motor paraparesis developed rapidly in three monkeys over 24-48 hours with marked loss of urinary bladder tone. Selective spinal cord angiography after irradiation disclosed nonfilling of major radicular feeding vessels of the artery of Adamkiewicz with collateral filling from arteries outside the radiation field. Histologic examination, however, disclosed demyelination of all long tract systems with no evidence of ischemic infarction. While the changes in larger lumbar arteries (200-600  $\mu$ m) are present after irradiation, the presence of adequate collateral supply to the thoracolumbar spinal cord provides for an intact arterial microarchitecture.



## EFFECTS OF IONIZING RADIATION ON SINGLE AND SIMPLE NERVE NETWORKS IN APLYSIA CALIFORNICA

Principal Investigators: J. A. Willis and D. O. Carpenter

In an attempt to elucidate the mechanisms underlying central nervous system dysfunction following ionizing radiation, experiments were carried out in the isolated abdominal ganglion of the marine gastropod Aplysia californica. Specimens were mounted in front of a collimated linear accelerator beam and exposed to varying numbers of 1200-rad pulses of 20 MeV electrons. Intracellular micropipettes were used to make simultaneous recordings of intracellular potential and membrane resistance. Synaptic potentials were recorded by stimulating connective nerve trunks known to make synaptic connections with the cells under study.

As previously reported, a consistent transient increase in pacemaker activity is found during the first 30 seconds following irradiation, and to some extent this increase is dose dependent. The mechanism underlying this increase was not discovered however. Membrane resistance, as measured by the change in membrane potential during intracellular current passage, did not change markedly during the transient increase in activity. Similarly, no noticeable change in the amplitude or duration of inhibitory postsynaptic potentials or excitatory postsynaptic potentials was noted, although there was some increase in their frequency during the transient excitation period, a finding consistent with transient activation of many pacemakers in the ganglion following irradiation. Inhibition of the electrogenic sodium pump with  $10^{-4}$  M ouabain did not abolish the transient response showing that the increase in firing following irradiation was not due to transient inhibition of the electrogenic pump. While the mechanism underlying the transient response of these cells to ionizing radiation is not yet understood, it is possible that this effect is important in the genesis of the early transient incapacitation seen in higher animals.

Spiking activity in most preparations was seen to continue following acute doses of up to 1 Mrad. Deterioration of the preparation over several hours occurred at much lower cumulative doses, 100 krads (see Figure 35). These data support the hypothesis that neuronal death following ionizing radiation occurs due to derangement of cellular metabolism rather than due to direct effects on the integrity and function of the excitable membrane.



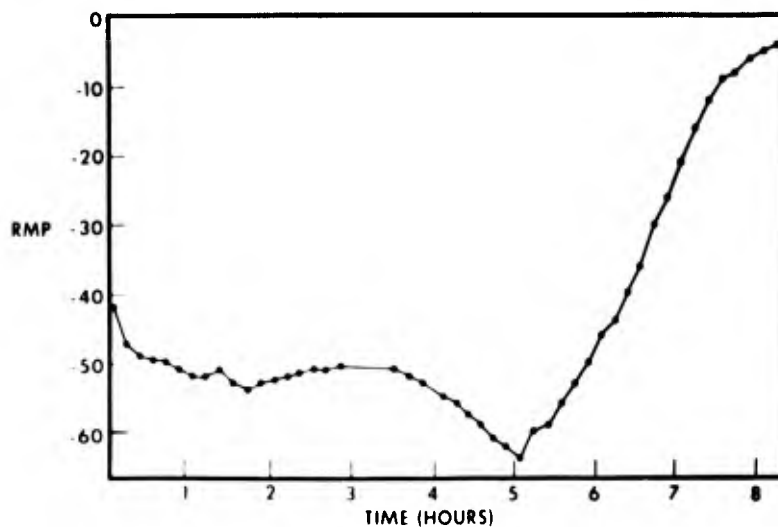


Figure 35. Resting membrane potential versus time postirradiation (100 krad)

\*\*\*\*\*

## CEREBRAL ISCHEMIA: LOCAL OXYGEN UTILIZATION AFTER MIDDLE CEREBRAL OCCLUSION

Principal Investigator: J. M. Fein

Technical Assistance: L. J. Parkhurst

Hemodynamic studies have previously demonstrated the augmentation of blood flow to the canine ischemic cerebral hemisphere after superficial temporal to middle cerebral cortical grafting. The increase in blood flow noted was significant when grafts were placed in proximity to the site of occlusion. In this study the regional changes in oxidative metabolism which might account for the specific effectiveness of a proximal graft were studied.

A polarographic circuit was utilized in nine dogs to obtain steady-state levels of oxygen availability after which a period of transient complete ischemia produced a slope proportional to the local oxygen extraction rate (LOER) and expressed as  $\Delta$  voltage/time. The mean LOER for 37 control determinations was  $1.4 \mu\text{V}/\text{sec}$  (see Figure 36). The onset of proximal middle cerebral artery clip occlusion was accompanied by a brief increase and a more sustained decrease in central LOER, and a frequent increase in peripheral LOER (see Figure 37). The different rates of oxygen extraction between these regions may reflect the presence of increased cortical functional activity at the periphery of an infarct. With the passage of 2-5 hours these differences in LOER were less marked although some regions retained an increased rate through 7 hours postocclusion.

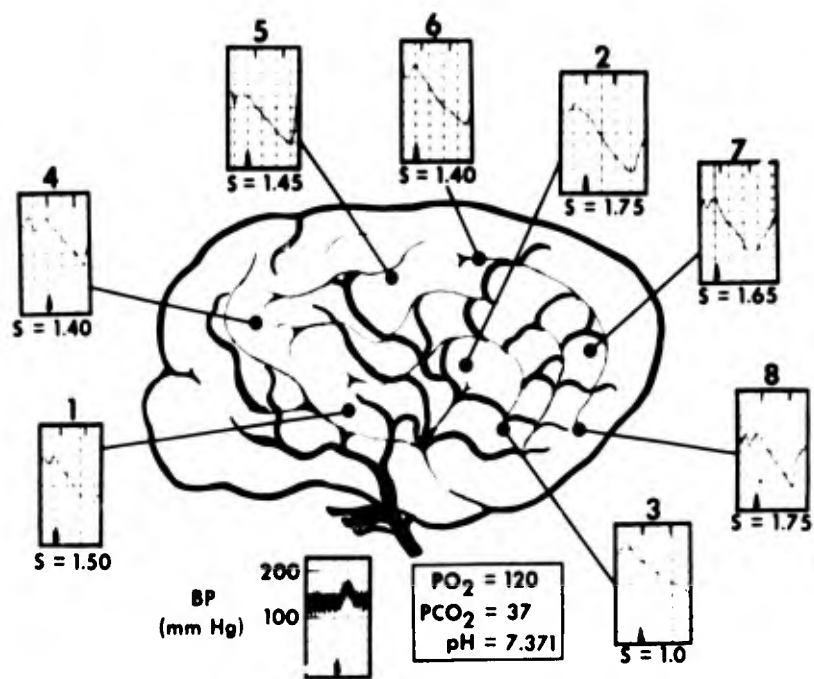


Figure 36. Local oxygen extraction rate

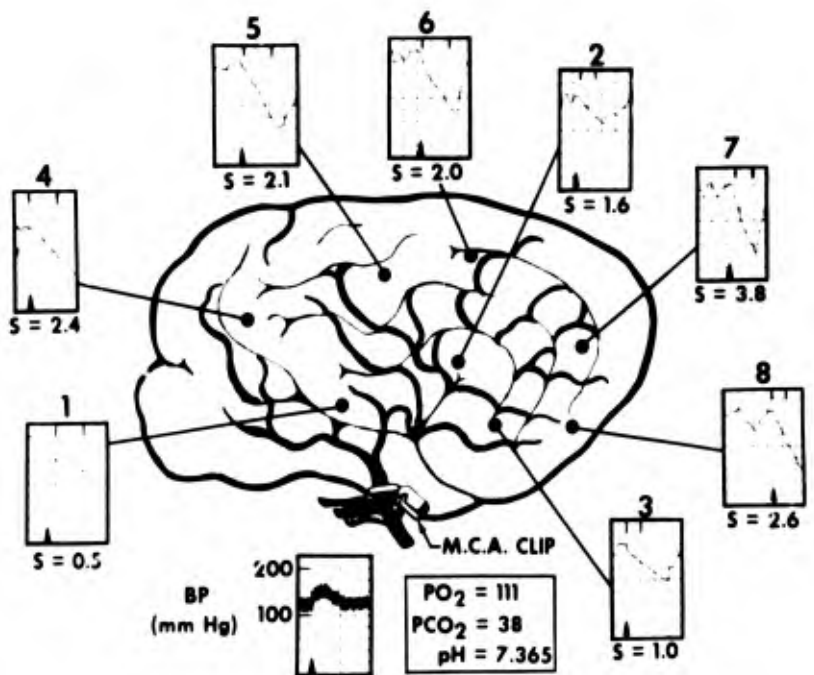


Figure 37. Local oxygen extraction rate after proximal middle cerebral artery clip occlusion



## CEREBRAL VASOSPASM

Principal Investigator: J. M. Fein

Technical Assistance: L. J. Parkhurst

The alterations of energy metabolism after subarachnoid hemorrhage (SAH) were evaluated in 26 rhesus monkeys. In the isobaric group (normal cisternal pressure), CSF lactate-pyruvate ratios, and cerebral metabolic consumption rates for oxygen ( $CMRO_2$ ) and glucose ( $CMR_{gluc}$ ) were consistent with an early decrease of both aerobic and anaerobic metabolism. Cerebral energy charge was maintained between 0.942 and 0.950. Evidence of ischemic injury and depression of energy charge were present between 1 and 5 hours after SAH. In the group with increased intracranial pressure (Figure 38) an early conversion to anaerobic metabolism was reflected in the first assays performed. Despite the accompanying decrease in cerebral perfusion pressure,

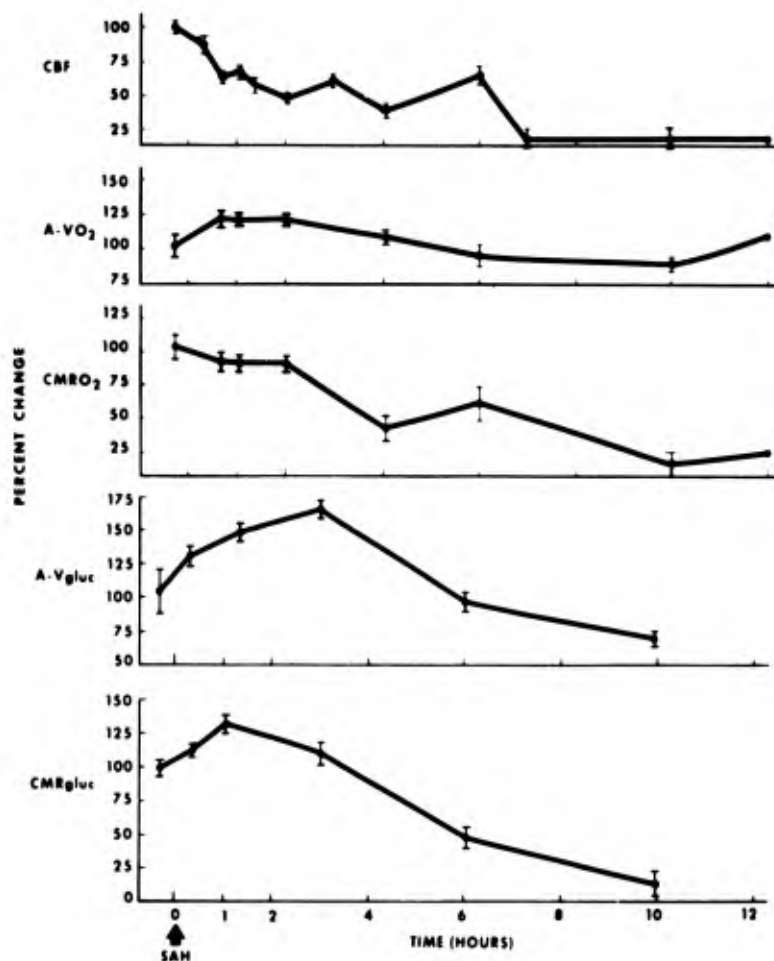


Figure 36. Cerebral blood flow and metabolism in the hyperbaric cisternal group. Intracranial pressure was allowed to rise after injection of blood and the decreased cerebral perfusion pressure was sufficient to cause a 40 to 60 percent decrease in flow between 1 and 6 hours after hemorrhage, with barely perceptible flow values thereafter. After a transient increase in anaerobic metabolism, both oxygen and glucose metabolism were depressed. A single study is indicated at 12 hours.

blood flow decreased more prominently demonstrating the probable occurrence of vaso-spasm and impaired autoregulation. Although oxygen extraction increased slightly compared to controls,  $CMRO_2$  decreased significantly. These studies indicate that the influence of cerebral metabolic requirements on blood flow rate after subarachnoid hemorrhage is restricted by the presence of intracranial hypertension.



## NEUROTRANSMITTERS IN THE NERVOUS SYSTEM OF APLYSIA

**Principal Investigators:** G. H. Zeman, P. J. Yarowsky and D. O. Carpenter

**Collaborators:** M. J. Brownstein, J. M. Saavedra and J. Axelrod,  
National Institutes of Health

**Technical Assistance:** T. K. Dalton and G. L. Gaubatz

The nervous system of the sea hare Aplysia is an ideal preparation for the study of neurotransmitter function since single nerve cells are very large and a number of these cells can be identified from one preparation to the next. Thus it is possible, because of their size, to perform chemical determinations of the content of various putative neurotransmitters and, because the cells can be identified, it is possible to study the electrophysiologic response to an iontophoretic application of various transmitters. We have used both of these techniques in an effort to identify those chemicals which function as neurotransmitters in Aplysia.

To study neuronal specificity as related to neurotransmitters we have investigated aspects of the functions of gamma-aminobutyric acid (GABA), glutamate and aspartate. These studies have included measurements of the distributions of these compounds in the Aplysia nervous system, characterization of the active transport mechanism by which some Aplysia ganglia accumulate these compounds from the extracellular milieu and electrophysiologic responses to these compounds.

GABA was detected in each Aplysia ganglion examined and in the foot muscle. Aspartate and glutamate were present in greater concentrations in nervous than nonnervous tissues, but, while ganglion glutamate concentrations were nearly equal, aspartate concentrations varied over twofold among the ganglia. Since GABA has not previously been considered to function as a neurotransmitter in molluscs, and because the aspartate content of the ganglia varied over a wide range, these two amino acids were studied further on a single neuron basis.

The GABA and aspartate content of selected Aplysia neurons is shown in Table XVIII. Each identified neuron examined contained GABA in greater than millimolar concentrations, and aspartate at concentrations ranging from 22 to 90 mM. An apparent correlation existed between the GABA and aspartate content of individual neurons, suggesting that these two amino acids may be involved in some complementary physiological function in nervous tissues.

Table XVIII. GABA and Aspartate Concentration (millimolar) in Identified Aplysia Neurons

	GABA	Aspartate
Abdominal ganglion		
L2-L6	1.3 ± 0.2	28 ± 3
L7	2.0 ± 0.2	34 ± 7
L11	1.4 ± 0.2	44 ± 4
R2	1.8 ± 0.3	25 ± 4
R3-R13	2.7 ± 0.8	22 ± 3
Buccal ganglion		
B1	5.7 ± 0.7	49 ± 6
B2	3.3 ± 0.4	85 ± 9
B4-B9	8.0 ± 1.7	90 ± 22
Cerebral ganglion		
C1	4.1 ± 1.3	34 ± 5
Pleural ganglion		
LPGC	1.6 ± 0.4	34 ± 5

The neurons of the buccal ganglion contained the greatest endogenous GABA concentrations. This ganglion was also found to be capable of accumulating exogenous GABA to a greater extent than were other ganglia (Table XIX). This accumulation was mediated by a high affinity, sodium dependent, temperature sensitive uptake mechanism which appeared to be located primarily in extraneuronal (glial) structures within the ganglion. These findings, together with other electrophysiologic results have led us to hypothesize that GABA may function as a neurotransmitter in the buccal ganglion of Aplysia. Further studies of this model nervous system are in progress.

Ganglion	Tissue:medium ratio
Buccal	20.0
Pleural	14.0
Abdominal	8.5
Cerebral	7.1
Pedal	1.7

Table XIX.  
Tissue:Medium Ratios for the Na<sup>+</sup> Dependent Accumulation of GABA by Aplysia Ganglia Incubated in 6  $\mu$ M <sup>14</sup>C-GABA

Table XX shows the content of seven different substances measured in four of the identified cells of Aplysia. Several things are remarkable. Classically it has been assumed that a given nerve cell contains only one neurotransmitter. However, in each of these four cells all of the assayed substances, with the exception of dopamine and norepinephrine, have been found in measurable quantity. The presence of multiple transmitters in the same cell does not prove a neurotransmitter function for these substances but the presence of such specific and unusual compounds is very suggestive as an indication that Dale's principle is not valid in Aplysia neurons. This is to suggest that a single nerve cell may synthesize, transport and release more than one neurotransmitter.

Table XX. Putative Neurotransmitters in Identified Neurons of Aplysia

	R2	R14	L11	C1
Serotonin	$1.8 \times 10^{-5} \pm 0.3$ (8)	$3.4 \times 10^{-5} \pm 1.2$ (5)	$1.1 \times 10^{-5} \pm 0.3$ (4)	$9.4 \times 10^{-4} \pm 3.1$ (10)
Histamine	$3.0 \times 10^{-6} \pm 0.5$ (5)	$7.0 \times 10^{-6} \pm 3.0$ (4)	$4.5 \times 10^{-6} \pm 0.7$ (4)	$1.4 \times 10^{-5} \pm 0.1$ (5)
GABA	$2.0 \times 10^{-3} \pm 0.3$ (4)	$4.0 \times 10^{-3}$ (1)	$1.3 \times 10^{-3} \pm 0.2$ (3)	$2.3 \times 10^{-3} \pm 0.6$ (4)
Octopamine	$2.5 \times 10^{-6} \pm 1.0$ (5)	$1.5 \times 10^{-4} \pm 0.5$ (5)	$1.4 \times 10^{-5} \pm 0.6$ (5)	N. D. (5)
Dopamine	N. D. (6)	N. D. (6)	N. D. (3)	--
Norepinephrine	N. D. (6)	N. D. (6)	N. D. (3)	--
Aspartate	$2.5 \times 10^{-2} \pm 0.4$ (10)	$2.7 \times 10^{-2} \pm 0.3$ (4)	$4.4 \times 10^{-2} \pm 0.4$ (8)	$3.4 \times 10^{-2} \pm 0.5$ (9)

Figure 39 shows an electrophysiologic experiment in which we have passed by iontophoresis four different substances into the region of the normal synaptic contacts on a single cell in the cerebral ganglion. In this case the cell was very responsive to octopamine, slightly responsive to phenylethanolamine and norepinephrine, but totally unresponsive to dopamine. The receptor in this cell thus appears to be specific for octopamine and this observation, plus the content of octopamine in whole ganglia and single cells, presents strong evidence for a role of octopamine as a neurotransmitter. We have obtained similar electrophysiologic data suggesting that dopamine, phenylethanolamine, histamine, serotonin and GABA all have roles as neurotransmitters in addition to that played by acetylcholine. Furthermore, for each of these substances three kinds of responses can be detected in different cells. These responses are due to conductance changes to sodium, chloride and potassium. Thus it would appear that each of these substances can function as either an excitatory or an inhibitory neurotransmitter, depending upon which ionophore the receptor is coupled with.

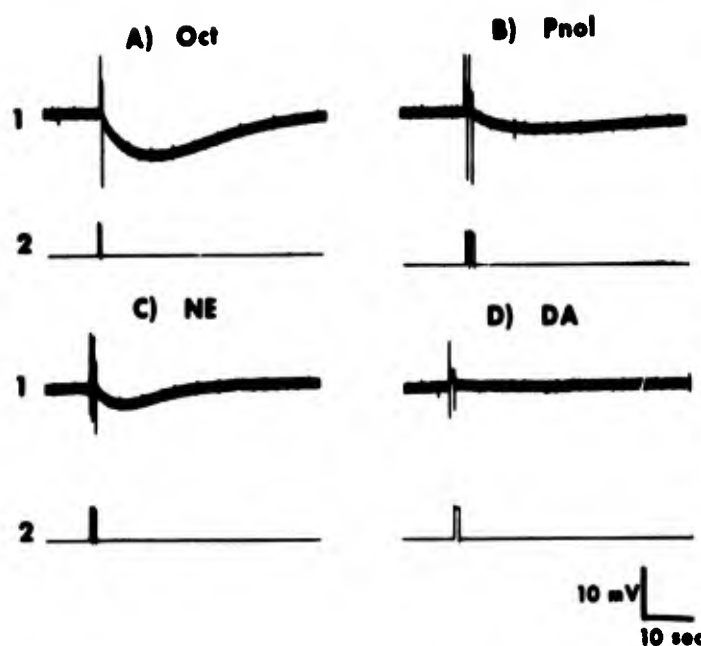


Figure 39. Intracellularly recorded responses (upper traces) to iontophoretic application of octopamine (Oct), phenylethanolamine (Pnl), norepinephrine (NE) and dopamine (DA) to a neuron in the cerebral ganglion. Pulses are indicated in the lower trace, where total charge passed was 1000 nC for Oct and DA and 2000 nC for Pnl and NE.



## CELL CULTURE OF NEURONAL TISSUES

**Principal Investigators:** W. G. Shain, Jr., P. R. Myers, R. A. Morantz and E. S. Chock

**Technical Assistance:** B. J. Bolden

This research has been divided into three different areas: (1) the development of new neuronal and glial cell lines, (2) the analysis of cell lines for neuronal characteristics, and (3) the development of cell culture models for studying synapse interactions.

Development of neuronal and glial cell lines. Since most neuronal cell lines are derived from transformed cells and as such demonstrate a certain heterogeneity in their genetic and phenotypic expression, it is of paramount importance to develop and use selective systems to obtain homogeneous cell lines. Recently Breakefield and Nirenberg<sup>1</sup> and Greene et al.<sup>3</sup> have demonstrated that cells with high tyrosine hydroxylase activity can be isolated by culture of heterogeneous cells in media lacking the amino acid tyrosine. Because this enzyme will also hydroxylate phenylalanine to make

tyrosine, cells with sufficiently high tyrosine hydroxylase activity will survive and divide while other cells will not. A number of cell lines have been isolated from the sympathetic ganglion cell  $\times$  neuroblastoma somatic cell hybrid X31. From Table XXI it is possible to see that though this cell line initially had relatively high levels of tyrosine hydroxylase activity ( $\sim 100$  units of activity) over a period of 80 generations of 10 subcultures, much of this activity was lost. However, an initial attempt to isolate cells in tyrosine-free media selected a heterogeneous population of cells with even higher tyrosine hydroxylase activity than the parent cell line ( $\sim 400$  units of activity).

Table XXI. Tyrosine Hydroxylase Activity of Sympathetic Ganglion Cell  $\times$  Neuroblastoma Somatic Cell Hybrid

Cell	Generation	Passage	Tyrosine hydroxylase specific activity (pmoles/min per mg%)
X31	20-40	3-4	98
X31	45-65	4-5	95
X31	120-150	15-16	27
TX31	120-150 + 10-13 in tyrosine-free media	T1	394

In addition to using the tyrosine-free selection as described above, two modifications were also used. The first modification was to select for cells in the presence of aminopterin (a drug that inhibits nucleic acid synthesis and applies a strong selective pressure for retention of the neuroblastoma genome). This was to demonstrate whether the expression of the gene for tyrosine hydroxylase could be expressed in the presence of the neuroblastoma genome. The second modification was to select cells in the presence of carbamylcholine. This was done to see if continued growth of cells in the presence of this agonist of acetylcholine would select for or against cells with acetylcholine receptors. To date over 30 cell lines have been isolated using the above selective pressures and these lines are presently being analyzed.

Three general types of other new cell lines are presently being adapted to cell culture and/or are being analyzed for specific neuronal or glial characteristics. Three tumors from rats injected with ethyl nitrosourea have been placed into culture. Two mouse schwannoma tumors obtained from D. J. Rice (Experimental Carcinogenesis Branch, National Cancer Institute) have been adapted to culture and a number of Schwann's cell clonal lines have been isolated. One human neurofibroma tumor has been placed in culture.

Analysis of cell lines for neuronal characteristics. Membrane transport and metabolism of dopamine in the somatic cell hybrid NX31. A detailed kinetic study of



the membrane transport of 3,4-dihydroxyphenylethylamine (dopamine) was carried out using the somatic cell hybrid NX31. There exists in this cell line a two-component uptake system, each operating at defined exogenous dopamine concentration ranges. A high affinity uptake system is apparent at low incubation medium dopamine concentrations. For concentrations greater than 0.1 mM dopamine, a low affinity transport system is seen to be predominant. A plot of velocity versus substrate concentration (Figure 40) shows two distinct slopes, each slope corresponding to separate uptake systems. The high affinity system is saturable, while the low affinity uptake was not saturable through 1 mM dopamine. Since the high affinity transport system is significant over physiological dopamine concentrations, it was subjected to a more detailed kinetic analysis.

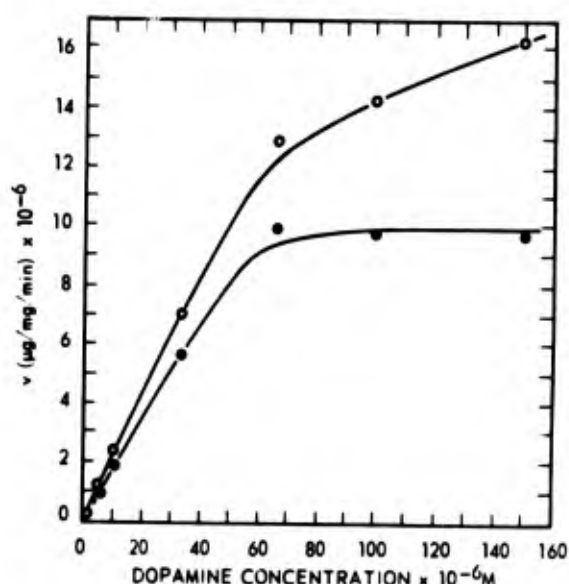


Figure 40. A plot of initial velocity of dopamine uptake versus dopamine concentration in the incubation medium. The open circles represent the plot of data which suggests two distinct uptake systems, one high affinity, apparent at low dopamine substrate concentrations, and one low affinity, seen at high dopamine substrate concentrations. The low affinity uptake system is nonsaturable. The closed circles represent the high affinity system corrected for the nonsaturable, low affinity system.

A double reciprocal plot (Lineweaver-Burk) (Figure 41) of velocity versus substrate concentration for the dopamine concentration range of  $1.4 \times 10^{-6}$  M to  $1 \times 10^{-4}$  M resulted in a nonlinear analysis. This suggested that the uptake system was not first order with respect to dopamine and that the system did not display classical Michaelis-Menten kinetics. Further investigations of mathematical models to describe the data showed that this membrane transport system was second order for dopamine. In addition, the data suggest not only a multiple substrate transport, but also that dopamine acts as an activator (multiple substrate-substrate as an activator). A Hill plot (Figure 42) of the data showed a coefficient of two, indicating that two dopamine molecules

are binding to a carrier prior to transport. Since one of the two carrier sites is an activator site, there exist two binding constants for the dopamine. The binding constants calculated from the model agree very well with the data.

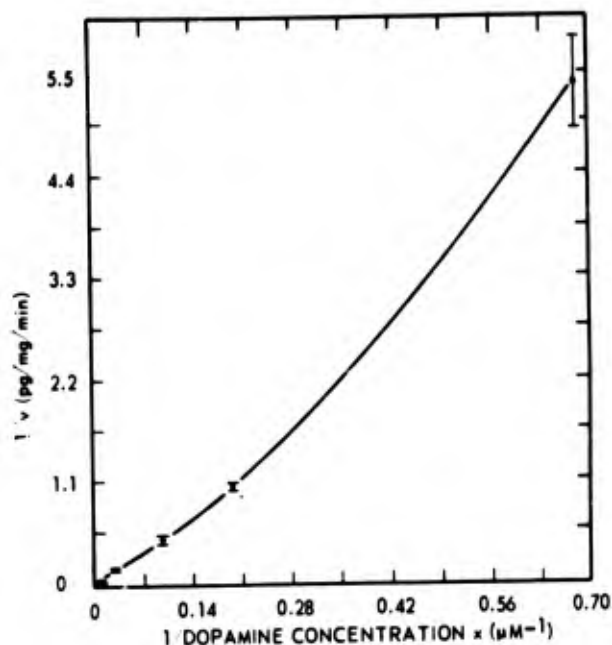


Figure 41. A double reciprocal plot of initial velocity of dopamine uptake versus dopamine incubation medium concentration. Note that the plot is nonlinear, indicating that the kinetics of dopamine uptake in X31 is something other than first order with respect to dopamine. Double reciprocal plots for multiple substrate reactions take on this characteristic nonlinear appearance.

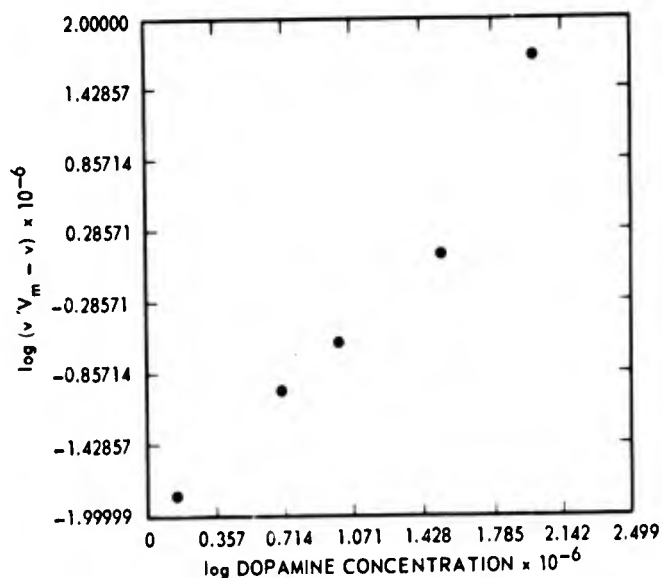


Figure 42. Hill plot of dopamine uptake data from X31. The slope of the line derived by linear regression analysis is 1.8, indicating that two substrate molecules (dopamine) bind to the carrier for transport.

Experiments were conducted to ensure that the high affinity uptake system was not an amino acid transport mechanism. The amino acid chosen for this study was tyrosine, the amino acid precursor of dopamine. Results showed that tyrosine and dopamine transport are mediated by separate systems. The uptake system is temperature sensitive and also inhibited by a number of pharmaceuticals, to include d-amphetamine, reserpine and benztropine.

The metabolism of accumulated dopamine is primarily by monoamine oxidase. No significant catechol-O-methyl transferase activity was detected. Likewise cells incubated in the presence of  $^3\text{H}$ -tyrosine showed no significant tyrosine hydroxylase activity. Previous tyrosine hydroxylase activity found in the cell line appeared only after the cells were treated with dibutyryl cyclic adenosine monophosphate.

The results indicate a neurotransmitter transport system is functional in these nondifferentiated cells. Although the kinetics appear to be more complex than first order, the existence of such a transport system in large populations of cultured cells lends itself to further investigations as to molecular basis of neurotransmitter membrane transport.

Models for studying synaptic interaction coculture experiments with X31 and smooth muscle. Recent experiments from a number of laboratories have demonstrated that when dissociated spinal cord cells are cocultured with previously prepared cultures of skeletal muscle, synaptic contacts will be made. Giller et al.<sup>2</sup> have also demonstrated that in such cocultures there is a significant increase in choline acetyl transferase activity when compared to spinal cord cell cultures alone. This suggests that there exists a feedback interaction by muscle on the differentiating innervating neuron. These experiments, though interesting, suffer from a number of difficulties associated with primary cultures of neurons and muscle, i.e., relatively small numbers of cells and a lack of homogeneity from culture to culture making it difficult to perform many biochemical experiments and to obtain consistency from experiment to experiment. Since the sympathetic ganglion cell-somatic cell hybrid X31 has demonstrated many properties of sympathetic neurons, coculture experiments have begun with X31 and smooth muscle to determine if a similar feedback mechanism exists in adrenergic synapse. In order to obtain homogeneous experimental conditions, cell lines have been developed from smooth muscle. To demonstrate that this is a specific interaction between a neuron and its target, two sources of smooth muscle were chosen. Muscle cultures were prepared from human oviduct and human umbilical artery. Muscle from the former source is heavily innervated while muscle from the latter source is reported to be noninnervated.

The initial effort was to develop procedures for not only procuring large numbers of viable and dividing populations of smooth muscle cells, but also to develop clonal cell lines of these cells to insure the homogeneity of these cells for anticipated biochemical characterization. To date, a number of authors have reported the cell culture of smooth muscle cell by placing tissue explants in culture and, over a period of

at least 4 weeks, allowing the various endothelial and fibroblast cells to migrate from the explant and die, and finally to obtain smooth muscle cells. In order to obtain more immediate results, we have minced the tissue into fine fragments and tested the ability of several enzyme procedures for dissociating muscle tissue into relatively homogeneous cell suspensions. Dissociations with trypsin (0.25 percent) and collagenase (0.2 percent) and chick serum (4 percent) were tried with relatively little success. A mixture of elastase (10 units/ml) and collagenase (20 units/ml) in calcium and magnesium-free Hanks' saline has permitted the complete dissociation of minced muscle into single cells. After four to five dissociation periods of 60 minutes duration at 37°C in a shaking water bath, large numbers of single muscle cells are isolated, which within 24 hours have begun to divide.

Preliminary coculture experiments suggested that continued division of X31 cells was inhibited by the presence of smooth muscle cells. To test whether this process required direct cell-cell interaction or is a result of a metabolic product of smooth muscle cells interacting with the neuronal cell, experiments have begun to test the media conditioned by the smooth muscle cells. Conditioned media from both oviduct and umbilical muscle cell cultures were collected and diluted with an equal volume of fresh media to insure that all nutrients were present in excess. This medium is called CM-50. After 3 days of culture in CM-50 prepared by all three methods, X31 cells showed an inhibition of cell division and extensive neurite formation. This effect was most pronounced in the cultures fed CM-50 from umbilical muscle cultures. Experiments are presently underway to measure more precisely the effect of conditioned media on the kinetics of X31 cell division and neurite formation as well as further isolation of the component(s) in the conditioned media responsible for this observation.

## REFERENCES

1. Breakefield, X. O. and Nirenberg, M. W. Selection for neuroblastoma cells that synthesize certain transmitters. *Proc. Natl. Acad. Sci.* 71:2530-2533, 1974.
2. Giller, E. L., Jr., Schrier, B. K., Shainberg, A., Fisk, H. R. and Nelson, P. G. Choline acetyltransferase activity is increased in combined cultures of spinal cord and muscle cells from mice. *Science* 182:588-589, 1973.
3. Greene, L. A., Shain, W. G., Chalazonitis, A., Breakefield, X. O., Minna, J. D. and Nirenberg, M. W. Neuronal properties of a neuroblastoma x sympathetic ganglion cell hybrid. *Proc. Natl. Acad. Sci.* (in press).



## OPIATE EFFECTS ON BRAIN TYROSINE

Principal Investigators: S. L. Cohan and J. R. Abbott

Tyrosine hydroxylase activity in morphine tolerant rats. Tyrosine hydroxylase (TH) activity has been measured in brains of rats acutely or chronically treated with morphine. Initial studies suggested that TH activity in thalamus and basal ganglia of rats chronically treated with morphine was decreased. These findings could be explained as a result of a morphine-induced shift of TH from particulate to soluble form. Experiments comparing the partition of TH between soluble and particulate forms following saline, acute morphine, or chronic morphine administration show no differences.

Role of prostaglandins in opiate tolerance and withdrawal. The analgesic effect of morphine was measured as a decreased response to pain induced by placing a rat on a hot plate at 55°C. Most rats develop tolerance to the morphine within 3 to 4 days (15 mg/kg subcutaneously, daily). Prostaglandin synthetase inhibitors (Indomethacin or aspirin) are administered to determine if prostaglandin depletion influences the rate or degree of tolerance development. The data from these experiments are too preliminary to draw any conclusion.

Three heroin addicts have been detoxified on the Clinical Study Unit at Georgetown Medical Center. Each of these patients received placebos as part of a feasibility study to determine if the patients could be managed on an open ward. The Clinical Study Unit Research Committee has reviewed the results from the first group of patients and has authorized continuation of the study. Drugs (Indomethacin or aspirin) or placebos will be administered in a double blind experiment to determine if prostaglandin depletion influences the signs and symptoms of acute withdrawal.

Pharmacokinetics of oral anticholinesterases in myasthenia gravis. The inhibition of serum nonspecific cholinesterase is used to reliably detect the presence of neostigmine or pyridostigmine in patients taking these drugs. These drugs, at serum concentrations of about  $10^{-8}$  M, are the mainstays in treatment of myasthenia gravis.

A second more direct method of measuring the concentrations of these drugs entails combustion of these quaternary ammonium compounds in the presence of iodine to produce methyl iodide. The methyl iodide is volatile and can be detected by electron capture on a gas chromatograph. At present, difficulty has been encountered in separating the methyl iodide peak from an artifactual water peak. This project is being conducted jointly with Dr. J. Pohlman, Night Vision Laboratory, Fort Belvoir, Virginia.

Control subjects and patients with myasthenia gravis will be studied with regard to: (1) the time of appearance and duration of pyridostigmine or neostigmine in serum after oral administration, and (2) the correlation between levels of serum anticholinesterases and their therapeutic effect in myasthenics.



## THE EFFECTS OF OPIATES ON RNA POLYMERASE ACTIVITY IN VIVO

Principal Investigators: J. H. Darden and G. N. Catravas

Previous studies in this laboratory using an in vitro assay system have shown oscillating changes in RNA polymerase activity in various brain areas following acute and chronic morphine treatment. Because of those results, attempts have been made to correlate the rate and degree morphine affects various brain sites, with possible morphine caused structural changes to RNA polymerase. This necessitated the development of an in vivo-in vitro assay system.

Briefly, a group of male adult rats were either administered twice daily doses of morphine (30 mg/kg body weight subcutaneously) for 7 days to render them tolerant to the drug (as determined by the hot-plate test) or were given a single dose (60 mg/kg body weight) for the acute studies. The animals were then injected intraventricularly under mild ether anesthesia with 6  $\mu$ Ci of  $^3$ H-uridine 1 hour after the last morphine injection and euthanatized by decapitation at various intervals of time ranging from 10 minutes to 2 hours after  $^3$ H-uridine injection. The brains were rapidly removed and dissected into four sections; brain stem (medulla), cerebellum, midbrain (hypothalamus, thalamus, hippocampus and basal ganglia) and cerebrum. These sections were immediately frozen in liquid nitrogen and stored at  $-90^{\circ}\text{C}$  until assayed.

Preliminary results in the acutely treated animals when compared to saline treated controls indicate no statistical difference. In the chronically treated animals, it was found that at 10, 20 and 30 minutes after  $^3$ H-uridine injection there were increases in RNA polymerase activity as compared to controls in the brain stem, cerebellum and midbrain sections. These data compare favorably with previously reported in vitro studies but data are insufficient at this time to report statistically valid results.



# MECHANISM OF MORPHINE ANTAGONISM OF RESERPINE-INDUCED DEPLETION OF BRAIN CATECHOLAMINES

Principal Investigators: J. C. Blosser and G. N. Catravas

A characteristic of the development of tolerance and dependence to morphine is an acquired resistance to the catecholamine depleting effects of reserpine in the brain. Reserpine is known to block the storage mechanism for biogenic amines in synaptic vesicles, rendering catecholamines susceptible to enzymatic degradation. The object of this study is to characterize the mechanism by which the morphine tolerance phenomena may be involved in blocking the action of reserpine. Our previous studies indicated a lack of interaction between morphine and reserpine *in vitro* with synaptic vesicle preparations. As seen in Table XXII, rats made tolerant to morphine (60 mg/kg) were significantly resistant to intraperitoneally administered reserpine (2.5 mg/kg). Levels of norepinephrine were only moderately reduced. However, if reserpine was given intravenously (0.5 mg/kg) to morphine tolerant animals, the antagonism of reserpine was no longer apparent (Table XXII). When  $^3\text{H}$ -reserpine was administered intraperitoneally to control and morphine tolerant animals, significantly less reserpine was found in the brains of tolerant animals (Table XXIII). This is consistent with the correspondingly higher levels of catecholamines found in animals treated with morphine intraperitoneally (Tables XXII and XXIII) and suggests that less reserpine is reaching the brains of tolerant animals. We conclude that an acquired resistance to the effects of reserpine cannot be correlated with CNS tolerance to morphine. Rather, a systemic inactivation of reserpine may be enhanced as a result of chronic morphine treatment.

Table XXII. Effect of Reserpine *In Vivo* on Levels of Norepinephrine in Control and Chronically Morphine Treated Rats

Reserpine	Norepinephrine (ng/g tissue $\pm$ S. D.)	
	Control	Morphine tolerant
0	498.5 $\pm$ 66.7	417.3 $\pm$ 71.9
2.5 mg/kg I. P.	82.1 $\pm$ 20.9	260.8 $\pm$ 67.1
0.5 mg/kg I. V.	89.9 $\pm$ 11.5	67.2 $\pm$ 9.9

Table XXIII. Levels of  $^3\text{H}$ -Reserpine and Norepinephrine in Brains of Control and Chronically Morphine Treated Rats

	Reserpine (ng/g tissue $\pm$ S. D.)	Norepinephrine (ng/g tissue $\pm$ S. D.)
Control	15.8 $\pm$ 1.3	82.1 $\pm$ 20.9
Morphine tolerant	6.8 $\pm$ 1.0	325 $\pm$ 40.3

◆◆◆◆◆◆◆◆◆◆

## FUNCTIONAL PROTEINS IN THE MEMBRANES OF NEURONS

Principal Investigators: W. G. Shain, Jr., D. O. Carpenter, D. R. Livengood  
and E. S. Chock

The snake neurotoxin  $\alpha$ -bungarotoxin ( $\alpha$ BT) has been used by a number of investigators to recognize, isolate, and purify the acetylcholine (ACh) receptor. In vertebrate systems the toxin binds only to nicotinic ACh receptors. Because of this apparent specificity of action experiments were initiated to determine if  $\alpha$ BT could be used to study in detail the ACh receptor in the nervous system of Aplysia. In an initial series of experiments it was demonstrated that  $\alpha$ BT blocked all three ionic responses to ACh and that the binding of  $\alpha$ BT could be blocked by not only a number of agonists and antagonists of ACh but also by drugs affecting (1) acetylcholinesterase, eserine and neostigmine, (2)  $\text{Na}^+ - \text{K}^+ - \text{ATPase}$ , ouabain, and (3)  $\text{K}^+$  ionophores, tetraethylammonium. To demonstrate the mode of action of these drugs, competitive binding studies have been performed. Kinetic analyses have been performed to determine if the inhibition of toxin binding is competitive, i.e., competing for the same site, uncompetitive, i.e., binding at a secondary site, causing inhibition, or noncompetitive, i.e., binding at a remote site causing conformational changes large enough to prevent toxin binding.

To determine if the inhibition of binding of  $\alpha$ BT was due to a direct interaction with the ACh receptor protein or to some adjacent protein, experiments were performed on a membrane preparation where the environment of the ACh receptor remained intact and in a Triton X-100 solubilized preparation where the ACh receptor should have been solubilized as a discrete protein. Data from the various experiments were first analyzed using Cleland's models of inhibition kinetics. A second analysis of the same data has begun using the Hill equation. Figure 43 demonstrates analysis of eserine inhibition using Cleland's inhibition kinetics. The hyperbolic curve in Figure 43B demonstrates that the inhibition is uncompetitive or that eserine is not binding to the same site as the  $\alpha$ BT but some site on the same molecule. All of the compounds studied to date have shown similar inhibition kinetics whether studied on the intact preparation or on the solubilized preparation.

Two types of experiments are now planned to further elucidate the mechanism of this inhibition. The first is to demonstrate that the solubilized receptor is completely free from additional enzyme, AChE, or ionophore activity. This will be performed by separation of the isolated preparation using sucrose gradient and column chromatographic procedures. The second set of experiments is to repeat competitive binding studies using well-known agonists of ACh.



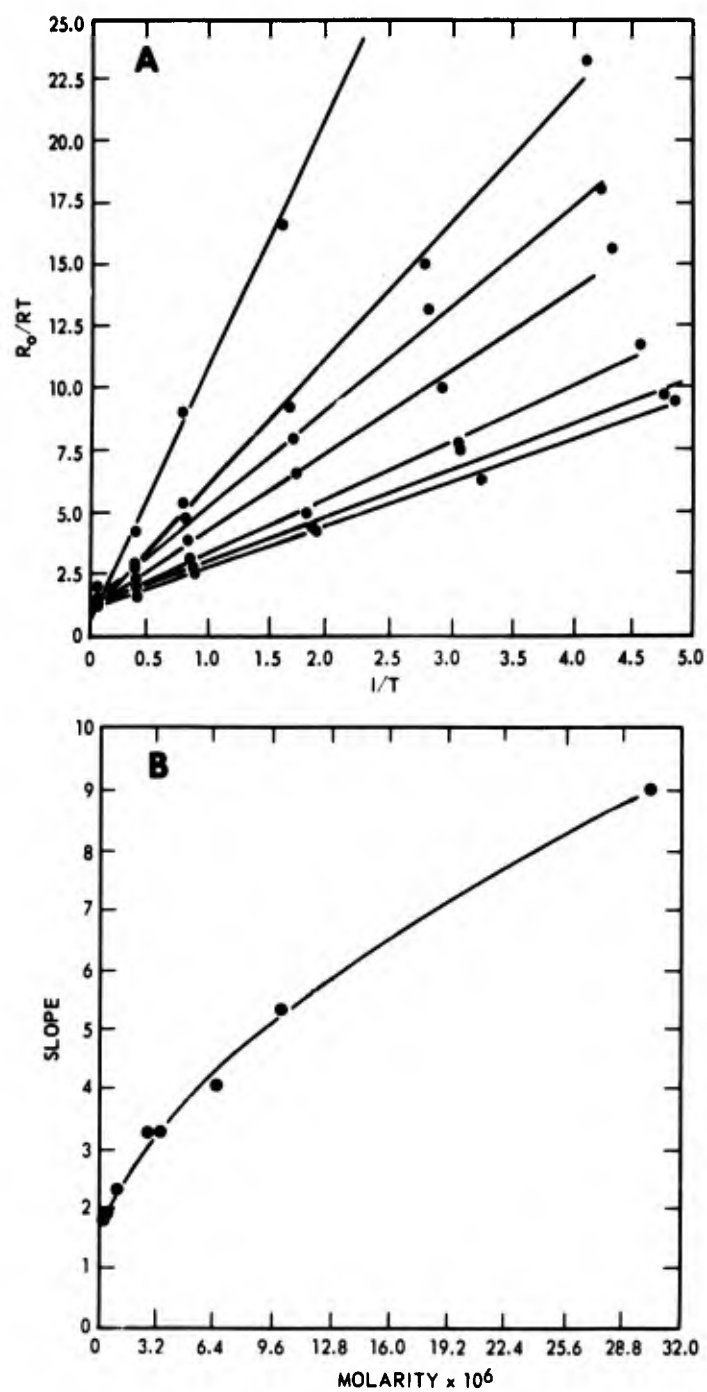


Figure 43. Analysis of eserine inhibition using Cleland's inhibition kinetics. A.  $R_0/RT$  versus  $1/T$  with lines drawn to linear regression. B. Slope versus eserine where slope values are from linear regression.

To gather further evidence that there is a single ACh receptor in Aplysia, a number of identified cells having different ACh responses were studied with regard to  $\alpha$ BT binding and the pharmacology of toxin binding. All cells showed similar kinetics of both  $\alpha$ BT binding and competition of binding, therefore demonstrating that  $\alpha$ BT only recognizes a single ACh receptor in Aplysia.

In addition to the  $\alpha$ -toxin used to study ACh receptors a number of other toxin peaks can be isolated from the crude Bungarus multicinctus venom (see Figure 44). A number of these are reported to function by inhibition of presynaptic events. To survey the effects of these various toxins, experiments were performed using the frog sciatic nerve-sartorius muscle preparation. The twitch responses of the muscle to evoked stimuli were measured. The nerve preparation was treated with a solution of the toxin and when inhibition was maximal or complete the preparation was washed overnight to demonstrate if the effect was reversible. The following day the preparation was tested for ACh sensitivity and direct electrical response to demonstrate that postsynaptic receptors were not blocked and to demonstrate that the muscle was still functional. The results of these experiments are summarized in Table XXIV. Peaks 9-11 have been selected for further study since they demonstrated increases not only in spontaneous activity but also in an increase in twitch magnitude to a constant stimulus. These results suggested that the toxins may be functioning by interfering with  $\text{Ca}^{++}$  flux across the presynaptic membrane and therefore disrupting normal release of neurotransmitter.

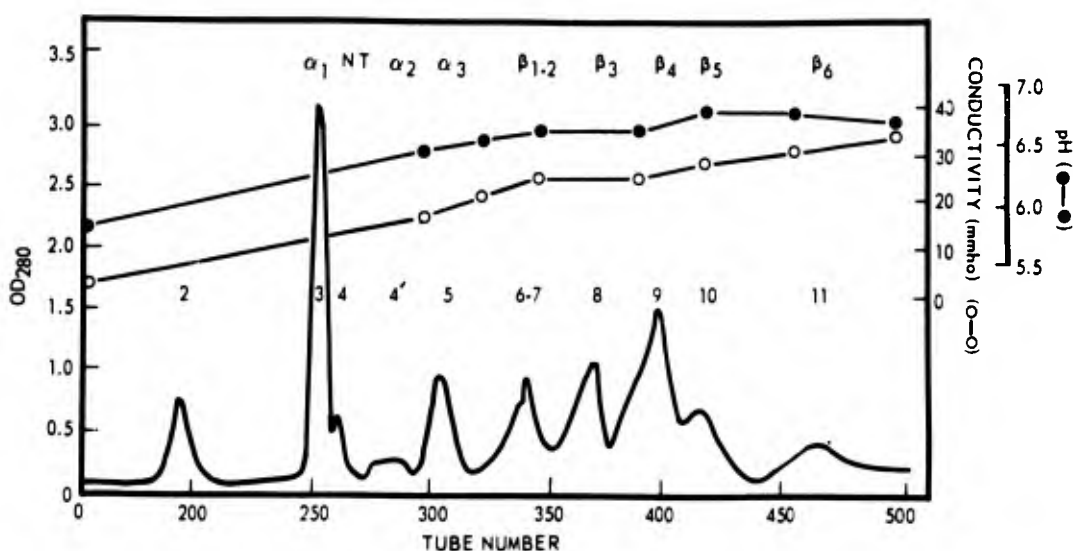


Figure 44. CM-25 Sephadex chromatography of crude Bungarus multicinctus venom. The venom is separated by means of concurrent pH-ionic strength gradients in 0.5-0.95 M ammonium acetate pH 5.8-7.2.

Table XXIV. Inhibition of Evoked Twitch Response

Peak number	Toxin designation	Synaptic effect	Toxin concentration ( $\mu\text{g/ml}$ )	Inhibition characteristics			Twitch response		ACh response
				$t_{50}$ (min)	Complete	Reversible	Spontaneous activity	Increase in magnitude	
3	$\alpha$	post	$2.5 \times 10^{-3}$	5.4	+	-	-	-	-
4	?	not studied							
5	$\alpha$	post	0.15	13	+	+	-	-	+
6-7	$\beta$	pre	0.25	14	+	-	-	-	+
8	$\beta$	pre	0.17	15	-	+	-	-	+
			0.19	4.2	-	+	-	-	+
9	$\beta$	pre	1.55	*	-	-	+	+	+
			3.1	43	+	-	+	+	+
10	$\beta$	pre	2.75	52	+	-	+	+	+
11	$\beta$	pre	0.14	33	+	-	+	+	+

\* No inhibition seen

To investigate this hypothesis, experiments have begun on the crayfish walking-leg preparation. This preparation was chosen (1) to demonstrate that the toxin can affect other than ACh synaptic mechanisms, (2) because with this preparation a single isolated nerve fiber can be stimulated and the evoked postsynaptic potential recorded, and (3) because the crayfish muscle has a  $\text{Ca}^{++}$  spike.

Treatment of the preparation is similar to that described for the frog nerve-muscle preparation. Experiments have been performed with peak 11 and have demonstrated that this toxin will block synaptic responses. In addition spontaneous postsynaptic potentials have been seen. A single experiment to study the effect of the toxin on the  $\text{Ca}^{++}$  spike mechanism has demonstrated that the spike is blocked by the toxin. These results indicated that this toxin may be functioning by blocking  $\text{Ca}^{++}$  ionophores associated with evoked synaptic release and the spike mechanism of the muscle. Experiments are now in progress to study peaks 9 and 10 and to elucidate the mode of action of these toxins.

◆◆◆◆◆◆◆◆◆◆

## NEURORADIOLOGY CORRELATIONS

**Principal Investigators:** S. A. Shatsky, D. E. Evans, W. A. Alter III, AFRRl;  
and V. Armbrustmacher, Armed Forces Institute of  
Pathology

**Technical Assistance:** L. J. Parkhurst

The physiologic and pathologic changes which occur after nonpenetrating head injury may be related to the displacement which the cerebral structures undergo during trauma. To date, studies of displacement during experimental impact have been limited to the observation of movements of surface blood vessels. To record the dynamic changes in external and internal anatomy during impact, a high speed cinefluorographic system was developed.

Anesthetized rhesus monkeys were accelerated to terminal velocities of 3 to 8 m/sec and impacted on the frontal, temporoparietal or occipital skull surface. To visualize the cerebral vasculature or ventricles, radiopaque medium was injected prior to impact, and a cinefluorographic record of the brain was obtained. Photographic data were analyzed for movement of intracranial anatomy and compression of the impacted skull surface. Gross and microscopic pathological examination was made from typical animals euthanatized 1 hour to 10 days postimpact.

Fifteen monkeys were prepared for cerebral arteriography and were accelerated to a terminal velocity of  $7.3 \pm 0.1$  m/sec (16.3 mph). Contact force ranged from 400 to 1000 lbs with a pulse duration of 3 to 6 msec. Accelerometers mounted at the bregma indicated that the skull underwent a deceleration of 500 to 1000 G over a similar time span. This wide range of impact parameters was probably due to variations in skull mass and occurrence of fractures as well as the specific skull impact site and orientation of the impactor.

Examples of the photographic records appear in Figure 45 and the data from this experiment appear in Table XXV. The cerebral vasculature is well defined in the pre-impact frame (Figure 45A). The midline common pericallosal artery (CPA) lies between two dark rectangles which are lead markers secured to the occipital surface. Stability of these markers postimpact indicates minimal lateral rotation. The vessels which appear below the markers are the middle cerebral arteries. This animal reached a terminal velocity of 7.1 m/sec and the force at impact on the temporoparietal skull surface was 506 lbs. The initial movement after impact was a compression of the skull at the impact site. Maximum compression (3.4 mm) occurred at 2 msec postimpact (Figure 45C). At this time the CPA was displaced toward the impact surface, whereas the left middle cerebral artery shifted toward the midline. Maximal displacement of the CPA was reached 5 msec postimpact (Figure 45D), and represented a movement of 1.4 mm from its normal midline position.

EXPERIMENT: A-4-69

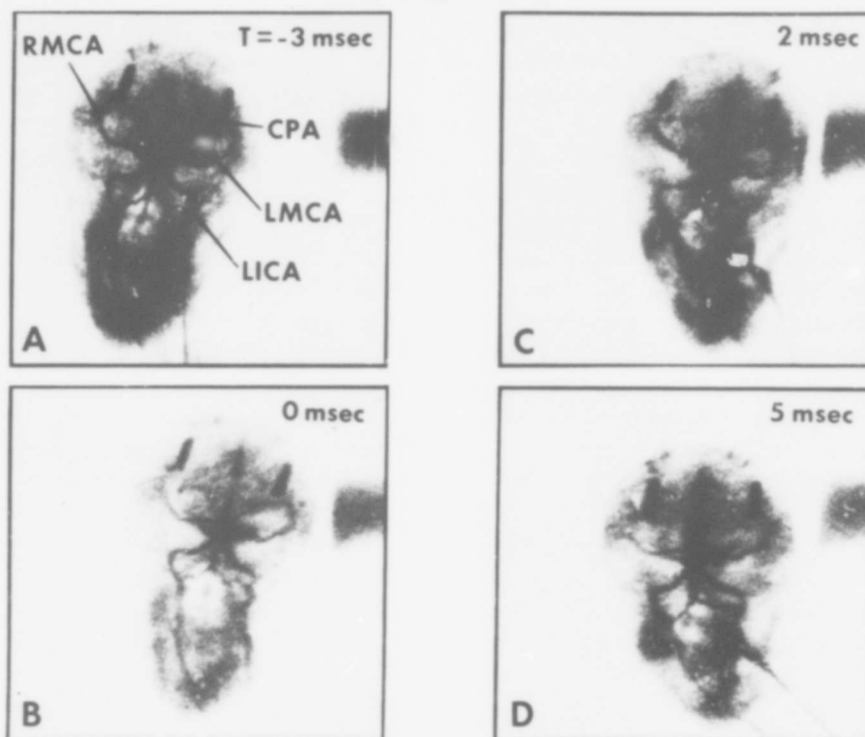


Figure 45. Temporoparietal impact of anesthetized rhesus monkey. Terminal velocity was 7.1 m/sec.

Table XXV. Effect of Temporoparietal Impact on Skull Parameters

Experiment A-4-69	
Impact force	506 lbs
Deceleration	532 G
Terminal velocity	7.1 m/sec
Lateral skull compression	3.4 mm at 2 msec
Displacement of the common pericallosal artery	1.4 mm at 3-5 msec (laterally)
Compression of the left cerebral hemisphere	3.8 mm at 3 msec
Displacement of the left middle cerebral artery	2.3 mm at 3 msec (medially)
Displacement of the right middle cerebral artery	1.3 mm at 0 msec (medially) 1.5 mm at 1 msec (laterally)

In summary, a relatively consistent pattern of movements occurred after temporo-parietal impact. The initial event was a significant decrease in the lateral skull diameter from a control value of  $5.85 \pm 0.01$  cm to  $5.69 \pm 0.06$  cm ( $p < 0.05$ ). The time of maximum skull compression was 0 to 2 msec postimpact in eight of nine experiments. During the first 10 msec, a significant displacement of the midline common pericallosal artery also occurred. The vessel was displaced from 0 to 17.6 percent toward the impacted skull surface, and this maximum was reached at approximately 4 to 5 msec postimpact. During this same time period, the normal pathway of this vessel was distorted just below its most superior extension (see Figure 45D). These complex wave patterns appeared to resolve, and the vessel returned to normal configuration by 10 msec postimpact. Compression of the left lateral skull surface and displacement of the common pericallosal artery toward this impacted surface resulted in a decrease in the vessel to skull distance of 0 to 6.3 mm. Based on these data we conclude that the lateral diameter of the left cerebral hemisphere decreased by up to 18.6 percent. The only other vessel to demonstrate consistent displacement was the middle cerebral artery ipsilateral to the impact site. Photographic data from five experiments revealed that the most lateral aspects of the vessel were displaced toward the midline 1.3 to 4 mm. The maximum displacement occurred from 0 to 3 msec postimpact. Movements during this time period indicate that compression of the skull resulted in a mass movement sufficient to displace the left middle cerebral artery medially, whereas within the next 5 msec, the midline common pericallosal artery was displaced toward the impact surface. Based on these findings, our conclusion is that inertial effects predominate near the brain midline, whereas compressional effects predominate nearer the impact site.

Gross pathological changes found in these animals include a separation of the left squamosal suture or depressed fracture of the left temporal bone. Cerebral cortices demonstrated contusions on gross examination of the left temporal surface in six of eight animals (coup contusions) as well as on the right temporal surface in four of eight animals (contrecoup contusions). Parasagittal petechial dural hemorrhages were observed in all animals as well as subarachnoid hemorrhages in the cerebellopontine angles, medulla, anterior pons and infundibulum. Only three of the animals died immediately postimpact and in these cases the pathology did not appear to be significantly different from the animals which were euthanatized up to 10 days postimpact.



## CARDIAC ARRHYTHMIAS RESULTING FROM EXPERIMENTAL HEAD INJURY

**Principal Investigators:** *D. E. Evans, W. A. Alter III and S. A. Shatsky*

Both clinical and experimental studies have demonstrated the occurrence of cardiac arrhythmias and other circulatory changes following head injury. Yet the significance of these cardiovascular changes and the mechanisms responsible for them remain poorly understood. Also largely unexplored is the question of rational therapy for cardiac arrhythmias resulting from head injury.

The purpose of this study was to systematically explore the cardiovascular events resulting from head injury in the primate and to determine the neural mechanisms responsible for these changes. A further goal of the study was to use this information to select drugs with specific autonomic actions and determine their antiarrhythmic efficacy against arrhythmias resulting from head injury.

The electrocardiogram and arterial blood pressure were recorded in anesthetized monkeys before and after the animals were subjected to graded impacts to the temporal-parietal surface of the head. The impacts were delivered by accelerating the animals to terminal velocities of 3-8 meters/second and impacting the skull surface against a fixed object. Impact forces of 400-800 lbs were recorded with an impulse duration of 3-6 msec.

Preliminary experiments using barbiturate anesthesia and impact forces of 200-400 lbs were found to produce consistent bradycardia but no shift in cardiac pacemaker activity to subatrial sites. Since barbiturates may have been depressing the autonomic nervous system, we developed a technique in which nitrous oxide and halothane combined with succinylcholine could be used to provide adequate levels of anesthesia with minimal depression of the autonomic nervous system. We also modified the sled impacting device so that higher impact forces could be achieved.

With the use of gaseous anesthetic techniques and impact forces of 400-800 lbs, cardiac arrhythmias have occurred immediately following temporal-parietal impact in every animal studied. The arrhythmias have taken the forms of: sinus arrest with A-V nodal rhythm, A-V dissociations rhythms, and premature ventricular contractions. An example of the rhythm changes following impact is shown in Figure 46. In this example, impact was immediately followed by sinus arrest and A-V nodal predominance with premature ventricular beats occurring approximately 90 seconds after impact.

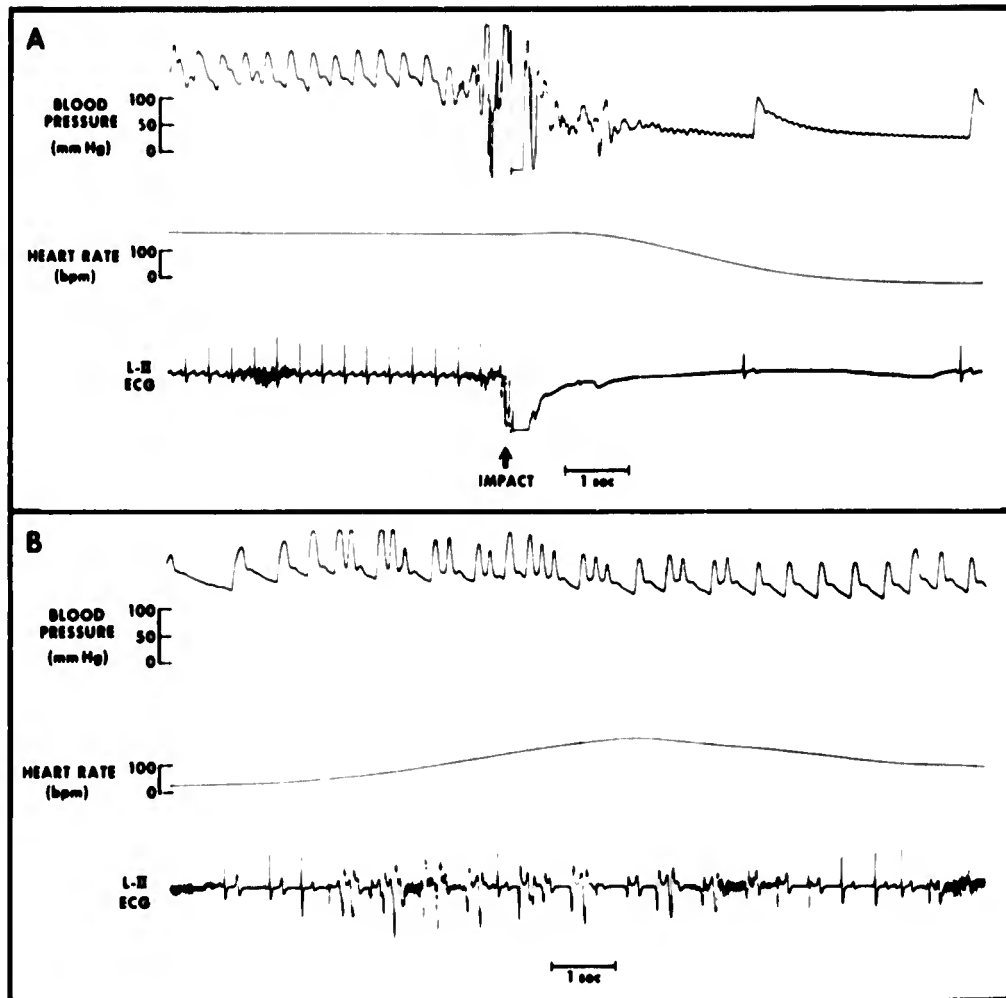


Figure 46. Rhythm changes (A) at temporoparietal skull impact, (B) 90 seconds after temporoparietal impact

The sinus arrest and slow A-V nodal rhythms which occur after temporal-parietal impact suggested that the arrhythmias were parasympathetic in origin. To test this we conducted a series of experiments in which the animals were treated with cholinergic blocking agents (atropine and propantheline) before impact. Cholinergic blockade was found to prevent arrhythmias from occurring in each animal tested. In addition, cholinergic blockade prevented any change in heart rate following temporal-parietal impact. These results confirmed that the arrhythmias were neural in origin and, more specifically, that they were mediated by the parasympathetic division of the autonomic nervous system. However to rule out the participation of the sympathetic division, another group of animals were pretreated with propranolol in beta-adrenergic blocking doses (0.5 mg/kg). In no instance did beta-adrenergic blockade prevent arrhythmias from occurring after temporal-parietal impact.



Our results to date indicate that cardiac arrhythmias consistently occur in the primate after temporal-parietal impacts of moderate force. We have further demonstrated that these arrhythmias are mediated by the parasympathetic division of the autonomic nervous system. In continuing these studies we are investigating the cardiovascular response to frontal and occipital impacts, and to impacts of greater force. We are also studying the efficacy of antiarrhythmic drugs in preventing and treating cardiac arrhythmias resulting from head injury.



## EFFECT OF $\text{PaCO}_2$ CHANGES ON THE RATE OF FORMATION OF CEREBROSPINAL FLUID IN THE MONKEY

Principal Investigators: A. N. Martins, A. I. Koblitz and T. F. Doyle

To improve our understanding of the intracranial pressure changes that attend changes in  $\text{PaCO}_2$  we measured simultaneously both cerebral blood flow (CBF) and rate of formation of cerebrospinal fluid (CSF) during hypocapnia.

Anesthetized rhesus monkeys underwent ventriculocisternal perfusion for 7 hours. Blue dextran and  $^{125}\text{I}$  serum albumin were added to the perfusate as nondiffusible indicators. A polarographic electrode of simple platinum wire was placed into the torcular Herophili to measure total CBF by the hydrogen clearance technique, as previously described.<sup>1,3</sup> Ventriculocisternal perfusion was carried out for 3 hours until the concentration of indicator in the effluent from the needle in the cisterna magna reached a steady state. Then the  $\text{PaCO}_2$  was changed by addition or removal of  $\text{CO}_2$  to the inspired air. CBF was also measured hourly, before and after  $\text{PaCO}_2$  changes. Table XXVI records our results. Our results do not agree with previously published reports<sup>2</sup> in that we failed to note a significant fall in rate of CSF formation when  $\text{PaCO}_2$  dropped. Additional experiments are planned in which  $\text{PaCO}_2$  will be lowered below 10 mm Hg. Perhaps monkeys require lower  $\text{PaCO}_2$  to affect CSF formation rate. The small difference in CBF between the hypocapnic and normocapnic groups is consistent with this speculation. Increasing  $\text{PaCO}_2$  failed to significantly change the rate of CSF formation, as previously reported. Hypercapnia produced the anticipated increase in CBF.

These results suggest that the protracted intracranial pressure changes that attend changes in  $\text{PaCO}_2$  are related to changes in CBF and the attendant changes in cerebral blood volume. These changes in the volume of the blood-brain unit act to alter resistance to CSF drainage, which in turn influences intracranial pressure. Changes in the rate of CSF formation appear to play no important role.

Table XXVI. Rate of Cerebrospinal Fluid Formation and Cerebral Blood Flow in Monkeys

	PaCO <sub>2</sub> mm Hg	Rate of CSF formation ml/min	CBF ml/100 g per min
Normocapnia N = 6	32 ± 1.0*	39.8 ± 3.8	59 ± 11
Hypocapnia N = 6	16 ± 4.6	36.5 ± 6.4	53 ± 19
Hypercapnia N = 6	57 ± 9.7	34.8 ± 3.6	156 ± 57

\* ± S.D.

#### REFERENCES

1. Martins, A. N., Kobrine, A. I., Doyle, T. F. and Ramirez, A. Total cerebral blood flow in the monkey measured by hydrogen clearance. *Stroke* (in press).
2. Oppelt, W. W., Maren, T. H., Owens, E. S. and Rall, D. P. Effects of acid-base alterations on cerebrospinal fluid production. *Proc. Soc. Exptl. Biol. Med.* 114:86-89, 1963.
3. Willis, J. A., Doyle, T. F., Ramirez, A., Kobrine, A. I. and Martins, A. N. A practical circuit for hydrogen clearance blood flow measurement. Bethesda, Maryland, Armed Forces Radiobiology Research Institute Technical Note TN74-2, 1974.

◆◆◆◆◆◆◆◆◆◆

#### THE EFFECTS OF TRAUMATIC INJURY ON SPINAL CORD BLOOD FLOW

Principal Investigators: T. F. Doyle, A. I. Kobrine and A. N. Martins  
 Technical Assistance: W. L. Stringfield

A 16-g weight was dropped 38 cm on the spinal cord of anesthetized monkeys which were allowed to recover and then observed long enough to infer that an injury of this severity results in permanent paraplegia. Using the hydrogen clearance technique, blood flow was measured in the lateral white matter and central gray matter of monkey

spinal cord before and after the trauma described. Blood flow in the center of the spinal cord started to decrease within 1 hour after injury and continued decreasing for up to 4 hours. After injury, blood flow in the lateral white matter more than doubled within 2 hours after injury and then fell to normal values where it remained for up to 24 hours. Because the axons which carry nerve impulses and whose dysfunction results in paralysis are situated in the lateral white matter it is clear that the paralysis which ensues after trauma is not due to lack of blood supply and is probably unrelated to the hemorrhagic ischemia of the central gray matter.



## SENSORY RECEPTOR PHYSIOLOGY

Principal Investigators: *M. L. Wiederhold and E. K. Gallin*

Technical Assistance: *P. Y. Okita and D. M. Paull*

The receptor cells of the *Aplysia* statocyst have been used as a model system in which to study the sensory transduction process in ciliated mechanoreceptor cells, such as the hair cells of the mammalian cochlea and vestibular labyrinth. Our studies have combined electrophysiology, scanning and transmission electron microscopy and differential interference phase contrast (Nomarski) microscopy.

In collaboration with A. E. McKee of the Naval Medical Research Institute, the fine structure of statocyst receptor cells has been studied by both scanning and transmission electron microscopy. Whereas each mammalian hair cell has only one true cilium (or none in the case of adult cochlear hair cells), the *Aplysia* statocyst has approximately 700 true cilia per cell. We have found the fine structure of these cilia to be quite similar to those of vertebrate hair cells, in that they contain nine peripheral and one central pair of filaments. The peripheral filaments extended down into a centriole where they fan out to form extensive lateral processes. Figure 47 is a low power scanning electron micrograph of a fixed, bisected cyst giving a view of the receptor cells' luminal surface with their numerous cilia and statoconia lying in close contact with them. Most of the statoconia have been washed out of this preparation to afford a better view of the cilia. The outlines of several receptor cells can be distinguished by sharp changes in the average reflection of electrons (change in average light level in the photograph).

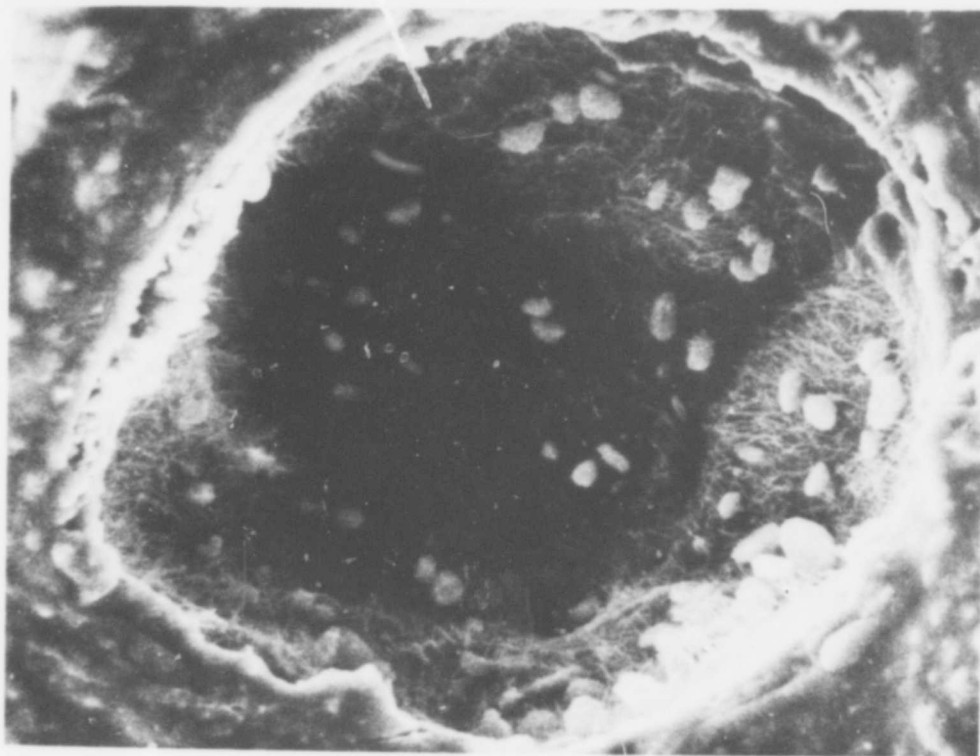


Figure 47. Scanning electron photomicrograph of a bisected statocyst showing numerous statoconia on the cilia-covered luminal surface. Diameter of cyst is 200  $\mu\text{m}$ . Note the close association of statoconia and cilia in the lower portion of the figure.

The *Aplysia* statocyst cells are large enough to penetrate with microelectrodes so that changes in membrane potential and permeability (measured as electrical conductance or resistance) can be observed during physiologic stimulation. It has been postulated for 25 years that hair cells perform their transduction in a manner analogous to that by which a carbon microphone operates: there is a potential difference maintained across the hair-bearing surface of the cell. When the cilia are deflected the resistance of the ciliated membrane was postulated to be changed (analogous to the compression of carbon particles in the carbon microphone) thus modulating the flow of current into the cell. This would in turn modulate the membrane potential at the site of neurotransmitter release in the case of cochlear hair cells or at the site of impulse initiation in the statocyst receptors. The cochlear hairs would be deflected by sound-induced movements of the tectorial membrane. When the statocyst is rotated about a horizontal axis the statoconia roll under gravity to deflect the cilia of those receptor cells at the bottom of the cyst. The data presented in Figure 48 represent the first case where it has been possible to directly observe changes in membrane potential and conductance during physiologic stimulation of this class of sensory receptor. In this experiment an

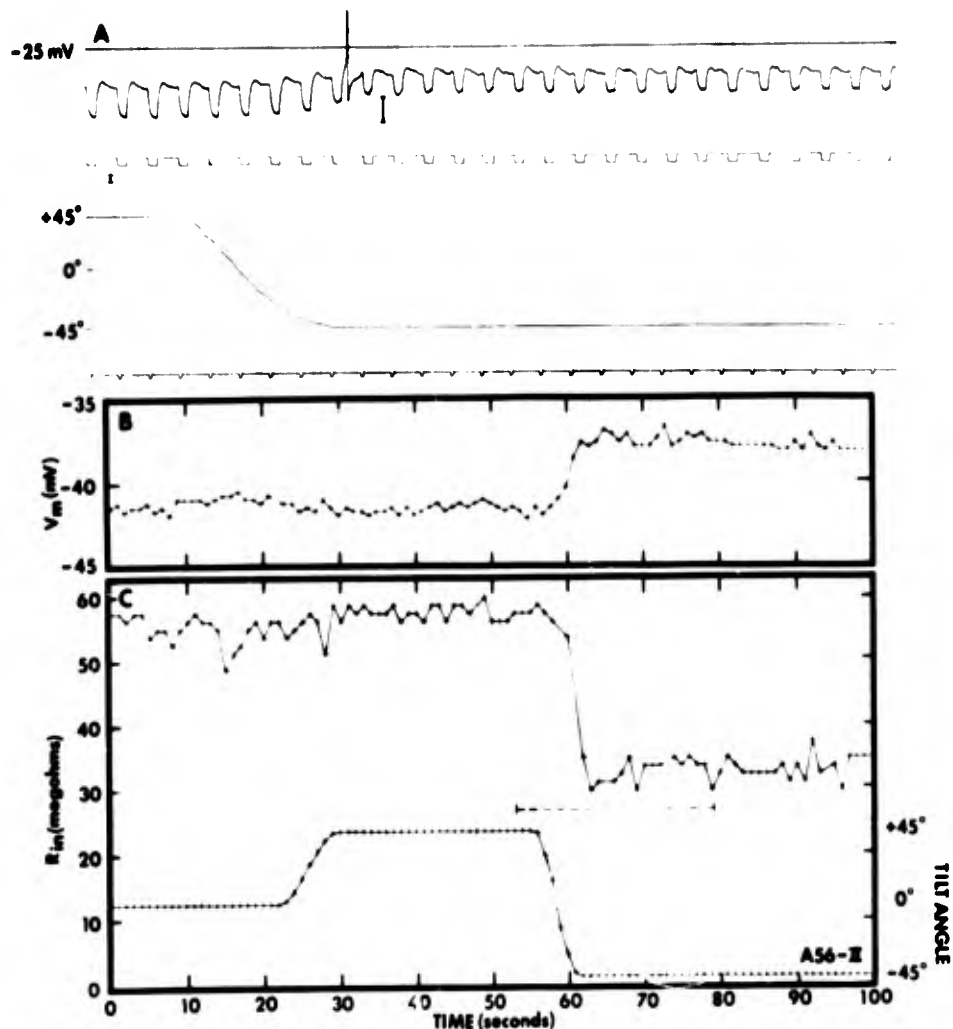


Figure 48. Measurement of change in cell input resistance during response to tilting. A. Upper trace: reference line of  $-25$  mV (intracellular potential relative to bath). Second trace: membrane potential, calibration bar  $\approx 10$  mV. Spikes were cut off photographically, actual spike amplitude:  $62$  mV peak to peak. Middle trace: current applied through recording electrode, calibration bar for current  $= 0.2 \times 10^{-9}$  A. Fourth trace: tilting table position,  $-45^\circ$  being maximum cell-down position. Table position was measured by means of a fixed potentiometer whose wiper was attached to the tilting platform. Bottom trace: 1-sec time markers. B. Receptor cell membrane potential in millivolts during a series of tilts from horizontal to cell-up position to cell-down (tilting table position indicated in lower trace of C). C. Receptor cell input resistance (upper trace, left-hand scale). The dashed line in C indicates portion of plot for which raw data are displayed in A. In B and C, plotted potential is that just before each current pulse, input resistance is this potential minus that just before end of pulse divided by the amplitude of the current. Table position is that at the beginning of each pulse. Current pulses were  $-0.2 \times 10^{-9}$  A, 300-msec duration, presented 1/sec.

Aplysia statocyst was mounted on a tilting table and a receptor cell penetrated with a micropipette electrode. Current pulses were passed through the recording electrode to measure membrane resistance during an excursion of the tilting table. Thus the larger the voltage deflection produced by the current pulse, the larger the membrane resistance. At the start of Figure 48A, the table was in the  $+45^{\circ}$  "cell up" position where the statoconia would not be in contact with the recorded cell, since they fall to the bottom of the cyst lumen. As the table is then moved to  $-45^{\circ}$  (recorded "cell down") a portion of the receptor cell comes into contact with the statoconia. A 5-mV depolarization of the cell is produced along with a 45 percent reduction in the cell's input resistance. The membrane potential, input resistance and tilt-table position are plotted in Figure 48B,C. Thus it has been demonstrated that loading the cilia, in the case of this receptor, does indeed reduce membrane resistance or increase conductance implying an increased ionic permeability.

When observed through the dissecting microscope the statoconia are often seen to "shimmer" indicating that they are in motion. This movement has been investigated further using Nomarski optics. To date we have not been able to distinguish individual cilia, but under this optical system it is clear that the movements of the cilia are much more vigorous and well organized than would be expected from Brownian motion. The movements are also greatest near the ciliated cyst wall, indicating that the movements are actively produced by the cilia. This observation raises the intriguing possibility that the statocyst cilia may be intermediate between sensory and motile cilia. This may not be a unique situation since paramecia produce an electrical response when stimulated mechanically near their motile cilia and several investigators in the 1930's noted shimmering reflected light from the cilia of fish labyrinthine hair cells in fresh preparations.



## STATE OF IONS AND WATER IN LIVING CELLS AND SOLUTIONS

Principal Investigators: D. O. Carpenter, M. J. McCreery and J. Bidinger

The cell bodies of a number of invertebrate neurons, the muscle fibers of the great barnacle, as well as several types of red blood cells have been shown to possess an internal electrical conductivity far lower than expected.<sup>1,2</sup> For example, this laboratory has demonstrated that the intracellular conductivity of *Aplysia* neurons is only 5 percent that of squid axoplasm or normal seawater. Evidence suggests that this depression is due neither to a low ionic concentration nor to an increased cytoplasmic viscosity, but rather is a function of the intracellular protein concentration. Our operating hypothesis is that the charged and polar groups of the protein cause sufficient ordering of cellular water to entrap ions and other small molecules in regions of high microviscosity. Under these circumstances, ion mobilities would be restricted and consequently their capacity to carry electrical current would be reduced. We have not only continued to probe the conductivity of other tissues, but also initiated experiments to determine the cause of this surprising phenomenon.

It seemed desirable to see if these observations would hold for a higher order animal such as the frog *Rana pipiens*. Forty-one measurements were made on 33 intact fibers of the whole sartorius (10 animals) muscle of *Rana pipiens* giving a mean fiber conductivity of  $9.6 \pm 2.6$  percent normal Ringer solutions. This corresponds to a resistivity of 833 ohm cm. Twenty-one measurements of 13 skinned fibers (single fiber segment having the membrane removed) gave a mean conductivity of  $67.4 \pm 14.3$  percent of the relaxing solution corresponding to a resistivity of 92.6 ohm cm (Table XXVII).

Table XXVII. Mean Conductivity and Resistivity of Intact and Skinned Fibers of Whole Sartorius Muscle of *Rana pipiens*

	Number of fibers	Mean conductivity (% bathing solution) (S. E.)	Mean resistivity (ohm cm)	Range (% bathing solution)
Intact	33	9.6 (0.45)	833	5 - 14.5
Skinned	13	67.4 (3.96)	92.6	37 - 85

Figure 49 shows sample voltage outputs with electrode calibrations for an intact fiber and a skinned fiber. Clearly our values for skinned fibers are much different from our values for intact fibers. From these observations it seems no longer appropriate to apply values measured in skinned fiber preparations to intact fibers as has been done by other investigators in the past. Considering that skinned fibers swell to about 2.3 times their normal diameter, perhaps the increased water content contributes in some way to the differences between intact and skinned fibers. We might suggest

the hypothesis that water in the intact fibers is more structured as the protein chains are closer together. Experiments measuring conductivity as a function of volume change in intact fibers are in progress.

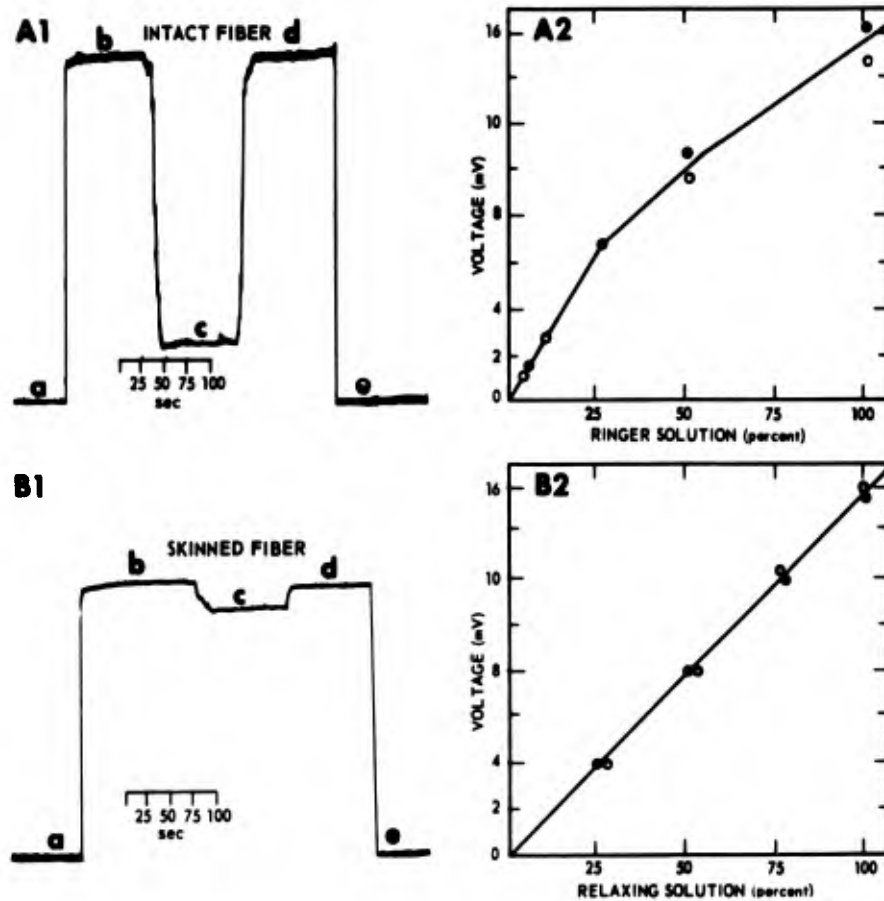


Figure 49. Voltage outputs with electrode calibrations for an intact and a skinned fiber. Letters indicate the position of the electrode as follows: (a) electrode is in the air; (b) electrode lowered into bathing solution, (c) electrode in the fiber, (d) electrode removed from fiber and back in bathing solution and (e) electrode back in air.

To elucidate the mechanism of our physiological observations, we are attempting to define a model solution of macromolecule-saltwater which will demonstrate a comparable lowering of conductivity. Once the model is found, physical-chemical measurements to include nuclear magnetic resonance, electron spin resonance, ion activity, and viscosity will be utilized to investigate its properties. Initial experiments have shown that a 50 mM sodium chloride solution containing 30 percent hemoglobin has a conductivity 50 percent less than expected.



## REFERENCES

1. Carpenter, D. O., Hovey, M. M. and Bak, A. F. Measurements of intracellular conductivity in *Aplysia* neurons: evidence for organization of water and ions. *Ann. N. Y. Acad. Sci.* 204:502-533, 1973.
2. Carpenter, D. O., Hovey, M. M. and Bak, A. F. Internal conductivity of axons, nerve cell bodies and large non-nervous cells. *J. Gen. Physiol.* (in press).



## IONIC MECHANISMS UNDERLYING NEURONAL THERMOSENSITIVITY

**Principal Investigators:** F. -K. Pierau and D. O. Carpenter

**Technical Assistance:** P. J. Torrey

There are temperature dependent processes functional in all nerve cells but some neurons are particularly temperature sensitive. These experiments were designed to attempt to determine the ionic and metabolic bases of neuronal thermosensitivity. In *Aplysia* neurons two temperature dependent processes have been described which have opposite effects on neuronal excitability. An electrogenic sodium pump tends to increase hyperpolarization with temperature and thus depresses firing as temperature rises. The membrane permeability to sodium tends to also increase with temperature and this mechanism tends to increase excitability as temperature rises. However, these neurons are not known to mediate temperature information and therefore we have investigated the mechanisms underlying neuronal thermosensitivity in primary temperature receptors from the scrotal skin of the rat.<sup>1</sup>

A greater percentage of the afferent fibers innervating the scrotal skin are primary temperature receptors than in most other mammalian preparations. We have analyzed and described this thermosensitivity of greater than 70 primary afferent fibers dissected from the pudendal nerve in intact animals. These afferent fibers fall into three primary categories. Greater than 50 percent of the fibers are mechanically sensitive but also temperature sensitive. Approximately 20 percent of the fibers are only temperature sensitive and are excited by cooling. Another population of fibers are not mechanically sensitive and are excited by warming. The mechanically sensitive afferents may be excited by cooling or by warming or may have a temperature optimum of an intermediate range.

By local infiltration of ouabain into the receptive field of these afferents we have been able to demonstrate that a cold fiber can be changed to a warm fiber. This observation is consistent with the hypothesis that an electrogenic sodium pump is the generator potential mechanism responsible for cold sensitivity.

To test this hypothesis more rigorously we have developed the isolated nerve skin preparation using the same tissue. This allows one to change the ionic medium and to add drugs and to be certain that the drug reaches the receptive field. Figure 50 shows activity recorded from an afferent fiber in an isolated rat scrotum skin preparation. The discharge characteristics of afferents in the isolated preparation are very similar to those of the intact preparation and are characterized by irregular discharges with bursts of activity, particularly at higher temperatures. Figure 51 shows that, when the isolated nerve skin preparation is perfused with a solution containing no potassium, the discharge frequency increases. Removal of extracellular potassium should depress excitability in the absence of a contribution of an electrogenic pump to membrane potential. Thus, the observation that discharge increases in potassium free solutions is evidence which strongly supports the hypothesis that the mechanism of cold sensitivity in these afferent fibers is activity of an electrogenic sodium pump.

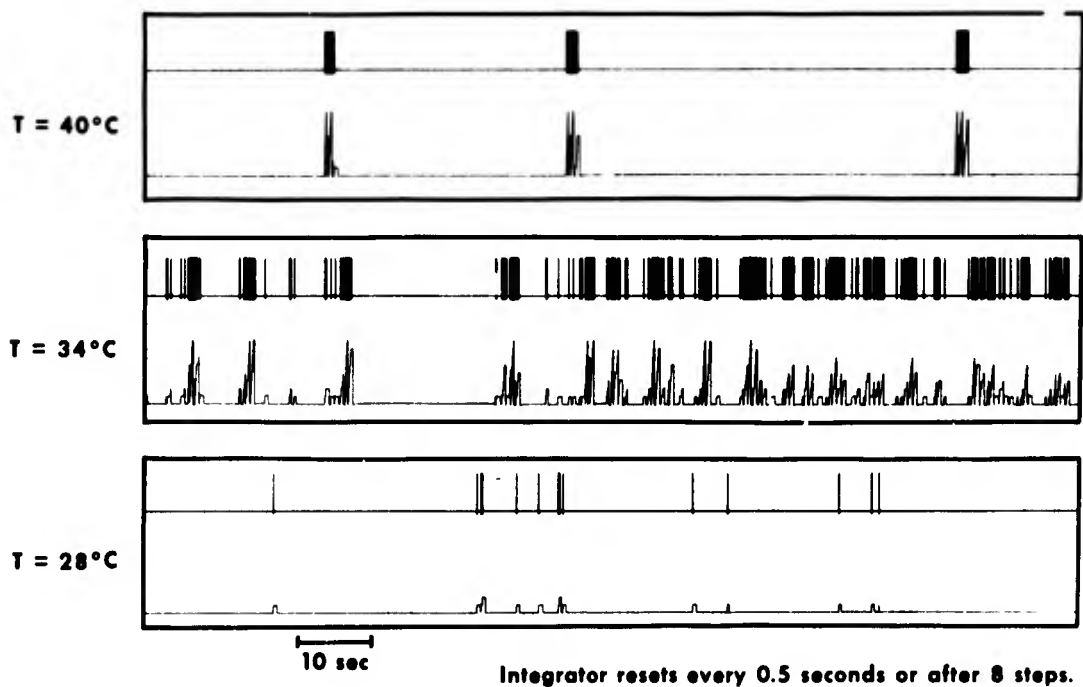


Figure 50. Activity recorded from an afferent fiber in an isolated rat scrotum skin preparation

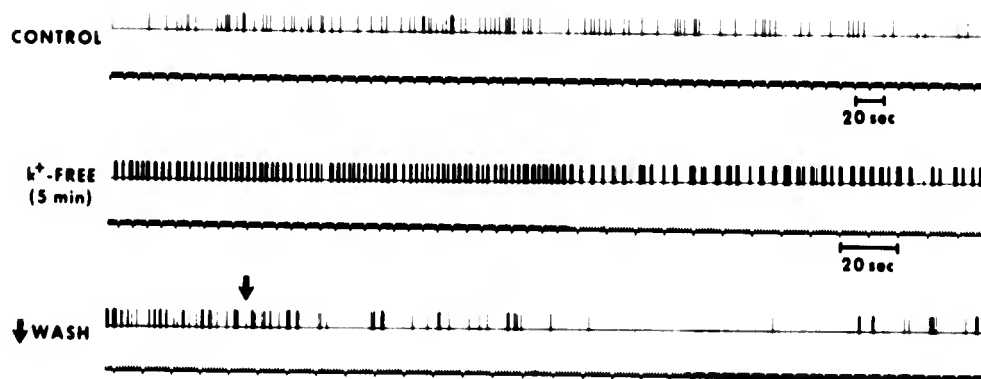


Figure 51. Activity recorded from an afferent fiber in an isolated rat scrotum skin preparation

#### REFERENCE

1. Carpenter, D. O., Pierau, Fr.-K. and Torrey, P. J. Mammalian cold receptor afferents: role of an electrogenic sodium pump in sensory transduction. Bethesda, Maryland, Armed Forces Radiobiology Research Institute Scientific Report SR74-15, 1974.



#### ELECTROPHYSIOLOGICAL STUDIES ON THE LOBSTER CARDIAC GANGLIA

Principal Investigator: *D. R. Livengood*

The lobster cardiac ganglion is currently being used to investigate the mode of action of Lioresal, a GABA derivative, which, like GABA, is effective in mammalian spinal cord as a dorsal root potential blocker.

GABA mimics the inhibitory neurotransmitter in the lobster cardiac ganglia. When applied in the bathing solution surrounding the cardiac ganglia GABA usually causes a slight hyperpolarization of the membrane associated with a rather large input resistance change, averaging 45 percent (see Table XXVIII and Figure 52, tracings 1 and 2). This membrane conductance change is apparently a change to chloride ions since an increase in internal chloride concentration caused a depolarization to GABA response. This is because an increase of internal chloride ions causes a positive shift in the Nernst potential for chloride, resulting in a depolarization of the membrane when GABA is applied. This can also be shown by removal

of the external chloride ions which again shifts the Nernst equilibrium potential for chloride and results in a depolarization when GABA is applied. GABA is blocked by the application of picrotoxin, a known GABA transmission blocker in the CNS. Lioresal, on the other hand, also frequently causes a slight hyperpolarization of the membrane. Lioresal also causes a slight reduction in the firing rate of the cardiac ganglia (Figure 53) as does GABA. Lioresal, however, does not produce a membrane resistance decrease as does GABA but rather a membrane resistance increase averaging about 17 percent. Therefore, the method of action of Lioresal, in the cardiac ganglia at least, seems to be considerably different from GABA. It seems likely that Lioresal causes a decreased membrane conductance to sodium.

Table XXVIII. The Effect of GABA and Lioresal on Membrane Properties of the Lobster Cardiac Ganglion

Condition	$\Delta E_m \pm S.D.$	$\Delta \text{Impact } R_m \pm S.D.$
GABA $10^{-3}$ M	$-0.5 \text{ mV} \pm 2.14$	decrease $45\% \pm 13$
GABA + Picrotoxin $10^{-3}$ M	0	0
GABA $10^{-3}$ M + increase of $[Cl]$	+ 20 mV	decrease 62%
GABA $10^{-3}$ M + decrease of $[Cl]$	+ 12 mV	decrease 22%
Lioresal $2 \times 10^{-3}$ M	$-15.5 \text{ mV} \pm 2.38$	increase $16.75\% \pm 9.7$

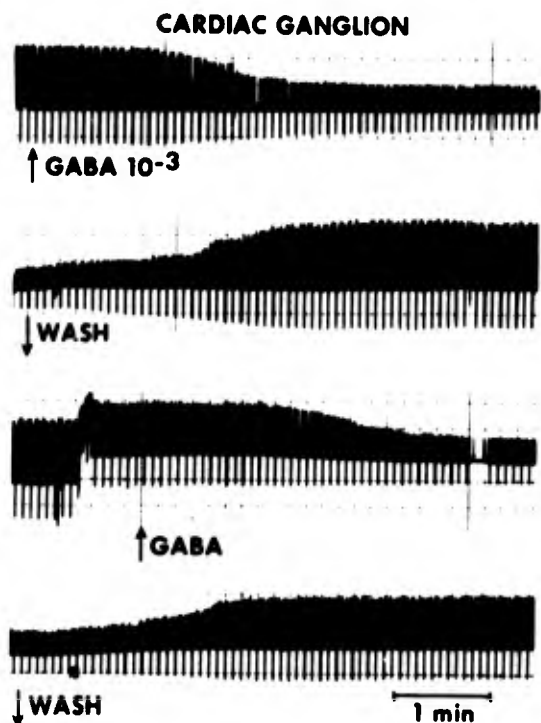


Figure 52.  
The effect of  $10^{-3}$  M GABA on the amplitude of burst potentials, membrane potential and membrane resistance. Without (traces 1 and 2) and with (traces 3 and 4) applied depolarization.



Figure 53. The effect of Lioresal on membrane potential, burst frequency and membrane resistance

••••••••••

## BIODYNAMICS AND PATHOPHYSIOLOGY OF TRAUMATIC UNCONSCIOUSNESS

**Principal Investigators:** *A. K. Ommaya, L. E. Thibault, National Institutes of Health; and D. O. Carpenter, AFRR*

**Technical Assistance:** *V. A. Kieffer*

Studies on the mechanism of head injury are of critical importance to both the clinician and the neuroscientist. This program aims at an understanding of the mechanisms of the injury to nervous tissue induced by sudden traumatic impact. We are approaching a study of experimental head injury both by subjecting primates to a sudden impact and by studying mechanisms of injury to simpler nervous tissues subjected to similar kinds of insults.

We have developed an apparatus which permits investigation of the effects of controlled and reproducible dynamic loading on the functional response of the sciatic nerve of a frog. The device is depicted schematically in Figure 54. A time varying force is applied to a piston closely fitted to the base of a liquid column. The piston motion produces a compressive disturbance which is acoustically propagated up the liquid column. The nerve is exposed over 1 cm of its length equivalent to the internal diameter of the column and thus is subjected to a transient hydrostatic pressure as well as normal and shearing strains resulting from fiber displacement. This complex loading condition is comparable to the type of loads predicted to occur at the tissue level when the head is subjected to impact or impulsive loading. In the case of head injury the duration of loading varies from approximately 3 to 5 msec for rigid flat plate impacts to 12 to 18 msec for padded impacts. This device permits variation of applied load duration over this range of interest. The pressure time history and column temperature in the vicinity of the nerve fiber are continuously recorded. Electrodes for stimulation and continuous recording of the compound action potential are located externally. Figure 55A shows a normal compound action potential resulting from a 5-volt stimulus. The action potential is modulated after loading (0.8 atm peak pressure, duration 10 msec) and returns to normal in approximately 10 minutes. Figure 55B derives from a subject subjected to 1.5 atm for 10 msec; the compound action potential does not fully recover. These experiments demonstrate that the compound action potential amplitude and duration, recorded from a frog sciatic nerve, can be reversibly or irreversibly modulated by dynamic mechanical loading with no obvious indication of macroscopic structural damage. Other nerve preparations are being studied.

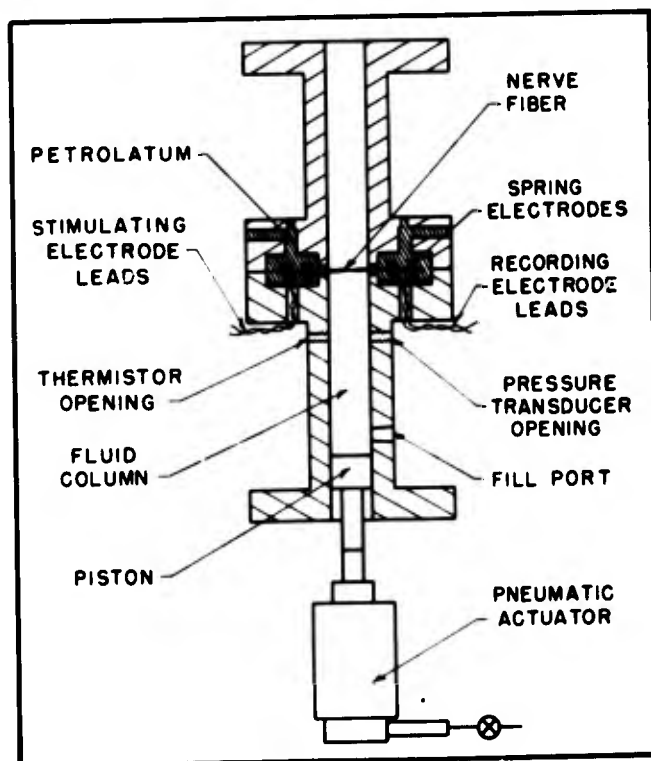


Figure 54. Schematic of apparatus

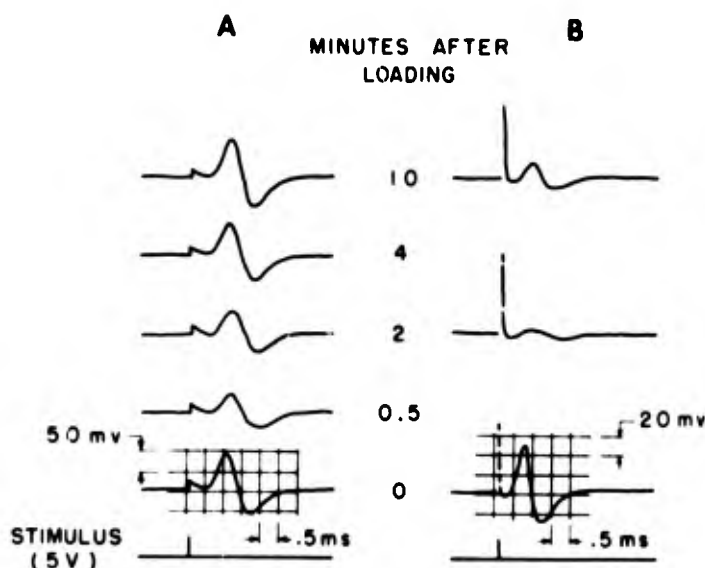


Figure 55. Compound action potentials



## STUDIES INTO THE MECHANISM OF ALCOHOL-INDUCED PHYSICAL DEPENDENCE IN THE RAT

Principal Investigator: W. A. Hunt

Alcohol dependence is being studied by two broad approaches: (1) the mechanism of alcohol-induced depression and (2) the mechanism of the development of physical dependence. Since alcohol is such a simple molecule and increases in depressant potency and lipid solubility as the length of the side chain is increased, it may not interact with a specific receptor in the classical sense as with drugs with more complicated structures. Because evidence has accumulated indicating an interaction between alcohol and membranes, the actions of alcohol in inducing depression may be more physicochemical in nature, and may involve a variety of disruptions to membranes. To explore this, studies have been initiated employing fluorescent probes, which provide information on various aspects of membrane structure, and a purified membrane preparation from rat brain. Because of the lack of a suitable method for isolating the latter, a procedure is being developed which utilizes differential centrifugation, an aqueous polymer two-phase system and gradient density centrifugation.

Development of alcohol dependence likely results from a secondary or adaptive change related to the primary mechanism of action of alcohol. Subtle changes in membrane structure with concomitant changes in membrane function may be the immediate cause of the addictive state. However, the definition of physical dependence maintains that upon withdrawal of the addicting drug, a series of behavioral and neurological symptoms develop which may involve a number of different systems in the brain. Neurotransmitter substances which play an important role in maintaining neuroexcitability may be related to the development of symptoms of the alcohol withdrawal syndrome. The possibility of neurotransmitter involvement in these phenomena is being explored using a model of alcohol dependence in the rat.<sup>4</sup> These animals display a withdrawal syndrome similar to that observed in man and have a greater susceptibility to seizures.<sup>1</sup> To date it appears that norepinephrine and dopamine<sup>3</sup> but not serotonin<sup>2</sup> are implicated in withdrawal phenomena. Current research is attempting to relate changes in catecholamine function to the various withdrawal symptoms observed. Also, other transmitters, such as acetylcholine and gamma-aminobutyric acid, are being investigated as to their possible role in alcohol dependence.

#### REFERENCES

1. Hunt, W. A. Changes in the neuro-excitability of alcohol-dependent rats undergoing withdrawal as measured by the pentylenetetrazole seizure threshold. *Neuropharmacology* 12:1097-1102, 1973.
2. Hunt, W. A. and Majchrowicz, E. Turnover rates and steady-state levels of brain serotonin in alcohol-dependent rats. *Brain Res.* 72:181-184, 1974.
3. Hunt, W. A. and Majchrowicz, E. Alterations in the turnover of brain norepinephrine and dopamine in alcohol-dependent rats. *J. Neurochem.* (in press).
4. Majchrowicz, E. Induction of physical dependence on alcohol and the associated metabolic and behavioral changes in rats. *Pharmacologist* 15:159 (Abstract 025), 1973.





## THE BRAIN AS AN IMMUNOLOGICALLY PRIVILEGED SITE

**Principal Investigators:** R. A. Morantz and W. G. Shain, Jr.

**Technical Assistance:** B. J. Bolden

Over the past 50 years the concept has arisen that the brain does not participate in the immune response of the organism to the same extent as other organs.

To investigate the extent of this phenomenon, inbred Fisher rats were injected both subcutaneously and intracerebrally with varying doses of tumor cells that had been cultured from an ethyl nitrosourea (ENU) produced rat glioma. In animals that were not immunosuppressed it was found that survival could be consistently obtained if the dose of tumor cells injected was less than  $2 \times 10^7$  cells. However, if genetically similar rats were immunosuppressed with antilymphocyte serum (ALS), then as little as  $5 \times 10^4$  injected tumor cells would consistently cause death within 30 days. Necropsy study of these animals revealed them to have intracerebral gliomas.

In addition, varying the time of injection of ALS with respect to tumor cell injection revealed that the essential time period for ALS injection (0.5 ml I. P.) was from days -1 to +6 (i.e., from 1 day prior to 6 days after tumor inoculation).

In a similar fashion, rats injected subcutaneously with tumor cells revealed the same phenomenon, i.e., large tumor doses could be rejected in normal rats but not in immunosuppressed rats. The subcutaneous tumors in normal rats reached maximum size on approximately day 7 and began to decrease in size by day 10. By day 30, after tumor injection, normal rats injected with less than  $2 \times 10^7$  EA or 8A rat glioma cells showed no evidence of tumor.

The implication of these data is that the brain as well as the periphery is participating in the immune rejection of this tumor. More quantitative studies using  $^{51}\text{Cr}$  microcytotoxicity tests and the injection of labelled lymphocytes are presently underway to compare the afferent and efferent limbs of the immune responses to tumor antigens injected into the brain and periphery.

Related to the previous issue is the question of whether or not the immune system carries out a surveillance function over the central nervous system in the same manner as it appears to do in certain cases of peripheral neoplasms. The concept of immune surveillance, originally proposed by Thomas<sup>2</sup> and amplified by Burnet,<sup>1</sup> implies that there is an immunologic mechanism by which the organism is constantly screening its internal environment for spontaneous cellular mutation which would then go on to become clinical neoplasia. To determine whether this immunologic screening is occurring in nervous system tumors, pregnant rats were given ENU at a dose of 20 mg/kg

intravenously within the last 3 days prior to term. The offspring were divided into three groups: control, immunosuppressed by neonatal thymectomy and weekly injections of ALS, and immunoenhanced with multiple injections of Bacillus Calmette-Guerin (BCG). At the termination of the experiment the latency frequency and distribution of neural and nonneural tumors will be evaluated to ascertain if altering the immune mechanisms of the host has affected neural oncogenesis.

## REFERENCES

1. Burnet, M. Somatic mutation and chronic disease. *Brit. Med. J.* 1:338-342, 1965.
2. Thomas, L. In: *Cellular and Humoral Aspects of the Hypersensitive States*, Lawrence, H. S., editor, p. 529. New York, N. Y., Paul B. Hoeber, Inc., 1959.

\*\*\*\*\*

## IDENTIFICATION OF SPECIFIC OPIATE RECEPTORS IN CULTURED CELLS

**Principal Investigators:** J. C. Blosser and W. G. Shain, Jr.

**Technical Assistance:** J. R. Abbott

The existence of specific opiate receptors of membrane origin has recently been demonstrated in the brain. The concept of an effector molecule binding to a receptor on the cell membrane and initiating changes in the metabolism of the cell is well established. However, elucidation of opiate-receptor mediated intracellular changes responsible for analgesia and dependence is complicated by the high degree of complexity and cell heterogeneity in the brain. Primary changes due directly to cell-drug interaction are difficult to differentiate from cell-cell induced secondary changes. These difficulties can be circumvented by using cell culture systems. The object of this study is to correlate opiate receptors with cell types and to identify drug-receptor induced intracellular changes in nerve cell metabolism.

Identification of opiate receptor sites is accomplished by cells with  $^3\text{H}$ -naloxone in the presence of either levorphanol, a potent opiate which binds to the receptor, or dextrorphan, its inactive enantiomer which does not bind to the receptor. Bound radioactivity is separated from unbound by collection on a Whatman GF/C filter. Specific

binding to receptors is differentiated from nonspecific binding by subtracting radioactivity bound in the presence of levorphanol from that bound in the presence of dextrorphan. Binding of opiate to receptors follows a langmuir saturation isotherm when plotted against concentration of opiate in solution. A comparison of specific with nonspecific binding of 2 nM  $^3\text{H}$ -naloxone to brain homogenates is depicted in Figure 56. Specific opiate binding requires several minutes to reach equilibrium, while nonspecific binding is linear over all of the ranges studied.

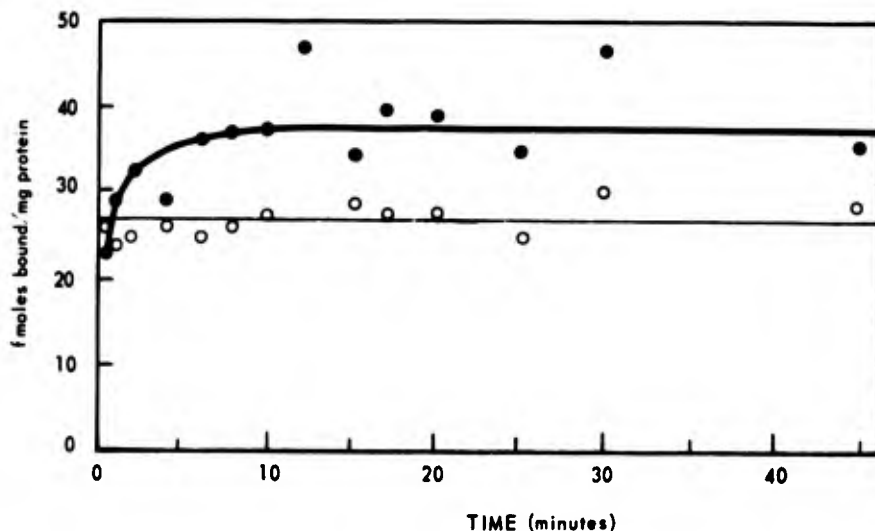


Figure 56. Specific (●) and nonspecific (○) binding of 2 nM  $^3\text{H}$ -naloxone to brain homogenates

Two different experiments are presently being carried out with cell cultures. The first series of experiments is to screen all of the available cell lines for  $^3\text{H}$ -naloxone binding activity. In these experiments, homogenates of cells are used for the assays. A number of cell lines have been studied to date (see Table XXIX); however, only a few lines have been found which bind  $^3\text{H}$ -naloxone. It is interesting to note that all of these cell lines are somatic cell hybrid lines derived from a common neuroblastoma parent (TGN2). However, this cell line has no opiate binding activity itself. From Table XXIX it is also possible to demonstrate that receptor activity cannot be correlated exclusively with cholinergic or adrenergic neurotransmitter systems.

The second series of experiments that have begun with the cell cultures is to develop an assay for monitoring opiate binding on intact cell cultures. Initial efforts are being made to demonstrate (1) interference of opiate binding with various ions in the media and (2) the relationships between the concentration of opiate required to saturate binding in cell homogenates, to saturate binding in intact cell preparations and to cause intracellular metabolic changes.

Table XXIX. Opiate Receptor Activity of Various Cell Lines and Related Neuronal or Glial Properties

Cell origin	Cell line	Neurotransmitter synthesis		Electrical activity	Response to acetylcholine	Opiate receptors
		Cholinergic	Adrenergic			
Neuroblastoma <u>X</u>						
Glioma somatic	H05	+*	-†	+	+	-
Cell hybrid	H15	+	-	+	+	+
Sympathetic ganglion cell <u>x</u>	X1	-	-	?‡	?	+
Neuroblastoma	X31	-	+	+	+	-
Somatic cell	X58	-	-	?	?	-
Hybrid	X93	-	-	?	?	-
Selected clones of X31	THX03	-	+	?	?	-
	THX11	-	+	?	?	-
	TX22	-	+	?	?	-
	TX23	-	+	?	?	-
	TX32	-	+	?	?	-
Neuroblastoma	TCN2	-	-	± §	±	-
Schwannoma	B6	?	?	?	?	-
	CII	?	?	?	?	-

\* + = significant response or synthesis  
† - = insignificant response or synthesis  
‡ ? = unknown  
§ ± = variable response

◆◆◆◆◆◆◆◆◆◆

## SPINAL CORD BLOOD FLOW MEASURED BY THE HYDROGEN CLEARANCE TECHNIQUE

Principal Investigators: T. F. Doyle, A. I. Kobrine and A. N. Martins

Technical Assistance: W. L. Stringfield

Attempts have been made in the past to measure spinal cord blood flow directly and indirectly, qualitatively and quantitatively, using a multitude of techniques, all of which have significant drawbacks. Much of the difficulty has been the inability to isolate flow in the cord. With the development of the hydrogen clearance technique, using

inhaled hydrogen as a tracer substance and microelectrodes as detectors, focal flow measurements in the spinal cord become accurate and reproducible.

Multiple blood flow determinations were made over 4-hour periods.<sup>1</sup> The average flow varied from  $13.6 \pm 1.2$  ml/min per 100 g to  $21 \pm 1.5$  ml/min per 100 g with a mean flow of  $16.84 \pm 2.5$  (S.E.) ml/min per 100 g.

## REFERENCE

1. Doyle, T. F., Kobrine, A. I. and Martins, A. N. Spinal cord blood flow measured by hydrogen clearance. Bethesda, Maryland, Armed Forces Radiobiology Research Institute Scientific Report SR74-20, 1974.



## VENTRICULOCISTERNAL PERFUSION STUDIES IN THE MONKEY

**Principal Investigators:** A. N. Martins and T. F. Doyle

**Technical Assistance:** W. L. Stringfield

Sixteen monkeys underwent standard ventriculocisternal perfusion with mock cerebrospinal fluid (CSF) to which  $^{125}\text{I}$  labeled human serum albumin and blue dextran were added as nondiffusible indicators. Dilution of the indicators provided a measure of the rate of formation of CSF ( $V_f$ ).

Eighty-five paired samples were available for analysis of the concentration of both  $^{125}\text{I}$ -RISA and blue dextran.

On Figure 57 is plotted  $V_f$ -albumin versus  $V_f$ -blue dextran. They are significantly ( $p < 0.001$ ) correlated ( $r = +0.806$ ). Mean  $V_f$  calculated from dilution of  $^{125}\text{I}$ -RISA was  $37.6 \mu\text{l/min}$  ( $\pm .74$  SEM) and mean  $V_f$  calculated from dilution of blue dextran was  $37.1 \mu\text{l/min}$  ( $\pm .70$  SEM). The difference is not significant (paired comparisons t-test).

As expected, these two large indicator molecules gave essentially identical mean rates of CSF formation. Apparently unbound  $^{125}\text{I}$  in the commercially available  $^{125}\text{I}$ -RISA is insignificant for the purpose of measuring rates of CSF formation. However, because of the counting variability of the RISA samples, which are related to the low energy levels of  $^{125}\text{I}$ , we have come to prefer blue dextran for ventriculocisternal perfusion studies.

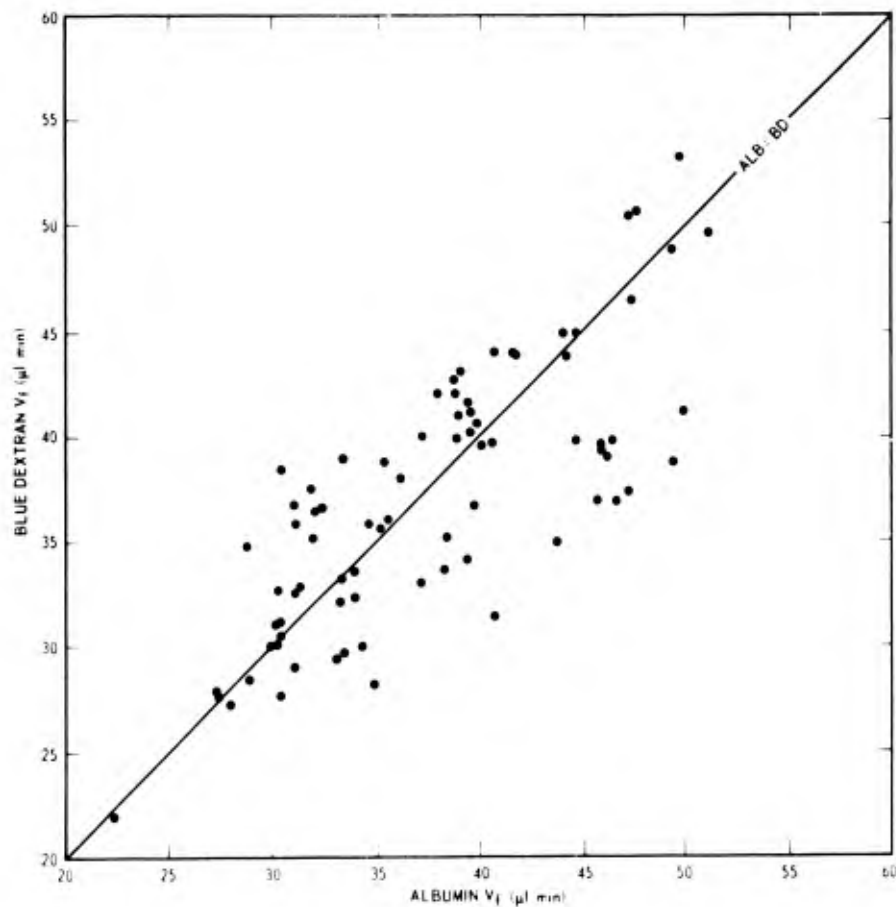


Figure 57. Scatter diagram in which the rates of formation of CSF ( $V_f$ ) calculated from the dilution of  $^{125}\text{I}$ -labeled albumin are plotted against those from the dilution of blue dextran.  $N = 85$ . Correlation of coefficient is 0.806 ( $p < .001$ ).

•••••

## COMPUTERIZED AXIAL-TRANSVERSE TOMOGRAPHY: THE ACTA SCANNER

**Principal Investigators:** *W. E. Kiker, T. W. Hinz, AFRRl; and R. S. Ledley,  
Georgetown University Medical Center*

**Technical Assistance:** *C. L. Bransford*

This research has resulted from a cooperative effort between Dr. R. S. Ledley, of the Georgetown University Medical Center, developer of the ACTA scanner, and members of the AFRRl staff. Since the scanner has been operational a continuing cooperative research program has been carried on.

Several papers describing the technique of computerized axial-transverse tomography have appeared recently so it will not be described in detail here. Briefly, the procedure is to measure the attenuation of a narrow beam of 120 kVp x rays as it is passed through a patient or phantom, each pass being from a different direction but always within a prechosen cross-sectional plane. The computer then calculates a map, or matrix, of numbers, proportional to x-ray attenuation coefficients within the plane. A typical head scan is shown in Figure 58.



Figure 58. Typical ACTA scan. The plane of the scan is at eye level. Included in the anatomical features seen are the orbits and mastoid sinuses.

Radiological physics measurement. A series of measurements were made to determine the radiation dose and dose distribution delivered to a patient during a scan. Radiographic film and thermoluminescent dosimeters (TLD) were used in the AFRRI Alderson Rando phantom for these measurements. Because of the dependence of the TLD calibration on x-ray energy, a series of measurements were made using the AFRRI Maxitron 300 kVp x-ray machine to calibrate our TLD's as a function of energy. A typical dose distribution diagram obtained for the head is shown in Figure 59.

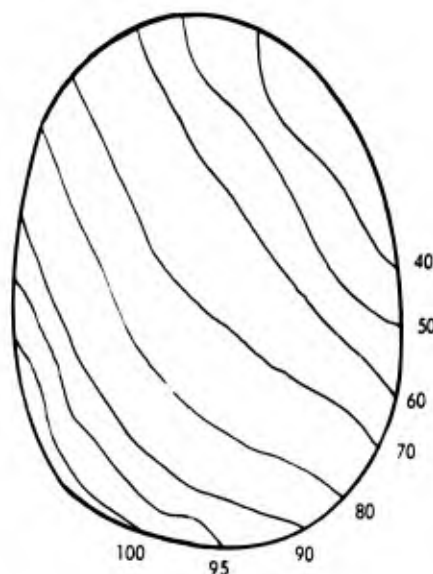


Figure 59. Depth-dose distribution film

Correlation of ACTA scanner numbers with electron density of material scanned. A series of measurements have been made to demonstrate the correlation of ACTA scanner numbers, which are proportional to x-ray attenuation coefficients, with electron density in scanned material. There has been a strong tendency to correlate these numbers with mass density. As part of the experiment, a calculation was made of the electron density of a typical blood clot and of whole blood to show that electron density and mass density do not change in the same way. Results of the calculation showed that the electron density of a clot relative to whole blood is 1.014 while the relative mass density is 1.021. Given the 0.5 percent resolution of the ACTA scanner, this difference is significant.

Experimentally the correlation between ACTA number and electron density was demonstrated by scanning a polystyrene phantom containing cavities filled with various fluids, as shown in Figure 60. For this experiment the fill fluids were aqueous solutions of acetic acid and ferrous nitrate. The electron and mass densities of each solution were calculated as a function of concentration, and the ACTA numbers measured. Results are shown in Figures 61 and 62. The solid curves in each case show the variation in electron and mass densities, while the points show the relative ACTA numbers. Clearly, for the low-Z acetic acid solution, the ACTA numbers follow the electron density curve while for the higher-Z iron, where the photoelectric cross section is appreciable, the correlation is with the density of iron atoms.

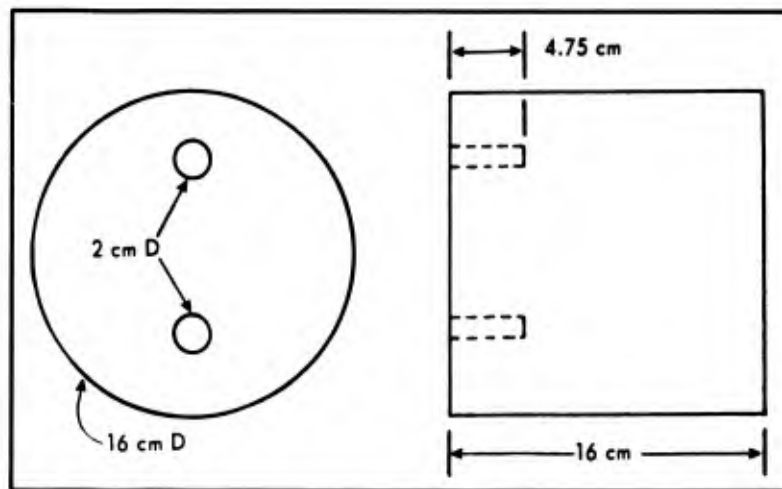


Figure 60. Polystyrene phantom



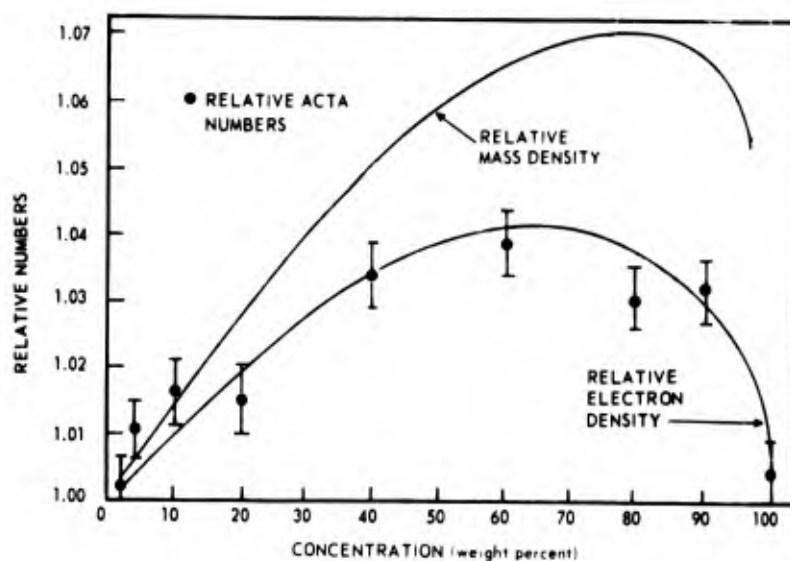


Figure 61. Variation of relative mass and electron densities and relative ACTA numbers for acetic acid solution

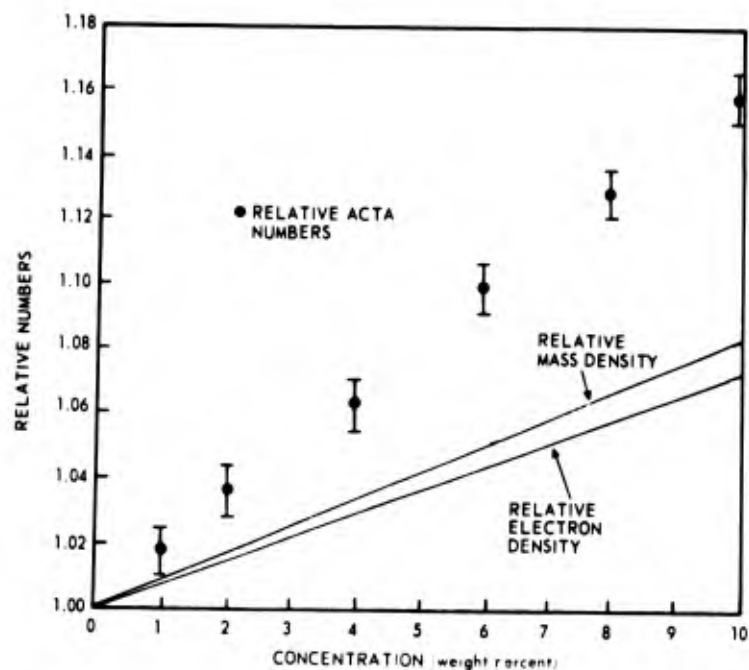


Figure 62. Variation of relative mass and electron densities and relative ACTA numbers for ferrous nitrate solution

••••••••••

## INTRACRANIAL PRESSURE SENSOR DEVELOPMENT

Principal Investigators: G. L. Hermann and W. E. Kiker

A long-term intracranial pressure sensor is desirable for many neurological conditions. Hydrocephalus, for example, normally requires repeated evaluation over a period of many years. This laboratory is pursuing the development of such a device based on the motion of fluid between two chambers of a small sensor that can be surgically implanted in the skull. The amount of fluid displaced is measured remotely with x-ray fluorescence. This method eliminates continuous penetration of the skin with tubes or wires over a long period of time.

A prototype sensor was assembled and tested with successful results. Figure 63 shows a schematic of the arrangement for the prototype test. A 5-mil thick gold foil and 4-mil thick rubber sheet were attached to a cork base. A syringe was used to introduce known volumes of  $0.3 \text{ g/cm}^3$  cesium nitrate solution into the sensor through the base. Each volume of fluid in the sensor was measured by irradiating it with a collimated beam of gamma rays from a  $^{99\text{m}}\text{Tc}$  source. The resulting 31 keV and 69 keV cesium and gold  $K_{\alpha}$  x rays were detected with a sodium iodide spectrometry system. Single channel analyzers were used to measure the counts in each of the two peaks. The ratio of cesium counts to gold counts was measured as a function of fluid volume in the chamber. Pressures corresponding to fluid volumes at  $21^{\circ}\text{C}$  were measured with a water manometer.

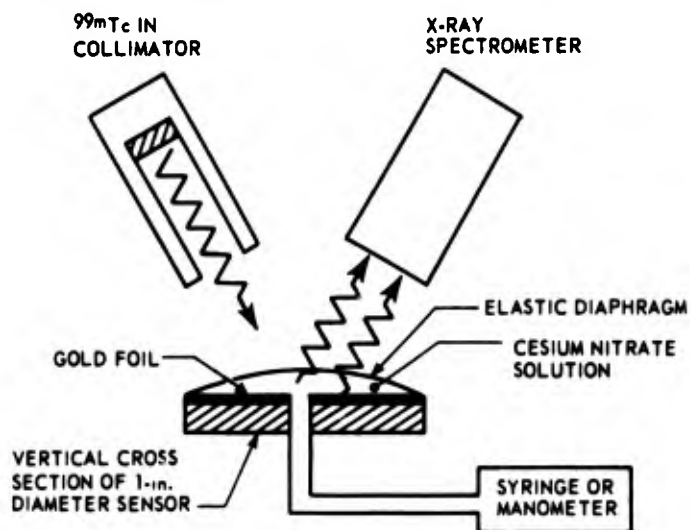


Figure 63. Equipment arrangement for measuring volume or pressure remotely with x-ray fluorescence

The results, shown in Figure 64, are linear over the range of measurement. Data points taken while increasing and decreasing the volume showed that no significant hysteresis occurred. Using a ratio of counts, rather than counts from only

the fluid, eliminates the need for efficiency calibration of the counting system. The location of the equipment shown in Figure 63 is therefore not critical.

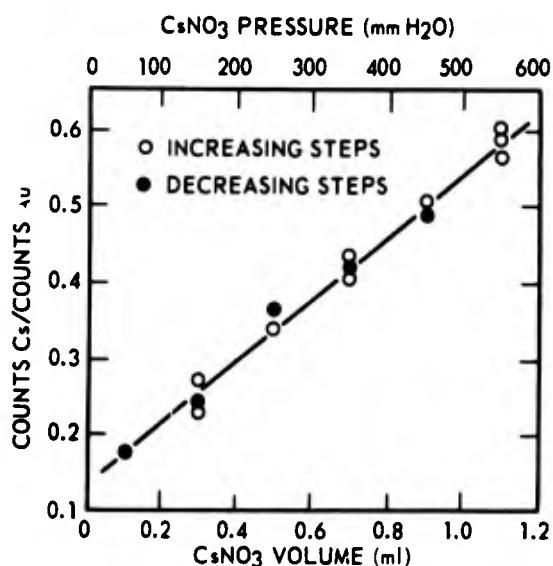


Figure 64. Ratio of cesium to gold fluorescence as a function of fluid volume or pressure

A cesium iodide solution is being employed to increase the sensitivity and accuracy of pressure measurements. The syringe is being replaced by a pressure sensitive tambour. Sensor size is being reduced and suitable materials are being used for in vivo application.

\*\*\*\*\*

## DEVELOPMENT OF A PROTOTYPE BURN WOUND DRESSING

**Principal Investigators:** G. M. Meaburn, C. M. Cole, J. L. Hosszu, AFRRl;  
C. W. Wade and J. C. Eaton, U. S. Army Medical  
Bioengineering Research & Development Laboratory,  
Ft. Detrick, Maryland

The radiation-induced graft polymerization of 2-hydroxyethyl methacrylate (HEMA) and other acrylic monomers to silicone rubber (Silastic) has been investigated with the objective of developing an effective burn wound dressing. Several acrylic polymers, e.g., the flexible contact lens material Hydron, are compatible

with body fluids but are mechanically weak and readily lose their elastomeric properties upon evaporative loss of water from the polymer matrix. The silicone rubbers are strong, possess excellent drape properties, and are biologically inert. Their lack of adherence to regenerating granulation tissue, however, contraindicates their use in direct contact with the wound surface. The covalently bonded laminates are designed to combine the desirable features of each material and reduce or eliminate the disadvantages.

Thin sheets of medical grade Silastic in contact with aqueous solutions of monomer are exposed to  $^{60}\text{Co}$  radiation under anaerobic conditions. Polymerization is initiated on one surface only of the elastomer. Grafts with two different surface properties have been developed. One is a heavy layer with a nonwetable surface, the other considerably lighter with a completely wettable surface. Factors which influence depth and morphology of the graft include radiation dose and dose rate, purity and concentration of the monomer, the extent of the competing homopolymerization reactions, and the thickness of the substrate. A typical dose curve is shown in Figure 65. The effect of substrate thickness on the total graft is shown in Figure 66.

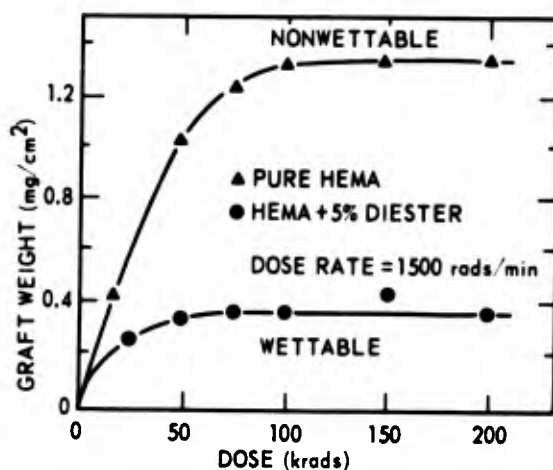
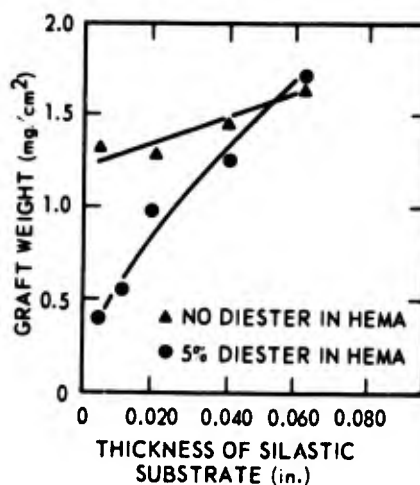


Figure 65.  
Effect of dose on grafting of 5 mil Silastic

Figure 66.  
Effect of substrate thickness on final graft yield



150 krads  $^{60}\text{Co}$   
AT 3000 rads/min  
SOLUTION: 10% MeOH  
10% HEMA  
80% H<sub>2</sub>O

Preliminary biological testing of these developmental dressings is being conducted at the U. S. Army Medical Bioengineering Research and Development Laboratory, Ft. Detrick, Maryland. Single and multiple grafts of both types of surfaces are being employed to promote healing of full-thickness excised wounds in rodents.



## PHOTONUCLEAR PRODUCTION OF POTASSIUM-38

**Principal Investigators:** C. M. Cole, F. C. Gray, G. M. Meaburn and J. S. Stevenson

Potassium-38 has been proposed by Myers <sup>2</sup> as a potentially useful radionuclide for *in vivo* studies. The rapid uptake of <sup>38</sup>K by the heart muscle is identical to that of <sup>43</sup>K, which has been demonstrated to be an effective agent for myocardial imaging. <sup>1</sup> This study was undertaken to evaluate the production of <sup>38</sup>K by the photonuclear reactions <sup>39</sup>K ( $\gamma, n$ ) <sup>38</sup>K and <sup>40</sup>Ca ( $\gamma, np$ ) <sup>38</sup>K using as the radiation source a bremsstrahlung field developed by the AFRRRI electron linear accelerator (LINAC).

The target materials used were KOH, for production of noncarrier-free <sup>38</sup>K, and calcium metal for the carrier-free radioisotope. Samples were sealed into quartz ampules and exposed to bremsstrahlung radiation developed by passing a high-energy LINAC beam through a thick water-cooled tantalum converter. In order to control the quantity of nonradioactive potassium in the final preparation, samples of KOH were limited to 0.25 g. After irradiation, sterile solutions of <sup>38</sup>KCl were prepared by acid digestion of the samples and were ready for use within one half-life (7.7 min) of removal of target material from the LINAC beam. In the case of the calcium metal target, the bulk of the calcium was removed from the preparation by precipitation as Ca(OH)<sub>2</sub>.

Typical radiopotassium yields are shown in Table XXX. Irradiation of calcium results in the production of <sup>42</sup>K and <sup>43</sup>K from competing ( $\gamma, np$ ) and ( $\gamma, p$ ) reactions, respectively, with <sup>44</sup>Ca present in natural abundance. The extent of this contamination is indicated in Table XXX.

Table XXX. Typical Radiopotassium Yields Achieved by Irradiating 1 g KOH or Calcium Metal for 30 Minutes in the Bremsstrahlung Beam Produced by 10 kW of 40 MeV Electrons

Target	Product	Yield	Yield delivered for injection
KOH	$^{38}\text{K}$	60 mCi	7 mCi*
Calcium	$^{38}\text{K}$	4 mCi	1 mCi
Calcium	$^{42}\text{K}$	4 $\mu\text{Ci}$	(co contaminant)
Calcium	$^{43}\text{K}$	17 $\mu\text{Ci}$	(contaminant)

\* KOH targets were limited to 0.25 g

Myocardial scans were performed on small (19-26 lb) and large (80-90 lb) dogs, using several millicuries of  $^{38}\text{K}$  per visualization. Hyperpotassemia in the animals was avoided by limiting total potassium injection to 4 meq. Potential problems of induced tachycardia resulting from this condition are completely eliminated by the use of the carrier-free radionuclide.

#### REFERENCES

1. Gray, F. C., Cole, C. M., Meaburn, G. M. and Brunhart, G. Electron linear accelerator production of potassium-43. Bethesda, Maryland, Armed Forces Radiobiology Research Institute Technical Note TN73-15, 1973.
2. Myers, W. G. Radiopotassium-38 for in vivo studies of dynamic processes. J. Nucl. Med. 14:359-360, 1973.

\*\*\*\*\*

#### ORGANOMETALLIC DOSIMETERS

Principal Investigators: G. M. Meaburn, J. L. Hosszu and W. E. Kiker

There is a continuing requirement for the development of dosimetry systems to be used in pulsed fields of ionizing radiation, particularly low-energy x radiation. A preferred dosimeter would be capable of live-time readout to monitor pulse profiles over a time scale of several nanoseconds. It also would be responsive to the spectral distribution of the x rays, i.e., able to discriminate between photons of different energies.

A homologous series of organometallic liquids, the tetraethyl compounds of silicon, germanium, tin and lead, are being considered for this purpose. Each member of the series contains one metal atom per molecule which absorbs preferentially in different regions of the x-ray spectrum. Little is known, however, about the radiation chemistry of this class of materials, particularly with regard to induced changes in physical properties that could be readily recognized and measured within the desired time scale.

The methods of pulse radiolysis and kinetic optical spectroscopy have been employed to observe the formation and decay of short-lived transient species present in these materials after exposure to single 200-nsec pulses of 40 MeV electrons delivered by the AFRRI electron linear accelerator (LINAC). Changes in optical absorption of each organometallic liquid were measured over the spectral range of 290-620 nm, using specialized photoelectric detection techniques in conjunction with a data analysis system responsive to fast nonrecurrent phenomena of this kind.<sup>1</sup>

All four tetraethyl compounds studied, as well as tetramethyl lead, exhibit transient absorption spectra in the visible and near ultraviolet regions following radiolysis. The spectra shown in Figure 67 are plotted from data recorded within 1  $\mu$ sec of target material receiving a 1-krad dose of radiation. The absorption bands of the tin and lead compounds exhibit well-defined shoulders which disappear within 10  $\mu$ sec of a LINAC pulse. This behavior is typified by the change observed in the spectrum of  $\text{Et}_4\text{Pb}$  as shown in Figure 68. The residual absorption is much longer lived and is still visible after several hundred microseconds. The shorter lived components are not found in the transient spectra of  $\text{Et}_4\text{Si}$  and  $\text{Et}_4\text{Ge}$ .

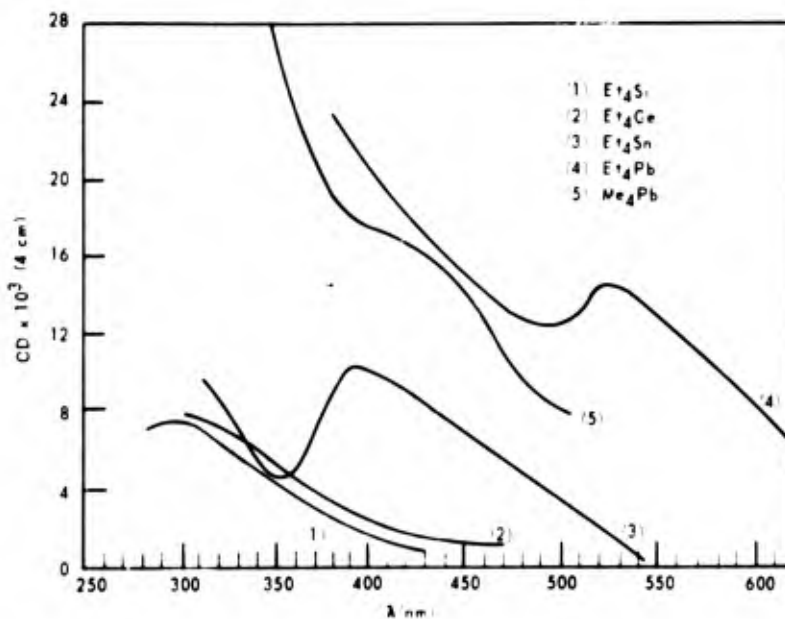


Figure 67. Transient absorption spectra of irradiated Group IV tetra-alkyls

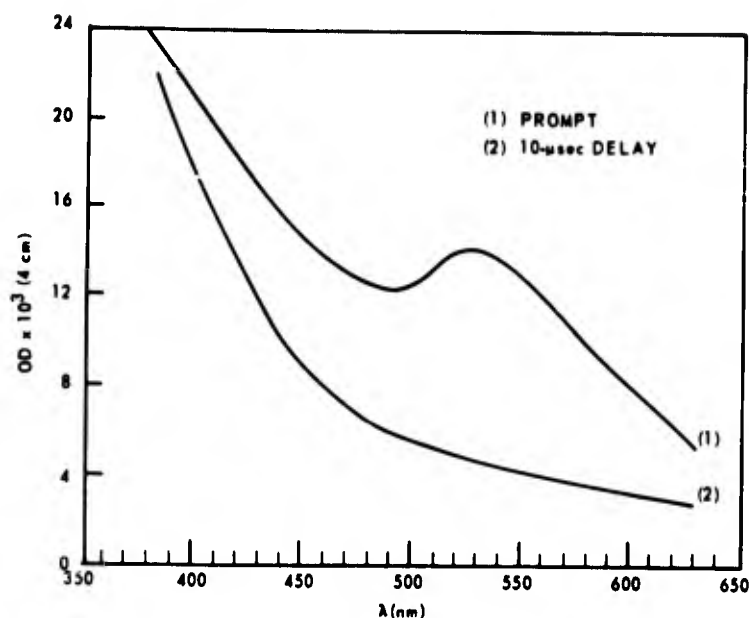


Figure 68. Decay of transient absorption spectra of irradiated  $\text{Et}_4\text{Pb}$

Detailed analysis of the decay kinetics in the different spectral regions indicates that trialkyl metal free radicals are probably responsible for much of the observed optical activity in all the irradiated compounds. Rupture of a metal to carbon chemical bond,  $(\text{C}_2\text{H}_5)_4\text{M} \xrightarrow{\text{radiolysis}} (\text{C}_2\text{H}_5)_3\text{M}\cdot + \cdot\text{C}_2\text{H}_5$ , is suggested as the major initial radiolytic reaction.

#### REFERENCE

1. Meaburn, G. M. and Isaacs, B. M. Digital recording of fast nonrecurrent phenomena in pulse radiolysis studies. Bethesda, Maryland, Armed Forces Radiobiology Research Institute Technical Note TN72-2, 1972.

◆◆◆◆◆◆◆◆◆◆



## FREE RADICAL REACTIONS: RADIATION-INDUCED OPTICAL CHANGES IN AQUEOUS DNA SOLUTIONS

Principal Investigators: G. M. Meaburn and J. L. Hosszu

Free radicals produced by the interaction of ionizing radiation with water react with deoxyribonucleic acid (DNA) in a complex and ill-understood manner. The highly organized macromolecular structure, essential to the biological function of DNA, is disrupted by attack of these highly reactive chemical species at specific sites in the biopolymer. The nitrogenous bases are damaged, sugar-phosphate linkages are broken, and the hydrogen bonds between the two complementary chains are lost. Destruction of the conjugated double bond system of the purine and pyrimidine bases, by addition of free radicals to these sites, results in loss of the light absorbing properties of DNA in the region of 260 nm. Radiation-induced changes in the optical absorption characteristics of DNA have now been investigated over the spectral range of 250 to 300 nm, thus providing additional information on the mechanisms of radiation damage in these in vitro systems.<sup>1</sup>

The methods of pulse radiolysis and kinetic spectroscopy were used to observe the radiation processes over a time scale of 1 to 800  $\mu$ sec. Dilute aqueous solutions of native or thermally denatured calf thymus DNA were exposed to single 0.5- $\mu$ sec pulses of 40 MeV electrons delivered by the AFRRI electron linear accelerator (LINAC). The absorbed radiation dose per pulse was approximately 4.8 krad. A pulsed xenon lamp was used to provide a sufficiently intense source of analyzing light in the spectral region under examination. The undesirable effects of stray light upon the photoelectric detection system were minimized by use of two high intensity monochromators coupled in tandem to obtain wavelength discrimination.

Over the time scale employed (800  $\mu$ sec), no change in optical absorption was observed in native DNA solutions exposed to a single LINAC pulse. This implies that (1) the conjugated double bonds of the bases are not attacked, or (2) damage to the base's chromophores is exactly balanced by loss of hypochromicity. Subsequent pulses delivered to the same sample produced a loss of optical absorption comparable to that seen in denatured DNA.

The radiation-induced optical changes in thermally denatured DNA, in which the bases are fully exposed but may be in a partially base-stacked configuration, are shown in Figure 69. The presence of  $N_2O$  in the solution effectively doubles the radiolytic yield of hydroxyl free radicals ( $\cdot OH$ ). Tertiary butanol, however, is an excellent  $\cdot OH$  scavenger but is unreactive towards hydrated electrons ( $e_{aq}^-$ ). The only radical species common to both solutions is the hydrogen atom ( $H\cdot$ ). The transient absorption band centered at 285 nm may be attributed, at least in part, to formation of an H-adduct of DNA. The half-life of this transient (50  $\mu$ sec) is identical for both solutions. Experimental observations in this absorption band are made difficult by the proximity of overlapping transient absorptions at higher wavelengths, due to

reaction of the various free radicals with sugar moieties or other sites on the bases. A further correction is necessary for denatured solutions because of the simultaneous loss of chromophoric activity following a radiation pulse.

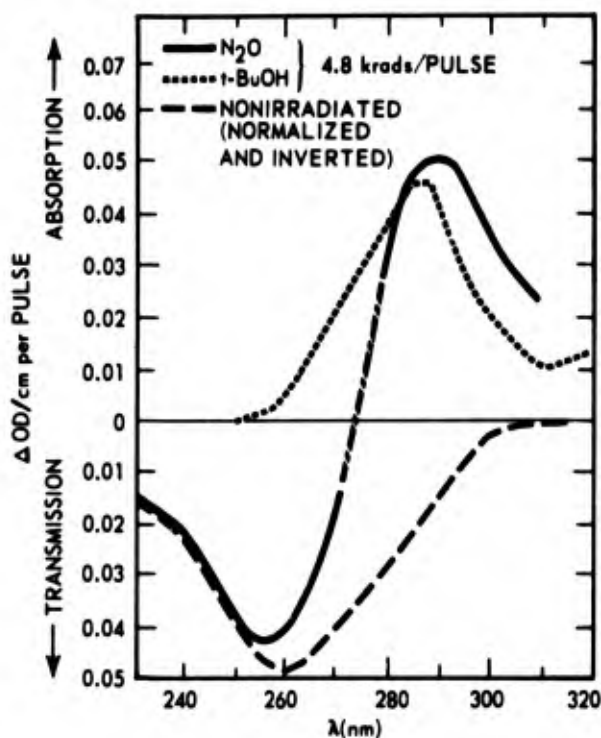


Figure 69. Composite absorption spectra of denatured DNA

This investigation emphasizes the important role of secondary structure in influencing the pathways of radiation damage in DNA. There appears to be little doubt that the double helical structure does afford some protection to the bases, thus confirming earlier conclusions based on a study of radiation-induced chain breakage of the polynucleotide.<sup>1</sup>

#### REFERENCE

1. Meaburn, G. M. and Cole, C. M. Free radical-induced chain breakage in irradiated aqueous solutions of DNA. Bethesda, Maryland, Armed Forces Radiobiology Research Institute Scientific Report SR74-3, 1974.

•••••

# INDEX TO PRINCIPAL INVESTIGATORS

	Page		Page
Abbott, J. R. ....	99	Kubota, H. ....	46
Adler, G. J. ....	48	Ledley, R. S. ....	132
Alter, W. A., III ....	106, 109	Ledney, G. D. ....	7, 10, 11, 22, 29
Armbrustmacher, V. ....	106	Levin, S. G. ....	44, 79
Barron, E. L. ....	44	Livengood, D. R. ....	102, 121
Baum, S. J. ....	1, 3, 19, 26	MacVittie, T. J. ....	26
Bidinger, J. ....	117	Martins, A. N. ....	83, 111, 112, 130, 131
Blosser, J. C. ....	80, 101, 128	Mathewson, N. S. ....	33, 57
Bright, R. W. ....	39	Matsson, J. L. ....	75, 79
Cagle, J. D. ....	48	McCarthy, K. F. ....	16, 26
Carpenter, D. O. ....	86, 90, 102, 117, 119, 123	McCreery, M. J. ....	117
Catravas, G. N. ....	80, 81, 83, 100, 101	McHale, C. G. ....	81
Chock, E. S. ....	93, 102	McManaman, V. L. ....	51, 62, 63, 64, 65
Cloud, C. L. ....	7, 11	Meaburn, G. M. ....	137, 139, 140, 143
Cohan, S. L. ....	99	Middleton, G. R. ....	69, 71, 73, 77
Cole, C. M. ....	137, 139	Morantz, R. A. ....	93, 127
Crawford, R. M. ....	10	Myers, P. R. ....	93
Crock, J. W. ....	75	Nelson, F. R. ....	39, 60
Curran, C. R. ....	69, 73	Newby, N. ....	83
Darden, J. H. ....	100	Ommaya, A. K. ....	123
Di Chiro, G. ....	85	Pierau, F.-K. ....	119
Donlon, M. A. ....	14	Reba, R. C. ....	46
Doyle, T. F. ....	83, 111, 112, 130, 131	Schneider, N. R. ....	1, 24
Dunson, G. L. ....	39	Shain, W. G., Jr. ....	93, 102, 127, 128
Eaton, J. C. ....	137	Shatsky, S. A. ....	106, 109
Eckelman, W. C. ....	44, 46	Short, D. B. ....	49
Ekstrom, M. E. ....	37	Sinclair, M. D. ....	51, 52, 65
Evans, A. S. ....	31	Skidmore, W. D. ....	3
Evans, D. E. ....	106, 109	Snyder, S. L. ....	57
Exum, E. D. ....	10	Sobocinski, P. Z. ....	33, 37, 44, 57
Fein, J. M. ....	85, 87, 89	Stevenson, J. S. ....	39, 44, 46, 48
Filo, R. S. ....	49		51, 52, 53, 55, 60, 62, 63, 64, 65, 139
Fink, M. P. ....	11	Takenaga, J. ....	81
Flor, W. J. ....	5	Taylor, J. F. ....	33
Franz, C. G. ....	69, 73	Teitelbaum, H. ....	80
Galley, C. B. ....	10, 29	Thibault, L. E. ....	123
Gallin, E. K. ....	113	Thrall, J. H. ....	63
Gambrill, M. R. ....	29	Wade, C. W. ....	137
Gray, F. C. ....	49, 139	Walker, R. I. ....	10, 14, 22, 29
Hermann, G. L. ....	136	Weathersby, P. K. ....	38
Hinz, T. W. ....	132	Wiederhold, M. L. ....	113
Hosszu, J. L. ....	137, 140, 143	Willis, J. A. ....	86
Hunt, W. A. ....	125	Woods, R. J. O. ....	37
Kelly, J. F. ....	48	Wyant, D. E. ....	3, 19
Kiker, W. E. ....	132, 136, 140	Yarowsky, P. J. ....	90
Kirchner, P. T. ....	49, 50	Young, R. W. ....	69, 71, 73, 77
Kobrine, A. I. ....	83, 111, 112, 130	Zeman, G. H. ....	83, 90